Crystallization of Molecular Glasses and Effect of Polymer Additives on Crystallization in Amorphous Solid Dispersion

By

Chengbin Huang

A Dissertation submitted in partial fulfillment of
the requirements for the degree of

Doctor of Philosophy
(Pharmaceutical Science)

at the
UNIVERSITY OF WISCONSIN-MADISON
2018

Date of final oral examination: 08/14/2018

The dissertation is approved by the following members of the Final Oral Committee:
Lian Yu, Professor, School of Pharmacy and Department of Chemistry
Mark D. Ediger, Professor, Department of Chemistry
Ronald Burnette, Professor, School of Pharmacy
Glen S. Kwon, Professor, School of Pharmacy

To my wife, Yilin

Acknowledgments

This thesis is not only a simple research summary in my Ph.D. study, but also a story of life experience by which I have been enriched in the past five years. While completing this thesis, I would like to express my sincere acknowledgment to my professors, mentors, colleagues, friends and family.

First of all, I would like to gratefully and sincerely thank my advisor, Prof. Lian Yu. His solid knowledge, enthusiasm and optimism have taught me how to do good science and how to be a qualified scientist. He has demonstrated how important is being fearless and curious in pursuing research ideas. Meanwhile, Lian is always patient. Whenever I have a question, Lian is always there with an open door, with an insightful comment, and with a smart solution. His unconditional support and absolute trust give me confidence to conquer any fear in my research projects and career growth.

I would like to thank Profs. Mark Ediger, Ronald Burnette, Glen S. Kwon, and Melgardt M. de Villiers as my preliminary exam and thesis committee members, for the helpful discussion and guidance. I would give my special thanks to Mark, who shares his knowledge, expertise, and resources in the lab during the past years. I would like to thank Dr. Geoff Zhang at AbbVie for help on the crystal nucleation project and support for my career development. I would express my appreciation to Dr. Chris Benmore at Argonne National Laboratory and Dr. Chenyang Shi at AbbVie for training me on synchrotron total X-ray scattering.

I own many thanks to all the past and current Yu group members: Prof. Ting Cai, Dr. Junshu Zhao, Dr. Caleb Brian, Dr. Siwei Zhang, Dr. Mariko Hasebe, Dr. Travis C. Powell, Dr. Wei Zhang, Dr. Men Zhu, Dr. Rattavut (M) Teerakapibal, Dr. Yinshan Chen, Dr. Shigang Ruan, Mr. Zhenxuan Chen, Ms. Yue Gui, Mr. Yuhui Li and Mr. Xin Yao. I would like to appreciate my research

collaborators, Prof. Feng Qian, Dr. Ankit Gujral, Dr. Jaritza Gómez, Dr. Yu Tong Tam, Dr. Niko Van den Brande, and Mr. Kushal Bagchi. I also want to thank all my friends outside the lab, who make my life colorful.

I would like to thank my mentors and colleagues during my summer co-op internship at Merck. I really appreciate help and support from Dr. Lei Zhu and Dr. Yongchao Su, who have mentored me scientifically and professionally. I also want to thank Drs. Adam Procopio, Gerard Klinzing, Jie Ren, Larry Rosen, Anthony Leone, Rubi Burlage, Fengyuan Yang, Hanmi Xi, Zhen Li and Wei Xu for their helpful assistance and discussion on projects.

Finally and most importantly, I would like to give my deepest thanks to my family, particularly my wife Yilin Wei, who love and support me regardless. I also want to thank my parents and parent-in-law for their spiritual support and encouragement.

CONTENTS

Abstract

Glasses are amorphous solids produced by cooling liquids, evaporating solutions, and condensing vapors while avoiding crystallization, with widespread applications ranging from optics to structural materials. There are many types of glasses, such as inorganic, polymeric, metallic and molecular glasses. Among them, molecular glasses have attracted increasing attention for applications in food, pharmaceutics, and organic electronics. In pharmaceutical science, molecular glasses are important for the delivery of poorly soluble drugs, because they are generally more soluble and bioavailable than their crystalline counterparts. Molecular glasses, however, readily crystallize. Therefore, a major task for developing these materials is to understand and avoid crystallization.

This study concerns the stability of molecular glasses and the effect of polymer additives on this property. It is organized around four topics. The first is the role of surface mobility in the crystallization of molecular glasses. The surface diffusion of amorphous griseofulvin was measured for the first time and was found to outpace bulk diffusion by a factor of 10^8 at the glass transition temperature T_g. This fast surface mobility explains the fast crystal growth on free surfaces. The second topic is crystal nucleation, the first step of a crystallization process that controls many of its properties. Homogeneous nucleation rates were measured in four glass-forming molecular liquids using two methods. For the systems studied (polyalcohols), the rates of crystal nucleation span at least 10 orders of magnitude, while the rates of crystal growth are comparable at the same temperature relative to T_g. At large supercooling, the rates of nucleation and growth share a similar temperature dependence, which suggests a similar kinetic barrier for both processes. The Classical Nucleation Theory provides a reasonable description of our data, showing no sign of failure as a result of a growing length scale for corporative rearrangement in

deeply cooled liquids, as recently suggested for lithium disilicate. The third topic focuses on a polymer's effect on the crystal growth and nucleation in molecular glasses. The rates of crystal growth were measured in many drug-polymer systems, and the results indicate a controlling role for the polymer's segmental mobility relative to host dynamics. The polymer effect on crystal nucleation was studied at temperatures at which the host molecules nucleate the fastest (slightly above T_g). The presence of a low-mobility polymer PVP in D-sorbitol effectively reduces the rate of crystal nucleation and the amount of reduction is similar to that seen for the growth rate. This argues that the decrease of molecular mobility by the polymer plays a controlling role. Our results, however, do not support the view that host-polymer hydrogen bonding controls the polymer's effect on crystallization. Finally, in the fourth topic, the structure of several polyalcohol liquids was studied by synchrotron total X-ray scattering to explore its relation to physical properties, such as crystallization tendency. The atomic pair-distribution functions from this work can be separated into intramolecular and intermolecular contributions to investigate the difference between the crystalline state and the liquid state in molecular structure and intermolecular hydrogen bonds. The findings of this thesis provide a better understanding of crystallization in molecular glasses and guide the selection of polymer additives to prevent the crystallization of molecular glasses.

Chapter 1. Introduction

Glasses are amorphous solids produced by cooling liquids, drying solution, and condensing vapors while crystallization is prevented. Glasses combine the mechanical strength of crystals and the spatial uniformity of liquids, and have widespread applications ranging from optics to structural materials. While better known glasses are inorganic (silicates), polymeric and metallic, molecular glasses are attracting more and more interests for applications in the delivery of poorly soluble drugs,[1] as matrices for preserving proteins,[2] and as photo- and electro-active materials.[3] Since the performance of amorphous materials rely on their non-crystalline structures, crystallization must be avoided. However, many molecular glasses easily crystallize,[4,5,6,7,8] making the understanding of crystallization in molecular glasses important in developing amorphous materials.

This thesis study focuses on the physical stability of amorphous materials against crystallization. Chapter 1 provides an overview of crystals, supercooled liquids (SCL) and glasses, discusses the crystallization (nucleation and growth) of amorphous materials, and reviews the polymer effect on the crystallization of amorphous materials. Chapter 2 describes the fast surface diffusion and crystallization of amorphous griseofulvin, as well as the general role of surface mobility in physical stability against crystallization. In Chapter 3, the first ever measurements of crystal nucleation rates in glass-forming molecular liquids is reported and discussed in the framework of the Classical Nucleation Theory (CNT). Chapters 4 and 5 describe the effect of polymer additives on crystal growth and nucleation in molecular liquids. Chapter 6 discusses the preliminary work to explore the structure of amorphous materials using total X-ray scattering. The last chapter describes possible future studies to further the understanding in the areas covered by this thesis.

1.1 Crystals, Supercooled Liquids (SCL) and Glasses

In Figure 1, the enthalpy and the specific volume of a crystal, a supercooled liquid and a glass are plotted against temperature. Upon cooling a liquid below its crystal melting temperature T_m, crystallization might happen. For some liquids, however, crystallization is easily avoided during cooling, producing a supercooled liquid. A supercooled liquid is a thermodynamically unstable phase in comparison to the crystal. Further cooling of a supercooled liquid causes the decrease of molecular mobility. At a certain temperature (the glass transition temperature T_g), molecular mobility is too slow to maintain the system in an equilibrium state, and a glassy state is produced. For a typical molecular liquid at T_g, the molecular mobility is approximately 100 s for structural relaxation time τ_α,[9,10] 10^{12} Pa·s for viscosity,[11] and 10^{-20} m^2/s for bulk self-diffusion coefficient.[12,13,14] Note that the glass transition is not a first-order transition, but rather a process of kinetic arrest. Because of its slow mobility, a glass behaves like a crystal in terms of mechanical properties.

Different from a crystal, which have both short-range and long-range orders, a glass lacks long-range order (Figure 2). This structural difference commonly offers the glass distinct properties, such as higher Gibbs free energy (physical instability), higher solubility, higher dissolution rate and lower density.[1,15,16]

Besides crystallization, a glass tends to age toward the equilibrium liquid state. Depending on the progress of the aging process, a glass can have different energies and densities. In theory, there are infinite numbers of glassy states. However, these different glasses should not be confused with *polyamorphism*, which distinguishes two amorphous phases by a first-order transition, *e.g.* water,[17,18] triphenyl phosphite (TPP),[19,20] and D-mannitol.[21,22]

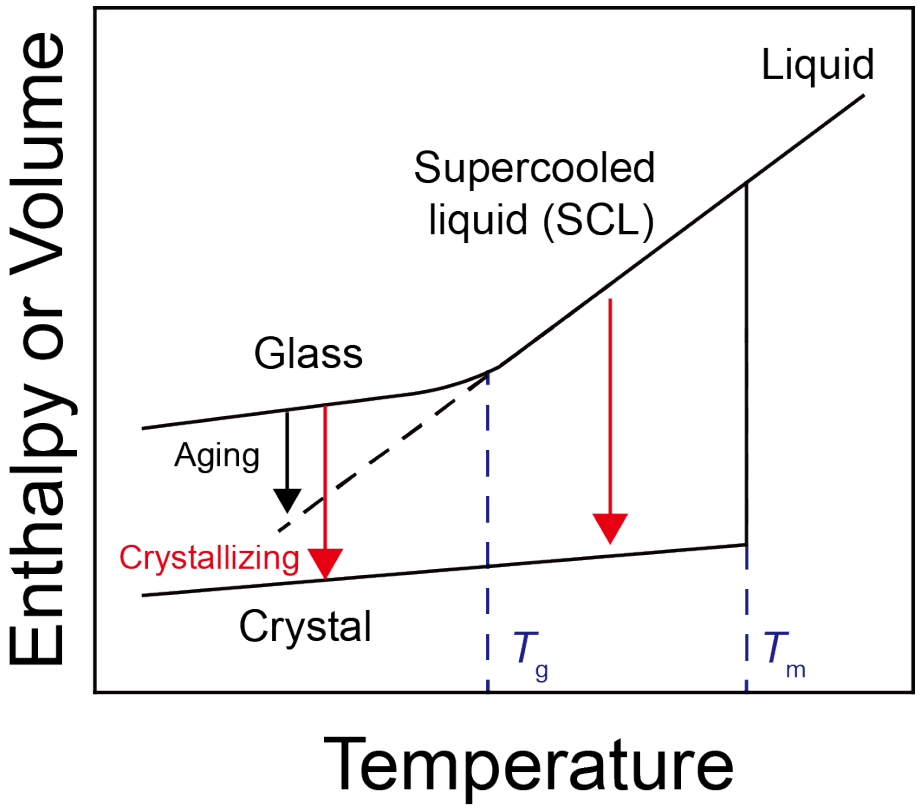

Figure 1 The enthalpy or specific volume of a crystal, a liquid or a glass as a function of temperature. Note that T_m and T_g represent the melting temperature and glass transition temperature, respectively.

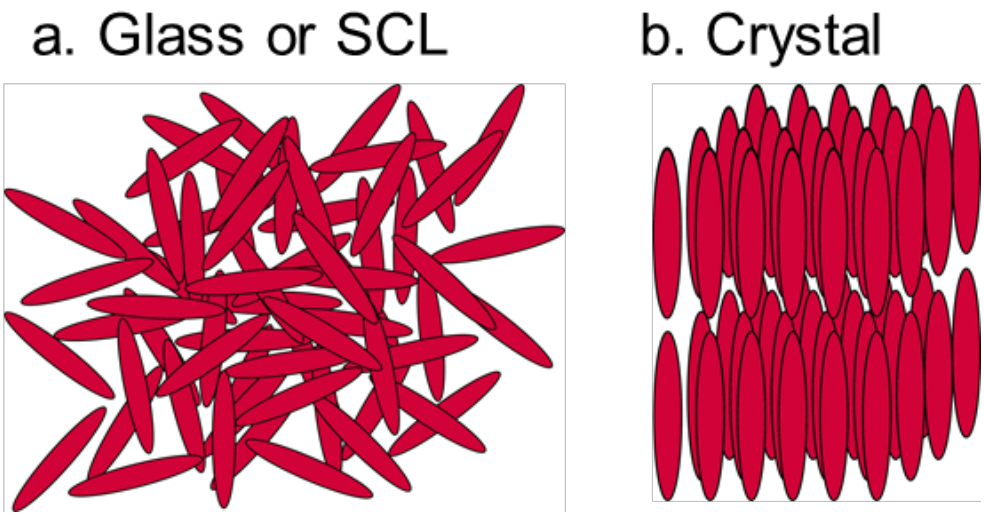

Figure 2 Schematic representation of the structures of a crystal and a glass, assuming a rod-like molecule. (a) Glass or SCL lacks long-range order, while (b) crystal has both short-range and long-range order.

1.2 Crystallization

Crystallization involves two elemental processes: nucleation and growth. When a critical nucleus forms and survives during the nucleation process, growth will occur and enlarge the nucleus to a macroscopic size. Nucleation and growth can have very different kinetics. The maximum rate of crystal nucleation is typically at a lower temperature relative to that of fastest crystal growth rate, which is shown in an example of lithium disilicate (Figure 3).[23,24] Therefore, such different kinetics makes it important to study crystal nucleation and growth as two independent processes.

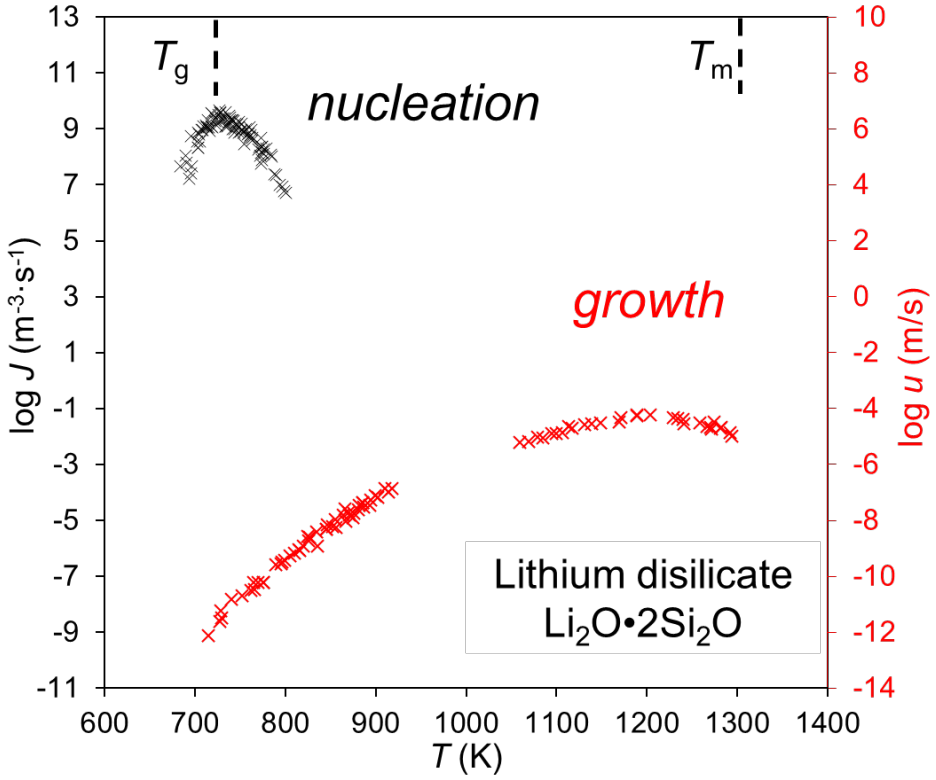

Figure 3. The rate of crystal nucleation *J* (ref. 23) and the rate of growth *u* (ref. 24) in amorphous lithium disilicate vs. temperature. Note that the rate of crystal nucleation reaches maximum at a lower temperature than that of crystal growth.

1.2.1 Crystal Nucleation

Being the first step of crystallization, nucleation determines whether crystallization is observed or not. The nucleation process has a strong impact on the microstructure of metals,[25,26] the formation of ice in the environment,[27] and the glass-forming ability of liquids.[23] However, the deep understanding on crystal nucleation is still lacking both in experimental data and theoretical models.

Experimentally, crystal nucleation can be categorized as homogeneous or heterogeneous nucleation. Homogeneous nucleation occurs without the aid of foreign surfaces, and is a stochastic process regardless of sample volume. Homogeneous nucleation rates have been reported for only a small number of systems: water[27], single-component metals,[25,26] and silicates,[23] while homogeneous nucleation in glass-forming molecular liquids have not been studied previously. In comparison, heterogeneous nucleation typically happens on active sites, like pre-existing interfaces and container surfaces. In this case, the rate of nucleation is expected to be fast at beginning but plateaus after exhaustion of preferred nucleation sites.

Theoretically, the classical nucleation theory (CNT), developed over a long history,[23] provides the basic understanding of crystal nucleation. According to the CNT, nucleation rate is given by

$$J = k_J \exp(-W_c/kT) \quad (1)$$

where $W_c = \frac{16\pi}{3}\frac{\sigma^3}{\Delta G_V^2}$ (thermodynamic factor) with σ being the crystal nucleus/liquid interfacial free energy and ΔG_v the free-energy difference between the crystal and the liquid, and k_J is a kinetic factor specifying the attempt frequency at which molecules join the nucleus. The thermodynamic term W_c in CNT describes the formation energy of crystal nucleus, which is the sum of the free energy to create the crystal nucleus/liquid interface (a positive term) and the volume-energy difference between the crystal and the liquid (a negative term). Assuming the shape of a critical

nucleus is spherical (radius, r), the interfacial surface energy ΔG_s can be described as $4\pi r^2\sigma$, while the volume-energy difference is represented by $4\pi r^3\Delta G_v/3$. In fact, crystal nuclei are metastable at small sizes, which is controlled by interfacial surface energy. With the fluctuational growth, the size of nuclei can reach the critical value ($r = r_{critical}$). Above $r_{critical}$, crystal growth is driven by the volume-energy difference (Figure 4).

At present, there are notable flaws in the CNT. In the thermodynamic factor W_c, the σ and volume-energy difference are typically taken as size-independent constants, while this assumption is questionable. In addition, independent measurements[28] or simulations[29,30] of σ value generally lack enough precision, while a small variation of it can change nucleation rate by many decades. This makes the CNT mostly a fitting model rather than predictive one. For kinetic factor k_J, the diffusion (or viscosity on basis of Stokes-Einstein relation) in the bulk liquid is usually assumed to describe kinetics of crystal nucleation. However, it is questionable that a bulk property can represent an interfacial property accurately and that Stokes-Einstein relation is valid at low temperatures (close to T_g).[12,13] Another approach to obtain k_J is to estimate the diffusivity using the lag time for nucleation, which also avoids the Stokes-Einstein relation. However, this approach requires an extraction of the lag time from the experimental induction time, while several factors should be carefully considered, for example the influence of thermal history from nuclei formation to detection as macroscopic crystals.[31]

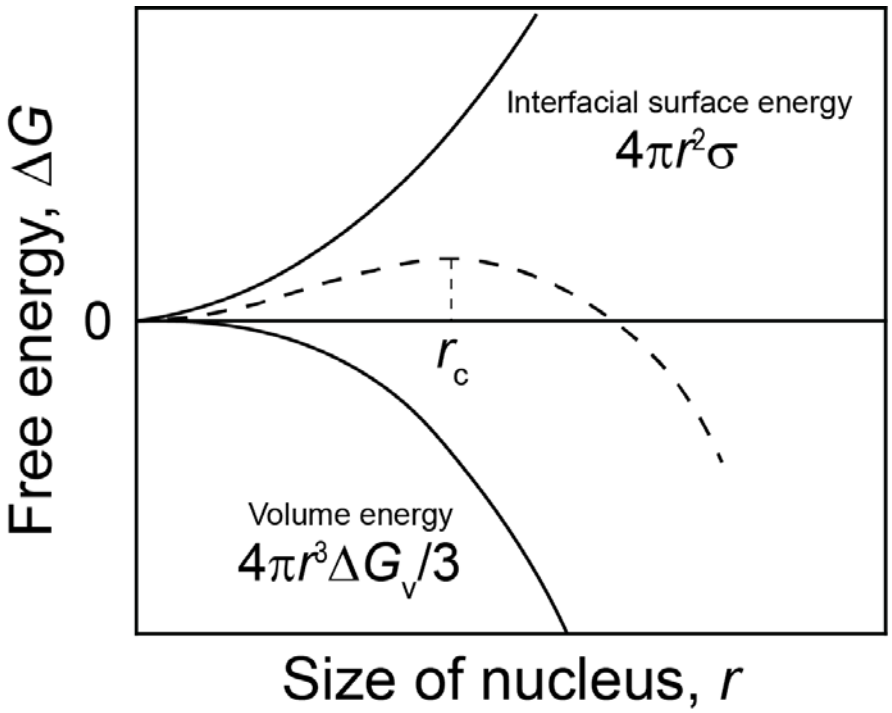

Figure 4. The interfacial surface energy and volume energy vs. size of crystal nucleus.

1.2.2 Crystal Growth

As a stable crystal nucleus ($r > r_{critical}$) forms, the nearby molecules in the liquid or glass can join the crystal front and the crystal subsequently grows. The crystal growth rate is usually measured by tracking the advance of a crystal front into the liquid or glass over time. The theory of crystal growth in a pure liquid began a century ago when Wilson[32] and Frenkel[33] proposed that the rate of crystal growth in a supercooled liquid is limited by the rate at which diffusion rearranges molecules. This model provides the reasonable description of crystal growth at temperatures above T_g, which is usually described as *diffusion-controlled crystal growth*. However, an anomalously fast crystal growth in *o*-terphenyl (OTP) was observed by Greet and Turnbull in 1967 near and below its T_g,[34] which does not follow the diffusion-controlled growth model and later termed the *glass-to-crystal* or *GC growth mode*.[35]

For the diffusion-controlled crystal growth, the rate in molecular liquids commonly increases and then decreases with supercooling, showing a "bell-like" pattern. When the temperature is close to melting point T_m, the thermodynamic driving force limits the rate of growth. At large supercooling, the growth rate is controlled by molecular mobility in the bulk liquid. The common explanation of crystal growth in molecular liquids is that diffusivity in liquid defines the kinetic barrier for crystal growth at large supercooling, *e.g. o*-terphenyl (OTP, Figure 5)[12,36] and α,α,β-tris-naphthyl benzene (TNB).[13,37] It is worth noting that viscosity is also utilized to represent liquid mobility. It has been demonstrated that crystal growth kinetics u is related to viscosity η by a power law of $u \sim \eta^{-\xi}$, with ξ value of approximately 0.75 for molecular liquids.[38] This is related to the decoupling between diffusion coefficient and viscosity at low temperatures.

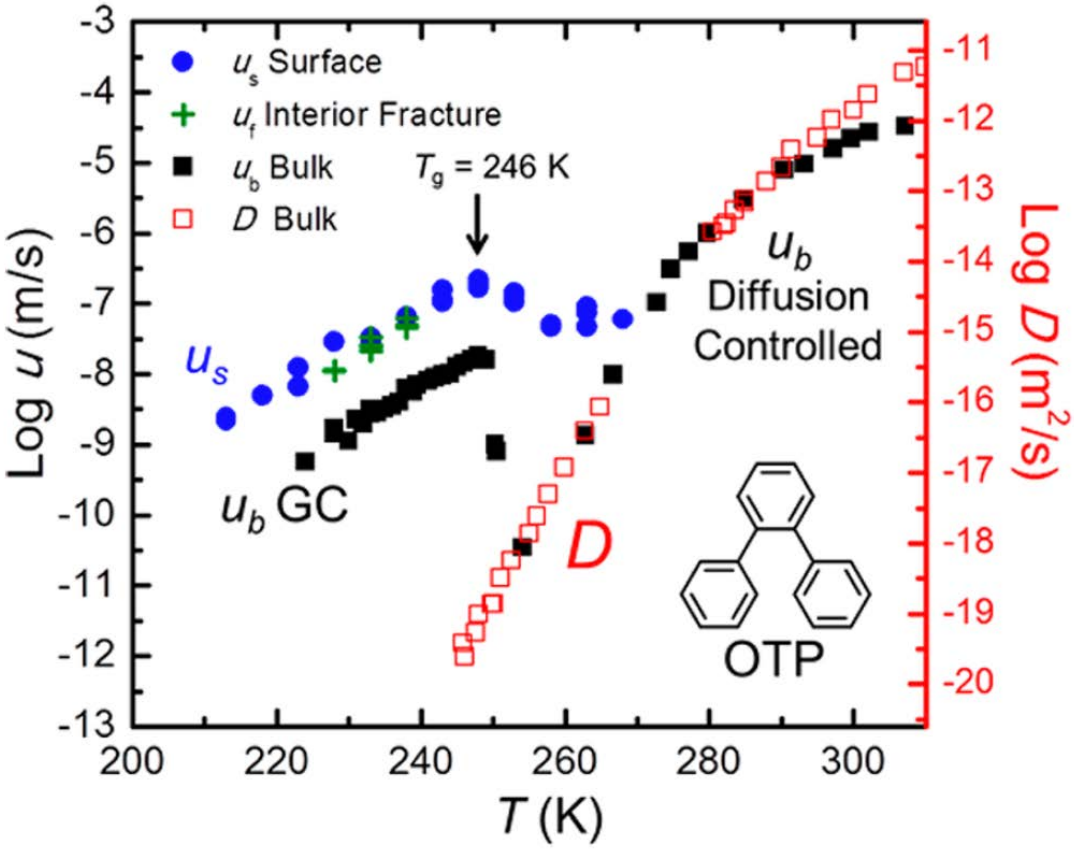

Figure 5. Crystal growth velocities in amorphous *o*-terphenyl (OTP) on a free surface u_s (blue circles, ref. 1), in the bulk u_b (black squares), and along cracks in the glass u_f (ref. 39). The bulk growth is diffusion-controlled at high temperatures (ref. 36) and escapes this control at low temperatures (GC mode; refs. 35 and 40). The second y-axis shows bulk diffusivity (open red squares, ref. 12). Reprinted with permission from Powell, C. T.; Xi, H.; Sun, Y.; Gunn, E.; Chen, Y.; Ediger, M. D.; Yu, L. *J. Phys. Chem. B* **2015,** *119*, 10124. Copyright 2015 American Chemical Society.

Based on understanding of diffusion-controlled growth model, crystal growth will be extremely slow when molecular liquids are supercooled near and below T_g. However, the crystal growth rate in some molecular glasses can exceed the Wilson-Frenkel limit by several orders of magnitude,[2,40,41,42] for example OTP in Figure 5. Among its several explanations,[39,40,42,43,44,45] Powell *et al.* proposed that GC growth involves crystallization-induced free surfaces by fracture and fast molecular motion on surfaces.[39] This hypothesis is based on that regardless of the density difference between crystal and glass, the conservation of overall volume is observed during crystallization. Free surfaces must be produced during the crystallization, which in turn accelerate molecular mobility (discussed later). This physical picture seems to be correct because the accelerated crystal growth has been observed along the artificially created cracks in molecular glasses.[39,46]

1.3 Surface-Enhanced Crystal Growth and Surface Mobility

A further discovery in this area occurred in the last decade is that the rate of crystal growth can be many decades faster on the free surface than in the interior. This surface-enhanced crystal growth has been reported in many organic molecules[1,2,4,47,48] and selenium.[49] One example is amorphous griseofulvin (GSF) shown in Figure 6, which compares the crystal growth rate on the surface and in the interior.[2] We can see that the surface crystal growth rate is faster than that in the interior over a wide temperature range (323 to 423 K); for example a factor of 10 is observed at T_g (361 K).

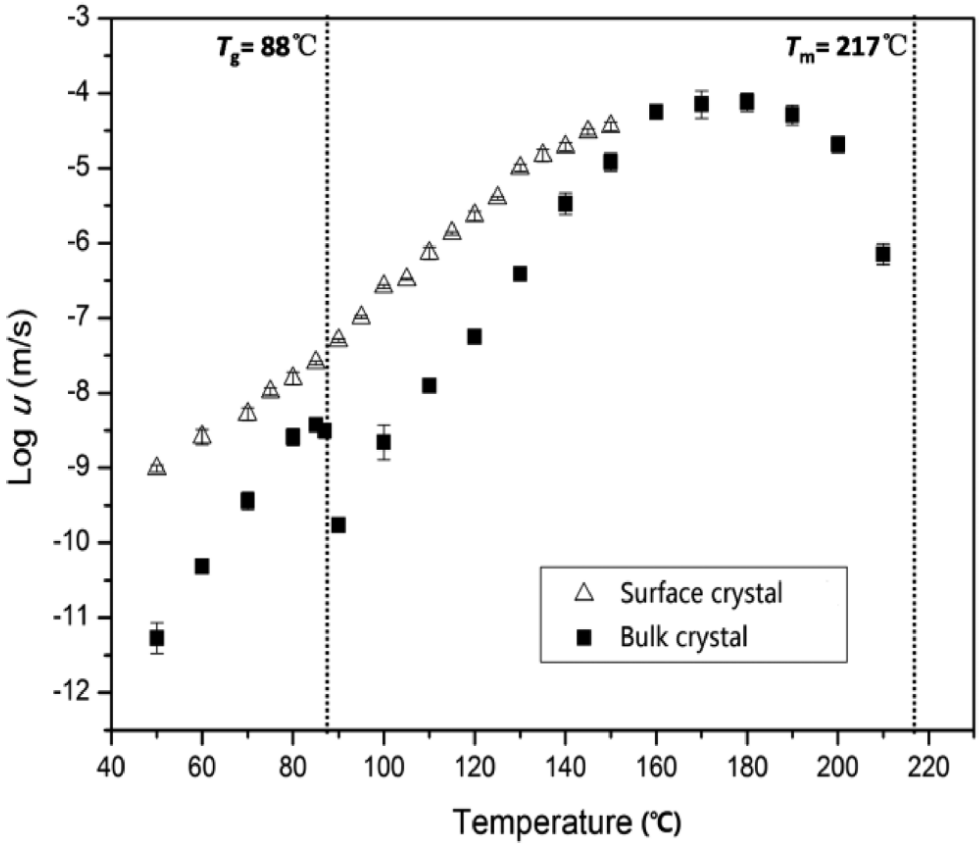

Figure 6. The crystal growth rate of griseofulvin (GSF) in the bulk and on the surface. Reprinted with permission from Shi, Q.; Cai, T. *Crystal Growth & Design* **2016,** *16*, 3279. Copyright 2016 American Chemical Society.

The most recent explanation for this surface-enhanced crystal growth is enhanced molecular mobility on free surfaces. This is supported by independent measurements of surface diffusion coefficients in amorphous materials, such as amorphous silicon [50] and molecular glasses.[48,51,52,53,54,55] Among these materials, the surface diffusion coefficients are determined using the method of surface-grating decay,[48,51,52,53,54] tracking the evolution of a stepped polymer film,[56] monitoring the evolution of a depletion zone near a surface crystal,[50,57] or following the response to particles placed on organic films.[55] For the grating decay method, Mullins[58,59] showed that the amplitude of a sinusoidal grating decays exponentially: $h = h_0 \exp(-Kt)$, and the decay constant is given by:

$$K = Fq + Aq^2 + Dq^3 + Bq^4 \qquad \text{where} \quad q = 2\pi/\lambda$$

$$F = \frac{\gamma}{2\eta}$$

$$A = \frac{p_0 \gamma \Omega^2}{(2\pi m)^{\frac{1}{2}}(kT)^{\frac{3}{2}}}$$

$$D = A' + C = \frac{\rho_0 D_G \gamma \Omega^2}{kT} + \frac{D_v \gamma \Omega}{kT}$$

$$B = \frac{D_s \gamma \Omega^2 \nu}{kT}$$

where λ is the grating wavelength; η is the viscosity; γ is the surface tension; p_0 is the equilibrium vapor pressure; Ω is the molecular volume; m is the molecular weight; k is the Boltzmann constant; T is the temperature; ρ_0 is the number density of vapor at equilibrium; D_G is the diffusion coefficient of the vapor molecules in the inert atmosphere; D_v is the bulk self-diffusion coefficient; ν is the number of molecules per unit area on surface. The four terms in Equation (1) correspond to different mechanisms of mass transport: viscous flow (F), evaporation-condensation ($A + A'$), bulk diffusion (C), and surface diffusion (B). In previous studies,[51,52,53] the grating decay process

can be tracked using the atomic force microscope (AFM) or laser diffraction for the determination of the decay constant. When the surface diffusion (*B* term) is the controlling mechanism, the corresponding surface diffusion coefficients, D_s, can be calculated based on the equations above.

The results in previous studies of organic glasses show that surface diffusion coefficients can vary significantly from one system to another. It turns out to be two leading molecular properties controlling this variation, which are molecular size and intermolecular hydrogen bonding. For hydrocarbons,[54] increasing the molecular size systematically slows down the surface diffusion when compared at T_g. Such effect can be attributed to a steep and similar mobility gradient beneath the surface of molecular glasses and the deeper penetration of a large molecule into the bulk where mobility is low. Meanwhile, at the similar molecular weight, intermolecular hydrogen bonding also slows down the surface diffusion.[60] One explanation is the persistence of hydrogen bonds as a molecule is moved from the bulk to the surface environment.

1.4 Polymer Effect on Crystallization

One important application of amorphous solids is for the delivery of poorly soluble drugs, since amorphous solids are generally more soluble than their crystalline counterparts. To take advantage of this high solubility, a key issue is to stabilize the amorphous solids during their shelf life. In context of inhibiting crystallization, one common strategy is addition of polymer additives, for example antifreeze proteins in arctic fish for inhibiting ice formation,[61,62] polymer additives for preventing crystallization of fuels and crude oils,[63,64] and polymer excipients for stabilizing amorphous drugs.[41,65,66,67,68,69,70] It is worth noting that at only 1 wt %, polyvinylpyrrolidone can slow crystal growth in glassy nifedipine by one decade at 12 K below T_g, suggesting the powerful effect of polymer additives on inhibition of crystallization in organic glasses.[67]

At present, it is unclear what is the mechanism of polymer's inhibition effect on crystal growth, and how to select appropriate polymer additives to meet the stabilization requirement of amorphous materials. Some propose that polymer's segmental mobility plays the controlling role, while others suggest the host-polymer interaction. Powell *et al.*[68] observed that a low-concentration polymer additive can either inhibit or accelerate the crystal growth in glassy nifedipine, and this effect has a strong correlation with the neat polymer's T_g. This suggests that the segmental mobility of polymer chain is the limiting step for crystallization of molecular glasses. Meanwhile, Mistry *et al.*[70] found that increasing the strength of ketoconazole-polymer interaction (ionic interaction > hydrogen bond > dipole-dipole interaction) can decrease the crystallization onset, which suggests the impact of host-polymer interaction.

While there are many studies of polymer effect on crystal growth, the understanding of polymer effect on crystal nucleation process is lacking. Some propose that polymer can serve as heterogeneous nucleation sites for the crystallization of small molecules,[71] but the polymer effect on homogeneous nucleation process is largely unknown.

1.5 Contribution of This Thesis

This thesis focuses on the physical stability of molecular glasses and amorphous solid dispersions against crystallization, involving nucleation and growth. It was found that the fast surface diffusion controls the fast crystal growth on free surfaces. Meanwhile, the rates of crystal nucleation in glass-forming molecular liquids are determined for the first time and discussed in the framework of the Classical Nucleation Theory (CNT), providing a fundamental understanding of crystallization in organics. The polymer effect on crystal growth and nucleation of small molecules

are further explored, guiding the selection of the appropriate polymer for stabilizing amorphous solids.

Chapter 2 will describe the correlation between the fast surface mobility and surface crystallization of amorphous griseofulvin, which is one of the fastest crystallization molecular glasses. we measured the surface diffusion in GSF using the method of surface grating decay. Surface diffusion in amorphous GSF is extremely fast, outpacing bulk diffusion by a factor of 10^8 at the glass transition temperature T_g (361 K). Among all molecular glasses studied (13 in all), GSF has the second fastest surface diffusion (to *o*-terphenyl) when compared at T_g. The GSF result fits the overall trend for molecular glasses without intermolecular hydrogen bonds, in which surface diffusion systematically slows down with increasing molecular size. This result is particularly noteworthy because GSF has many hydrogen-bond acceptors (ether and carbonyl) but no donors, indicating that so long as they do not participate in hydrogen bonding, the polar functional groups have a similar effect on surface diffusion as the non-polar hydrocarbon groups. In contrast, the formation of intermolecular hydrogen bonds strongly inhibits surface diffusion. The surface crystal growth rate of amorphous GSF is nearly proportional to its surface diffusion coefficient, as noted for other systems, supporting the view that surface crystal growth is controlled by surface diffusion. In addition, the fast surface diffusion of GSF glasses explains the fast crystal growth along fracture surfaces and provides a basis to understand fast crystal growth *in the bulk* through continuous creation of micro-cracks.

Chapter 3 will demonstrate the first ever measurements of crystal nucleation rates in glass-forming molecular liquids. We measured the rate of crystal nucleation rate in four glass-forming molecular liquids: D-sorbitol, D-arabitol, D-xylitol and glycerol. These polyalcohols have similar rates of crystal growth when compared at the same temperature relative to T_g (the glass transition

temperature), peaking near 1.4 T_g, while the nucleation rates J are vastly different. In D-sorbitol and D-arabitol, J reaches a maximum of ~ 10^8 $m^{-3}\cdot s^{-1}$ near 1.1 T_g, whereas $J < 10^{-2}$ $m^{-3}\cdot s^{-1}$ in D-xylitol and < 1 $m^{-3}\cdot s^{-1}$ in glycerol based on no nucleation in large samples after long waits. This confirms the fundamentally different mechanisms for nucleation and growth. Near T_g, both nucleation and growth slow down with a similar temperature dependence, suggesting a similar kinetic barrier for the two processes. This temperature dependence is significantly weaker than that of viscosity η, approximately following $\eta^{-0.75}$. This indicates that viscosity is a poor representative of the kinetic barrier for nucleation, and a better choice is the crystal growth rate. Under the latter assumption, the classical nucleation theory (CNT) describes our data reasonably well, yielding σ = 0.013 J/m^2 for D-sorbitol and 0.026 J/m^2 for D-arabitol, where σ is the critical nucleus/liquid interfacial free energy. There is no strong indication that the CNT fails as the length scale for corporative rearrangement exceeds the size of the critical nucleus, as recently suggested for lithium disilicate.

Chapter 4 will present the polymer effect on crystal growth is correlated with polymer segmental mobility relative to host dynamics. We measured the velocity of crystal growth in two molecular glasses, nifedipine (NIF) and *o*-terphenyl (OTP), each doped with 4 or 5 different polymers. For each polymer, the concentration was fixed at 1 wt % and a wide range of molecular weights was tested. We find that a polymer additive can strongly alter the rate of crystal growth, from a 10-fold reduction to a 10-fold increase. For a given polymer, increasing molecular weight slows down crystal growth and the effect saturates around DP = 100, where DP is the degree of polymerization. For all the systems studied, the polymer effect on crystal growth rate forms a master curve in the variable $(T_{g\ polymer} - T_{g\ host})/T_{cryst}$, where T_g is the glass transition temperature and T_{cryst} is the crystallization temperature. These results support the view that a polymer's effect on crystal

growth is controlled by its segmental mobility relative to the host-molecule dynamics. In the proposed model, crystal growth rejects impurities and creates local polymer-rich regions, which must be traversed by host molecules to sustain crystal growth at rates determined by polymer segmental mobility. Our results do not support the view that host-polymer hydrogen bonding plays a controlling role in crystal growth inhibition.

Chapter 5 will discuss the polymer effect on crystal nucleation in a glass-forming molecular liquid. We measured the crystal nucleation rate in liquid D-sorbitol in the presence of polyvinylpyrrolidone (PVP) of different concentrations and molecular weights, and compared with the rate of crystal growth measured under the same conditions. The presence of PVP can significantly reduce the rate of nucleation. At the temperatures studied (near the temperature of maximal nucleation rate in pure sorbitol), 10 wt % PVP can reduce the rate of nucleation by a factor of 40, and the effect increases with polymer concentration and with falling temperature. At a fixed polymer concentration (10 % wt), the polymer's inhibition effect becomes stronger with increasing molecular weight. Under the conditions of this study, the polymer additive shows a similar effect on the rate of crystal growth, suggesting a similar kinetic inhibition of nucleation and growth by the polymer. These results can be explained by the reduction of molecular mobility in the presence of the polymer. They do not support the view that polymer-host hydrogen bonding is the controlling factor since PVP of different molecular weights form the same number of hydrogen bonds per monomer but have very different effects on nucleation and growth at the same weight fraction.

Chapter 6 will demonstrate utilization of synchrotron total X-ray scattering to characterize the hydrogen bonds (HBs) in three polyalcohols in the crystalline state and the amorphous state (liquid or glass). For each system, the atomic pair distribution function (PDF) shows a well-resolved peak

at 2.7 Å after removing intramolecular contributions. This peak corresponds to the O…O distance in an intermolecular HB. We find that the O…O bond length does not change significantly from the crystal to the liquid or glass, while the O…O coordination number (the number of HBs formed by each OH group) is ~10% lower in the amorphous phase. The distribution of the O…O distance is slightly narrower in the amorphous phase than in the crystal, perhaps a result of many distinct O…O distances in a crystal (static disorder) in order to achieve regular 3D packing. Furthermore, the O…O distance obtained from total is systematically shorter that that found in single-crystal structures (by ~0.03 Å). This might result from the fact that single-crystal diffraction yields mean atomic positions, whereas total scattering yields correlations between atomic pairs.

1.6 References

[1] Yu, L. Amorphous pharmaceutical solids: preparation, characterization and stabilization. *Adv. Drug Deliv. Rev.* **2001,** *48*, 27-42.

[2] Crowe, J. H.; Carpenter, J. F.; Crowe, L. M. The role of vitrification in anhydrobiosis. *Annu. Rev. Physiol.* **1998,** *60*, 73-103.

[3] Shirota, Y. Photo- and electroactive amorphous molecular materials - molecular design, syntheses, reactions, properties, and applications. *J. Mater. Chem.* **2005,** *15*, 75-93.

[4] Hasebe, M.; Musumeci, D.; Powell, C. T.; Cai, T.; Gunn, E.; Zhu, L.; Yu, L. Fast surface crystal growth on molecular glasses and its termination by the onset of fluidity. *J. Phys. Chem. B* **2014,** *118*, 7638-7646.

[5] Shi, Q.; Cai, T. Fast crystal growth of amorphous griseofulvin: relations between bulk and surface growth modes. *Crystal Growth & Design* **2016,** *16*, 3279-3286.

[6] Sun, Y.; Zhu, L.; Kearns, K. L.; Ediger, M. D.; Yu, L. A. Glasses crystallize rapidly at free surfaces by growing crystals upward. *Proc. Natl. Acad. Sci. U. S. A.* **2011,** *108*, 5990-5995.

[7] Wu, T.; Yu, L. Surface crystallization of indomethacin below Tg. *Pharmaceutical Research* **2006,** *23*, 2350-2355.

[8] Wu, T.; Yu, L., Origin of Enhanced Crystal Growth Kinetics near Tg Probed with Indomethacin Polymorphs. *The Journal of Physical Chemistry B* **2006,** *110* (32), 15694-15699.

[9] Menon, N.; O'Brien, K. P.; Dixon, P. K.; Wu, L.; Nagel, S. R.; Williams, B. D.; Carini, J. P., Wide-frequency dielectric susceptibility measurements in glycerol. *Journal of Non-Crystalline Solids* **1992,** *141* (Supplement C), 61-65.

[10] Wagner, H.; Richert, R., Equilibrium and Non-Equilibrium Type β-Relaxations: d-Sorbitol versus o-Terphenyl. *The Journal of Physical Chemistry B* **1999,** *103* (20), 4071-4077.

[11] Angell, C. A. Formation of glasses from liquids and biopolymers. *Science* **1995,** *267*, 1924-1935

[12] Mapes, M. K.; Swallen, S. F.; Ediger, M. D. Self-diffusion of supercooled o-terphenyl near the glass transition temperature. *The Journal of Physical Chemistry B* **2006,** *110*, 507-511.

[13] Swallen, S. F.; Traynor, K.; McMahon, R. J.; Ediger, M. D.; Mates, T. E. Self-diffusion of supercooled tris-naphthylbenzene. *The Journal of Physical Chemistry B* **2009,** *113*, 4600-4608.

[14] Urakawa, O.; Swallen, S. F.; Ediger, M. D.; von Meerwall, E. D. Self-diffusion and viscosity of low molecular weight polystyrene over a wide temperature range. *Macromolecules* **2004,** *37*, 1558-1564.

[15] Lipinski, C. A.; Lombardo, F.; Dominy, B. W.; Feeney, P. J., Experimental and computational approaches to estimate solubility and permeability in drug discovery and development settings. *Adv. Drug Deliv. Rev.* **1997,** *23* (1), 3-25.

[16] Lipinski, C. A., Drug-like properties and the causes of poor solubility and poor permeability. *Journal of Pharmacological and Toxicological Methods* **2000,** *44* (1), 235-249.

[17] Mishima, O.; Calvert, L. D.; Whalley, E., 'Melting ice' I at 77 K and 10 kbar: a new method of making amorphous solids. *Nature* **1984,** *310* (5976), 393-395.

[18] Mishima, O.; Suzuki, Y., Propagation of the polyamorphic transition of ice and the liquid–liquid critical point. *Nature* **2002,** *419*, 599.

[19] Ha, A.; Cohen, I.; Zhao, X.; Lee, M.; Kivelson, D., Supercooled Liquids and Polyamorphism. *The Journal of Physical Chemistry* **1996,** *100* (1), 1-4.

[20] Kobayashi, M.; Tanaka, H., The reversibility and first-order nature of liquid–liquid transition in a molecular liquid. *Nature Communications* **2016,** *7*, 13438.

[21] Zhu, M.; Wang, J.-Q.; Perepezko, J. H.; Yu, L., Possible existence of two amorphous phases of d-mannitol related by a first-order transition. *The Journal of Chemical Physics* **2015,** *142* (24), 244504.

[22] Zhu, M.; Yu, L., Polyamorphism of D-mannitol. *The Journal of Chemical Physics* **2017,** *146* (24), 244503.

[23] Fokin, V. M.; Zanotto, E. D.; Yuritsyn, N. S.; Schmelzer, J. W. P., Homogeneous crystal nucleation in silicate glasses: A 40 years perspective. *Journal of Non-Crystalline Solids* **2006,** *352* (26–27), 2681-2714.

[24] Nascimento, M. L. F.; Zanotto, E. D., Does viscosity describe the kinetic barrier for crystal growth from the liquidus to the glass transition? *The Journal of Chemical Physics* **2010,** *133* (17), 174701.

[25] Turnbull, D., Kinetics of Solidification of Supercooled Liquid Mercury Droplets. *The Journal of Chemical Physics* **1952,** *20* (3), 411-424.

[26] Bokeloh, J.; Rozas, R. E.; Horbach, J.; Wilde, G., Nucleation Barriers for the Liquid-To-Crystal Transition in Ni: Experiment and Simulation. *Physical Review Letters* **2011,** *107* (14), 145701.

[27] Laksmono, H.; McQueen, T. A.; Sellberg, J. A.; Loh, N. D.; Huang, C.; Schlesinger, D.; Sierra, R. G.; Hampton, C. Y.; Nordlund, D.; Beye, M.; Martin, A. V.; Barty, A.; Seibert, M. M.; Messerschmidt, M.; Williams, G. J.; Boutet, S.; Amann-Winkel, K.; Loerting, T.; Pettersson, L. G. M.; Bogan, M. J.; Nilsson, A., Anomalous Behavior of the Homogeneous Ice Nucleation Rate in "No-Man's Land". *The Journal of Physical Chemistry Letters* **2015,** *6* (14), 2826-2832.

[28] Jackson, C. L.; McKenna, G. B., The melting behavior of organic materials confined in porous solids. *The Journal of Chemical Physics* **1990,** *93* (12), 9002-9011.

[29] Laird, B. B.; Davidchack, R. L., Direct Calculation of the Crystal−Melt Interfacial Free Energy via Molecular Dynamics Computer Simulation. *The Journal of Physical Chemistry B* **2005,** *109* (38), 17802-17812.

[30] Gerges, J.; Affouard, F., Predictive Calculation of the Crystallization Tendency of Model Pharmaceuticals in the Supercooled State from Molecular Dynamics Simulations. *The Journal of Physical Chemistry B* **2015,** *119* (33), 10768-10783.

[31] Deubener, J.; Montazerian, M.; Krüger, S.; Peitl, O.; Zanotto, E. D., Heating rate effects in time-dependent homogeneous nucleation in glasses. *Journal of Non-Crystalline Solids* **2017,** *474*, 1-8.

[32] Wilson, H. W. On the velocity of solidification and viscosity of super-cooled liquids. *Philosophical Magazine* **1900,** *50*, 238-250.

[33] Frenkel, J. Note on a relation between the speed of crystallization and viscosity, *Physikalische Zeitschrift der Sowjetunion*, **1932**, *1*, 498-500.

[34] Greet, R. J.; Turnbull, D. Glass transition in *o*-terphenyl. *The Journal of Chemical Physics* **1967,** *46*, 1243-1251.

[35] Xi, H.; Sun, Y.; Yu, L., Diffusion-controlled and diffusionless crystal growth in liquid o-terphenyl near its glass transition temperature. *The Journal of Chemical Physics* **2009,** *130* (9), 094508.

[36] Magill, J. H.; Li, H.-M., Physical properties of aromatic hydrocarbons: V. The solidification behavior of 1:2 diphenylbenzene. *J. Cryst. Growth* **1973,** *20* (2), 135-144.

[37] Magill, J. H.; Plazek, D. J., Physical Properties of Aromatic Hydrocarbons. II. Solidification Behavior of 1,3,5-Tri-α-Naphthylbenzene. *The Journal of Chemical Physics* **1967,** *46* (10), 3757-3769.

[38] Ediger, M. D.; Harrowell, P.; Yu, L., Crystal growth kinetics exhibit a fragility-dependent decoupling from viscosity. *The Journal of Chemical Physics* **2008,** *128* (3), 034709.

[39] Powell, C. T.; Xi, H.; Sun, Y.; Gunn, E.; Chen, Y.; Ediger, M. D.; Yu, L. Fast crystal growth in *o*-terphenyl glasses: a possible role for fracture and surface mobility. *The Journal of Physical Chemistry B* **2015,** *119*, 10124-10130.

[40] Hikima, T.; Adachi, Y.; Hanaya, M.; Oguni, M., Determination of potentially homogeneous-nucleation-based crystallization in o-terphernyl and an interpretation of the nucleation-enhancement mechanism. *Phys. Rev. B* **1995,** *52* (6), 3900-3908.

[41] Ishida, H.; Wu, T. A.; Yu, L. A. Sudden rise of crystal growth rate of nifedipine near Tg without and with polyvinylpyrrolidone. *Journal of Pharmaceutical Sciences* **2007,** *96*, 1131-1138.

[42] Sun, Y.; Xi, H. M.; Chen, S.; Ediger, M. D.; Yu, L. Crystallization near glass transition: transition from diffusion-controlled to diffusionless crystal growth studied with seven polymorphs. *J. Phys. Chem. B* **2008,** *112*, 5594-5601

[43] Konishi, T.; Tanaka, H. Possible origin of enhanced crystal growth in a glass. *Phys. Rev. B* **2007,** *76*, 220201.

[44] Stevenson, J. D.; Wolynes, P. G. The ultimate fate of supercooled liquids. *The Journal of Physical Chemistry A* **2011,** *115*, 3713-3719.

[45] Caroli, C.; Lemaître, A. Ultrafast spherulitic crystal growth as a stress-induced phenomenon specific of fragile glass-formers. *The Journal of Chemical Physics* **2012,** *137*, 114506.

46 Zhu, L.; Jona, J.; Nagapudi, K.; Wu, T. Fast surface crystallization of amorphous griseofulvin below Tg. *Pharmaceutical Research* **2010,** *27*, 1558-1567.

[47] Zhu, L.; Wong, L.; Yu, L., Surface-Enhanced Crystallization of Amorphous Nifedipine. *Molecular pharmaceutics* **2008,** *5* (6), 921-926.

[48] Ruan, S.; Zhang, W.; Sun, Y.; Ediger, M. D.; Yu, L., Surface diffusion and surface crystal growth of tris-naphthyl benzene glasses. *The Journal of Chemical Physics* **2016,** *145* (6), 064503.

[49] Barták, J.; Valdés, D.; Málek, J.; Podzemná, V.; Slang, S.; Pálka, K., Comparison of Lateral Crystal Growth in Selenium Thin Films and Surface of Bulk Samples. *Crystal Growth & Design* **2018,** *18* (7), 4103-4110.

[50] Sallese, J. M.; Ils, A.; Bouvet, D.; Fazan, P.; Merritt, C. Modeling of the depletion of the amorphous-silicon surface during hemispherical grained silicon formation. *J. Appl. Phys.* **2000,** *88*, 5751-5755.

[51] Zhu, L.; Brian, C. W.; Swallen, S. F.; Straus, P. T.; Ediger, M. D.; Yu, L. Surface self-diffusion of an organic glass. *Physical Review Letters* **2011,** *106*, 256103.

[52] Brian, C. W.; Yu, L. Surface self-diffusion of organic glasses. *The Journal of Physical Chemistry A* **2013,** *117*, 13303-13309.

[53] Zhang, W.; Brian, C. W.; Yu, L. Fast surface diffusion of amorphous *o*-terphenyl and its competition with viscous flow in surface evolution. *The Journal of Physical Chemistry B* **2015,** *119*, 5071-5078.

[54] Zhang, W.; Yu, L. Surface diffusion of polymer glasses. *Macromolecules* **2016,** *49*, 731-735.

[55] Zhang, Y.; Potter, R.; Zhang, W.; Fakhraai, Z. Using tobacco mosaic virus to probe enhanced surface diffusion of molecular glasses. *Soft Matter* **2016,** *12*, 9115-9120.

[56] Chai, Y.; Salez, T.; McGraw, J. D.; Benzaquen, M.; Dalnoki-Veress, K.; Raphaël, E.; Forrest, J. A. A direct quantitative measure of surface mobility in a glassy polymer. *Science* **2014,** *343*, 994-999.

[57] Hasebe, M.; Musumeci, D.; Yu, L., Fast Surface Crystallization of Molecular Glasses: Creation of Depletion Zones by Surface Diffusion and Crystallization Flux. *The Journal of Physical Chemistry B* **2015,** *119* (7), 3304-3311.

[58] Mullins, W. W. Theory of thermal grooving. *J. Appl. Phys.* **1957,** *28*, 333-339.

[59] Mullins, W. W. Flattening of a nearly plane solid surface due to capillarity. *J. Appl. Phys.* **1959,** *30*, 77-83.

[60] Chen, Y.; Zhang, W.; Yu, L. Hydrogen bonding slows down surface diffusion of molecular glasses. *The Journal of Physical Chemistry B* **2016,** *120*, 8007-8015.

[61] Knight, C. A.; Cheng, C. C.; Devries, A. L., Adsorption of alpha-helical antifreeze peptides on specific ice crystal-surface planes. *Biophys. J.* **1991,** *59* (2), 409-418.

[62] Sicheri, F.; Yang, D. S. C., Ice-binding structure and mechanism of an antifreeze protein from winter flounder. *Nature* **1995,** *375* (6530), 427-431.

[63] Hutter, J. L.; Hudson, S.; Smith, C.; Tetervak, A.; Zhang, J. H., Banded crystallization of tricosane in the presence of kinetic inhibitors during directional solidification. *J. Cryst. Growth* **2004,** *273* (1-2), 292-302.

[64] Tinsley, J. F.; Prud'homme, R. K.; Guo, X. H.; Adamson, D. H.; Callahan, S.; Amin, D.; Shao, S.; Kriegel, R. M.; Saini, R., Novel laboratory cell for fundamental studies of the effect of polymer additives on wax deposition from model crude oils. *Energy Fuels* **2007,** *21* (3), 1301-1308.

[65] Kestur, U. S.; Lee, H.; Santiago, D.; Rinaldi, C.; Won, Y. Y.; Taylor, L. S. Effects of the molecular weight and concentration of polymer additives, and temperature on the melt crystallization kinetics of a small drug molecule. *Crystal Growth & Design* **2010,** *10*, 3585-3595.

[66] Kestur, U. S.; Taylor, L. S. Role of polymer chemistry in influencing crystal growth rates from amorphous felodipine. *CrystEngComm* **2010,** *12*, 2390-2397.

[67] Cai, T.; Zhu, L.; Yu, L. Crystallization of organic glasses: effects of polymer additives on bulk and surface crystal growth in amorphous nifedipine. *Pharmaceutical Research* **2011,** *28*, 2458-2466.

[68] Powell, C. T.; Cai, T.; Hasebe, M.; Gunn, E. M.; Gao, P.; Zhang, G.; Gong, Y. C.; Yu, L. Low-concentration polymers inhibit and accelerate crystal growth in organic glasses in correlation with segmental mobility. *J. Phys. Chem. B* **2013,** *117*, 10334-10341.

[69] Kothari, K.; Ragoonanan, V.; Suryanarayanan, R. The role of drug–polymer hydrogen bonding interactions on the molecular mobility and physical stability of nifedipine solid dispersions. *Molecular pharmaceutics* **2015,** *12*, 162-170.

[70] Mistry, P.; Mohapatra, S.; Gopinath, T.; Vogt, F. G.; Suryanarayanan, R., Role of the Strength of Drug–Polymer Interactions on the Molecular Mobility and Crystallization Inhibition in Ketoconazole Solid Dispersions. *Molecular pharmaceutics* **2015,** *12* (9), 3339-3350.

[71] Lang, M.; Grzesiak, A. L.; Matzger, A. J., The Use of Polymer Heteronuclei for Crystalline Polymorph Selection. *J. Am. Chem. Soc.* **2002,** *124* (50), 14834-14835.

Chapter 2. Fast Surface Diffusion and Crystallization of Amorphous Griseofulvin

As published in ***The Journal of Physical Chemistry B***

2017, vol. 121 (40), page 9463–9468

Chengbin Huang [1], Shigang Ruan [2], Ting Cai [3], Lian Yu [1,2,*]

[1] School of Pharmacy, University of Wisconsin-Madison, Madison, Wisconsin 53705, United States.

[2] Department of Chemistry, University of Wisconsin-Madison, Madison, Wisconsin 53705, United States.

[3] State Key Laboratory of Natural Medicines, Jiangsu Key Laboratory of Drug Discovery for Metabolic Diseases, Department of Pharmaceutics, College of Pharmacy, China Pharmaceutical University, Nanjing 210009, China

2.1 Abstract

Among molecular glasses, griseofulvin (GSF) is one of the fastest crystallizing. To understand this property, we have measured the surface diffusion in GSF using the method of surface grating decay. Surface diffusion in amorphous GSF is extremely fast, outpacing bulk diffusion by a factor of 10^8 at the glass transition temperature T_g (361 K). Among all molecular glasses studied (13 in all), GSF has the second fastest surface diffusion (to *o*-terphenyl) when compared at T_g. The GSF result fits the overall trend for molecular glasses without intermolecular hydrogen bonds, where surface diffusion systematically slows down with increasing molecular size. This result is particularly noteworthy because GSF has many hydrogen-bond acceptors but no donors, indicating that so long as they do not participate in hydrogen bonding, the polar functional groups have a similar effect on surface diffusion as the non-polar hydrocarbon groups. In contrast, the formation of intermolecular hydrogen bonds strongly inhibits surface diffusion. The surface crystal growth rate of amorphous GSF is nearly proportional to its surface diffusion coefficient, as noted for other systems, supporting the view that surface crystal growth is controlled by surface diffusion. In addition, the fast surface diffusion of GSF glasses explains the fast crystal growth along fracture surfaces and suggests a basis to understand fast crystal growth *in the bulk* through continuous creation of micro-cracks.

2.2 Introduction

Crystal growth in supercooled liquids and glasses is an important problem in many areas of science and technology. Work on this problem began at least a century ago, when it was proposed that the velocity of crystal growth in a supercooled liquid is limited by the rate at which diffusion (or viscous flow) rearranges molecules.[1,2] This Wilson-Frenkel model has proved reasonably

accurate in describing crystal growth in many glass-forming liquids above the glass transition temperature T_g. In 1967, however, Greet and Turnbull briefly reported the "anomalously rapid" crystal growth in the molecular liquid *o*-terphenyl (OTP) near and below its T_g,[3] with its velocity exceeding the Wilson-Frenkel limit by 4 orders of magnitude. This fast mode of crystal growth (later termed the glass-to-crystal or GC growth mode) is now known for many molecular liquids and has received many explanations.[4,5,6,7,8,9,10] It is noteworthy that GC growth occurs in the *interior* of a molecular glass. A further progress in this area was the discovery that the velocity of crystal growth can be even faster at the *free surface* of a molecular glass than in its interior.[11,12,13] This suggests that surface molecules are highly mobile and able to crystallize even when bulk mobility is low. This notion gained support from independently measured surface diffusion coefficients,[14,15,16,17,18,19] indicating that surface diffusion can be 8 orders of magnitude faster than bulk diffusion when compared at T_g. It was also established that the growth velocity of surface crystals is approximately proportional to the surface diffusion coefficient,[15,16] further confirming the relation between the two processes. In 2016, on the basis of this result, Powell *et al.*[10] proposed a new explanation for the now 50-year-old puzzle of GC growth. They argued that despite being a bulk process, GC growth is fundamentally linked to surface mobility because the crystal growth process continuously creates voids and free surfaces (a consequence of the higher density of the crystal than the glass), which in turn accelerates local transformation through high surface mobility.

The purpose of this work is to further evaluate the current understanding of crystallization in molecular glasses using griseofulvin (GSF, see Scheme 1) as a model system. GSF is an antifungal drug and a well-studied glass-forming molecular liquid.[20,21,22,23] The glass of GSF shows remarkably fast crystal growth on the free surface;[20,21] its velocity is the second fastest on record

(to OTP). This property suggests very fast surface diffusion in GSF, a hypothesis to be tested in this study. In this context, another intriguing property of GSF is that its crystallization process causes a large increase of density by 8 %;[20] this value is larger than the values reported for any other molecular glasses (5 % or less).[3,7,20] It suggests that the crystallization process can create a large amount of void space and free surfaces, which in turn accelerate local transformation. Indeed, fast crystal growth has been observed not only on the free surface of a GSF glass but also in its interior (GC growth).[21] It is noteworthy that crystal growth in a GSF glass is greatly accelerated along fracture surfaces,[20] suggesting a growth mechanism involving microcracks and surface mobility.

We expect GSF to play an important role in understanding the *molecular dependence* of surface diffusion in molecular glasses. Previous work[17,24] has shown that the rate of surface diffusion can vary significantly from one system to another, with two leading factors controlling the variation being the molecular size and intermolecular hydrogen bonding. For example, for a series of aromatic hydrocarbons – OTP,[15] α,α,β-tris-naphthyl benzene (TNB),[16] and polystyrene (PS) oligomers[17] (see Scheme 1), surface diffusion systematically slows down with increasing molecular size when compared at T_g. Meanwhile, for molecules of similar sizes, introducing intermolecular hydrogen bonds also slows down surface diffusion; this trend is evident by comparing OTP and TNB (no hydrogen bonds) with nifedipine (NIF),[18] indomethacin (IMC),[14] and the triazines[19] (limited hydrogen bonds) and with poly-alcohols (extensive hydrogen bonds)[24]. In this context, GSF provides a valuable new system. Similar to the simple aromatic hydrocarbons, GSF forms no hydrogen bonds (it has only acceptors but no donors); but unlike these previous molecules, GSF has many polar groups (ether and carbonyl). Is the surface diffusion of

GSF fast like that of OTP and TNB, or slow like that of the polyalcohols? Answering this question will sharpen the understanding of the molecular factors controlling surface mobility.

We report that the surface diffusion of a GSF glass is extremely fast, outpacing bulk diffusion by approximately a factor of 10^8 at T_g. Among all molecular glasses studied to date, GSF has the second fast surface diffusion (to OTP). The fast surface diffusion of GSF is consistent with its fast surface crystal growth. The correlation plot between surface crystal growth and surface diffusion is approximately linear, indicating a fundamental relation between the processes. Despite its abundant polar functional groups, GSF has a similar rate of surface diffusion as a simple aromatic hydrocarbon of similar size (OTP and TNB). This indicates that as long as they are not engaged in hydrogen bonds, polar functional groups have no more influence on surface diffusion than the hydrocarbon groups, whereas the formation of intermolecular hydrogen bonds has a strong inhibitory effect on surface diffusion.

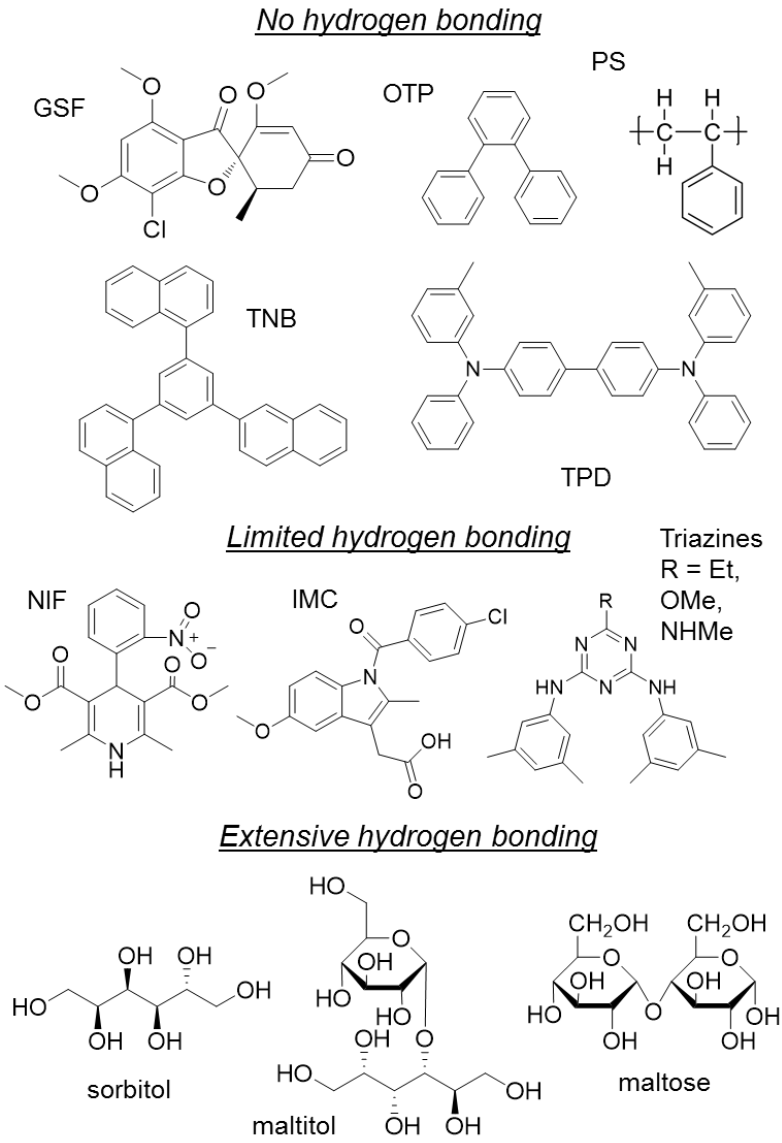

Scheme 1. Structures of griseofulvin (GSF) and other molecules discussed in this work. OTP: *ortho*-terphenyl; TNB: *tris*-naphthyl benzene; TPD: *N*, *N'* -Bis(3-methylphenyl)-*N*, *N'* –diphenylbenzidine; PS: polystyrene; NIF: nifedipine; IMC: indomethacin; Et/OMe/NHMe triazines: bis(3,5-dimethyl-phenylamino)-1,3,5-triazine with different functional groups R (Et, OMe, and NHMe).

2.3 Experimental Section

Griseofulvin (GSF, purity > 99%) was obtained from J&K Scientific Co. Ltd. and used as received. To prepared a GSF glass with a surface grating, a supercooled liquid on a round silicate coverslip (diameter = 12 mm) was covered by a master grating at 408 K and was cooled to 353 K (T_g – 8 K), at which the master was detached to yield a GSF glass film with a corrugated surface. Notice that cooling to much lower temperature caused fracture of the GSF glass owing to the stress created by the coverslip's smaller thermal expansion coefficient than GSF's. The master gratings were purchased from Rainbow Symphony (wavelength λ = 1000 and 2000 nm), separated from commercial data-storage discs (1500 nm for CD and 730 nm for DVD), or duplicated from glass gratings purchased from Spectrum Scientific (550, 3300 and 8200 nm) through a UV-curing polymer (Norland Optical Adhesive 61). All masters were gold-coated to minimize the transfer of contaminants. The surface profiles of all master gratings were sinusoidal except for those of wavelength 3300 and 8200 nm, which had a sawtooth profile. We emphasize that the thickness of each embossed GSF glass film was *ca.* 40 μm and much greater than the wavelength of the surface grating, ensuring that the substrate had no effect on surface evolution.

The decay process of a surface grating was monitored by atomic force microscopy (AFM, Bruker Veeco Mutiple Mode IV) or laser diffraction. AFM was performed in the tapping mode at room temperature; the height profile was Fourier transformed to obtain the amplitude of the sinusoidal surface or in the case of a sawtooth profile, that of the first harmonic. In a diffraction measurement, a HeNe laser (λ = 632.8 nm, Uniphase Corp.) passed through the GSF film and the intensity of the first-order diffraction was recorded with a Si-amplified photodetector (Thorlabs) interfacing with a National Instruments LabVIEW program. The square root of the first-order diffraction intensity was shown to be proportional to the grating amplitude. The two methods yielded consistent results

at the same temperatures where both were applied. For both methods, temperature was controlled with a Linkam THMS 600 hot stage purged with dry N_2.

2.4 Results

Figure 1 shows the typical decay kinetics of GSF surface gratings recorded by AFM (Figure 1a) and laser diffraction (Figure 1b). AFM directly yielded the grating amplitude h; the laser diffraction experiment yielded the first-order diffraction intensity I, which is proportional to h^2. The decrease of h over time t is exponential, $\phi = \exp(-Kt)$, where ϕ is h/h_0 and K is the decay constant, or stretched-exponential, $\phi = \exp[-(Kt)^{\beta}]$, with β close to 1.

Figure 2a shows the temperature dependence of the decay constant K at λ = 1000 nm. To expand the temperature range, the K value at the highest temperature (388 K) was calculated from the decay rate of a longer wavelength grating (λ = 8200 nm), based on the wavelength dependence of K (discussed below). In total, the measured decay rates cover five orders of magnitude.

We also measured the wavelength dependence of K at different temperatures. Figure 2b shows the results at 383 K and 333 K. At 383 K (T_g + 22 K), the decay constant, K, is proportional to λ^{-1}; at 333 K (T_g - 28 K), we find $K \propto \lambda^{-4}$. These wavelength dependences of K indicate that the surface decay at 383 K occurs by viscous flow, while the process at 333 K is by surface diffusion, as we explain below.

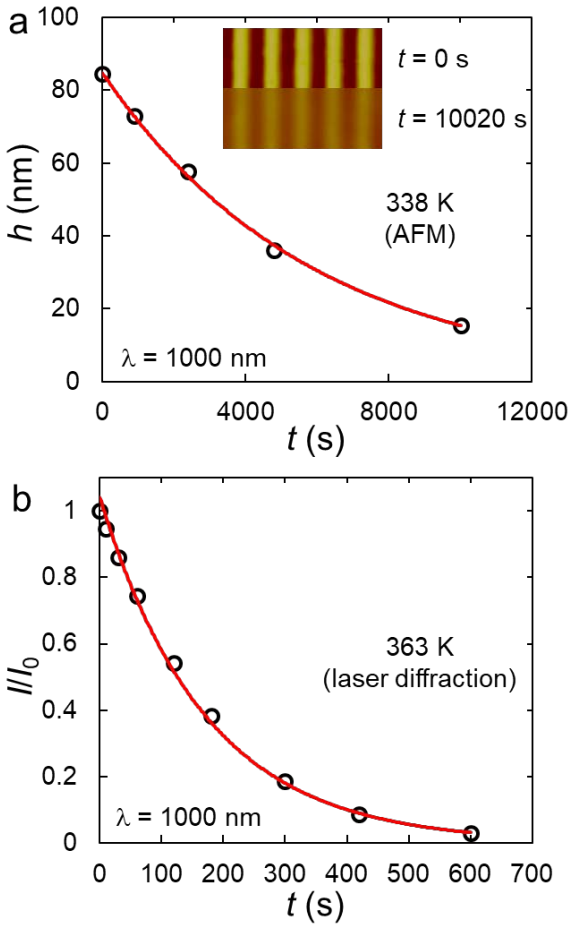

Figure 1. Typical decay kinetics of GSF surface gratings (λ = 1000 nm). (a) At 338 K recorded by AFM. Insert: AFM images at 2 time points. (b) At 363 K recorded by laser diffraction. I/I_0 is normalized diffraction intensity.

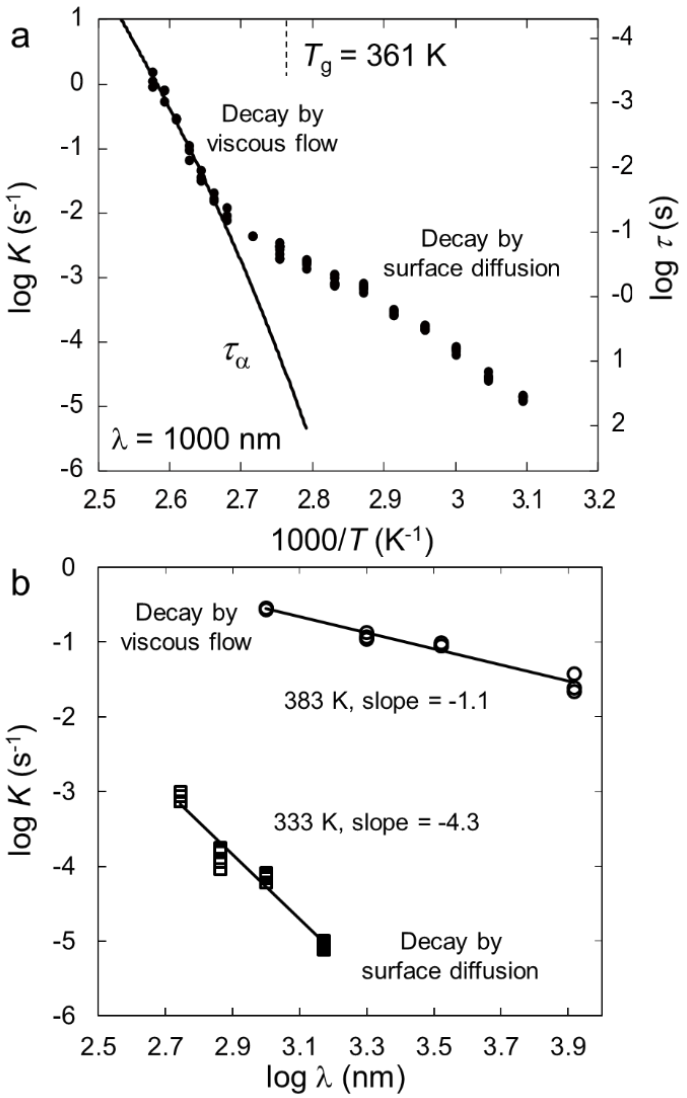

Figure 2. (a) The temperature dependence of decay constant, *K*, at λ = 1000 nm for amorphous GSF (solid circles). The structural relaxation time, τ_α, is shown as a curve. (b) The wavelength dependence of *K* at 333 K and 383 K.

Mullins[25,26] showed that the amplitude of a sinusoidal grating decays exponentially and the decay constant is given by

$$K = Fq + Aq^2 + Dq^3 + Bq^4 \qquad (1)$$

where $q = 2\pi/\lambda$

$$F = \frac{\gamma}{2\eta}$$

$$A = \frac{p_0 \gamma \Omega^2}{(2\pi m)^{\frac{1}{2}}(kT)^{\frac{3}{2}}}$$

$$D = A' + C = \frac{\rho_0 D_G \gamma \Omega^2}{kT} + \frac{D_v \gamma \Omega}{kT}$$

$$B = \frac{D_s \gamma \Omega^2 \nu}{kT}$$

where λ is the grating wavelength; η is the viscosity; γ is the surface tension; p_0 is the equilibrium vapor pressure; Ω is the molecular volume; m is the molecular weight; k is the Boltzmann constant; T is the temperature; ρ_0 is the number density of vapor at equilibrium; D_G is the diffusion coefficient of the vapor molecules in an inert atmosphere; D_v is the bulk self-diffusion coefficient; ν is the number of molecules per unit area on surface. The four terms in Equation (1) correspond to different mechanisms of mass transport: viscous flow (F), evaporation-condensation ($A + A'$), bulk diffusion (C), and surface diffusion (B).

Notice that each term in eq. (1) has a distinct wavelength dependence. For example, the viscous flow term scales as λ^{-1} and the surface diffusion term as λ^{-4}. These are the wavelength dependences observed for GSF decaying at high and low temperatures (Figure 2b). Thus, we assign the high-temperature decay as occurring through viscous flow and the low temperature decay through surface diffusion. In what follows, we offer additional justification for these assignments.

Among the four terms in eq. (1), the evaporation-condensation and bulk-diffusion terms are shown to be much smaller than the observed decay constant, K, by at least 10,000 times. For this calculation, the following values are used: $p_0 = 6.8\times10^{-11}$ Pa (predicted by the ACD software[27]), ρ_0 was calculated from p_0 using the ideal gas law, $\Delta H_{vap} = 86$ kJ/mol (predicted value at the boiling point by ACD[27]), $\gamma = 0.0526$ N/m (predicted by ACD[27]), $D_G \approx 0.00001$ m^2/s (typical value of organic molecules at ambient pressure[28]), and D_v is assumed to be the same as OTP[29] or TNB[30] at the same T_g–scaled temperature. In addition, Ω is calculated from $M/(\rho N_A)$, where M is the molecular weight, N_A is Avogadro's number, and ρ is the density of a GSF glass (1.35 g/mL),[20] to yield $\Omega = 4.0\times10^{-28}$ m^3.

The assignment that the high-temperature decay occurs by viscous flow can be tested against the expected temperature dependence of K. While there is no viscosity data on GSF, the structural relaxation time τ_α is known[22] and can be used to describe the temperature dependence of viscosity because of the relation $\eta \propto \tau_\alpha$.[31] In Figure 2a, τ_α is plotted on the second y axis. It is seen that the τ_α curve has the same temperature dependence as K at high temperatures, as expected for the viscous flow mechanism. This agreement holds above 375 K (T_g + 14 K) for the 1000 nm wavelength grating, but breaks down at lower temperatures (Figure 2a), indicating that a different mechanism is operative. By elimination, surface diffusion is the only mechanism remaining that is responsible for the low-temperature decay. Again, this assignment is supported by the wavelength dependence test (Figure 2b), which finds $K \propto \lambda^{-4}$, as expected for this mechanism.

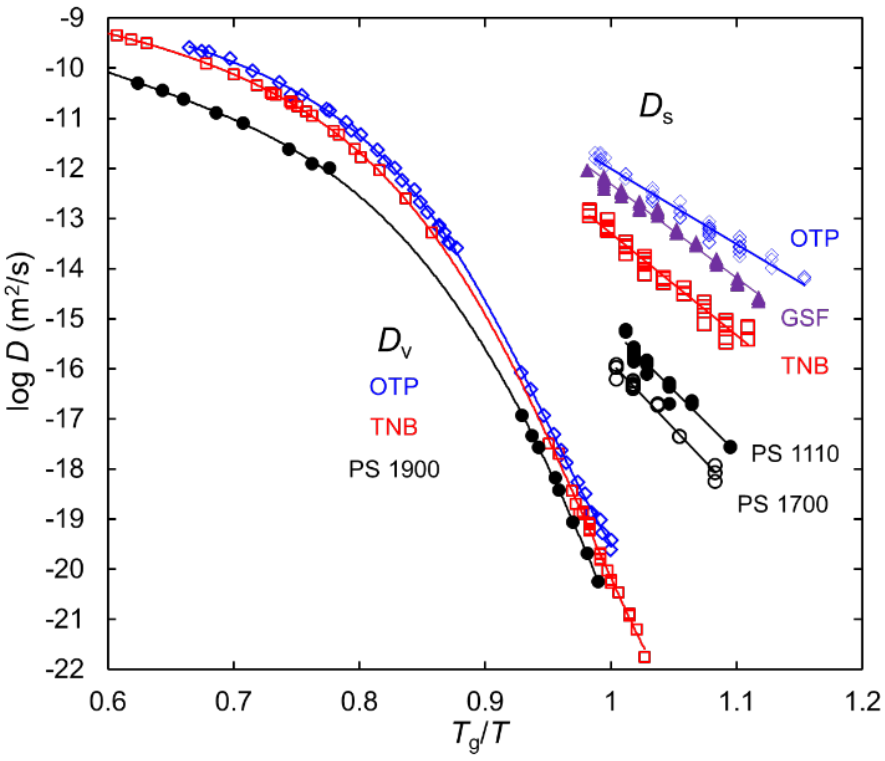

Figure 3. D_s and D_v of several glass-forming molecular liquids against T_g-scaled temperature. T_g is from DSC (onset temperature during heating): 246 K for OTP, 347 K for TNB, 307 K for PS1110, 319 K for PS1700 and 361 K for GSF).

Assigning surface diffusion as the mechanism for surface-grating decay at low temperatures, the corresponding surface diffusion coefficients, D_s, can be calculated. Figure 3 shows the result of this calculation, along with the previous results on simple aromatic hydrocarbons: OTP, TNB, and two PS oligomers (M_w = 1110 and 1700 g/mol). Figure 3 also includes the D_v values of OTP[29], TNB[30], and a PS oligomer[32] (M_w = 1900 g/mol). In this plot, the temperature has been scaled by T_g. In this format, the D_v values of the various systems nearly collapse to a master curve, and it is reasonable to expect that the D_v of GSF falls close to the master curve.

Notice that surface diffusion in a GSF glass is remarkably fast; its rate is similar to that of OTP, the fastest system on record. The ratio D_s/D_v is approximately 10^8 at T_g and increases with cooling. The D_s of GSF has an approximately Arrhenius dependence on temperature with an activation energy of 131 kJ/mol. From OTP to GSF and to the other systems in Figure 3, surface diffusion slows down, with the D_s/D_v at T_g decreasing from 10^8 to 10^4, and the activation energy for surface diffusion also increases.

In Figure 4, the D_s value at T_g is plotted against the molecular weight M. To expand our comparison, other data are included for molecular glasses that form intermolecular hydrogen bonds: IMC,[14] NIF,[18] three triazines[19] (Et, OMe, and NHMe), and two polyalcohols (sorbitol and maltitol).[24] All these data were obtained by the method of surface-grating decay. In addition, three data points are included that were obtained by other methods: TPD (surface evolution around a nano-particle),[33] PS 2400 (spontaneously roughening),[34] and PS 3000 (smoothing of a step)[35]. In Figure 4, solid symbols indicate systems without intermolecular hydrogen bonds, and open symbols systems with intermolecular hydrogen bonds.

For the non-hydrogen-bonding group (solid symbols), the D_s value decreases with increasing molecular weight. Note that the GSF point fits in this overall trend very well. This is noteworthy because GSF is the only system in this group that is *not* a simple aromatic hydrocarbon. GSF has many polar functional groups (ether and carbonyl). This result argues that in terms of its effect on surface diffusion, each polar group in GSF has no more influence than a non-polar hydrocarbon group. The molecular size dependence of D_s has been attributed to a steep and similar mobility gradient beneath the surface of molecular glasses and the deeper penetration of a larger molecule into the bulk where mobility is low.[17]

Figure 4 also shows that the correlation between D_s and molecular weight vanishes if the data points are included for hydrogen-bonded glasses (open symbols). Here, we note a different effect: compare the molecules of similar sizes but varying degrees of hydrogen bonding (the vertical column of open symbols). Observe that D_s decreases from molecules forming no hydrogen bonds (GSF) to those forming limited hydrogen bonds (NIF, IMC and the triazines) to those forming extensive hydrogen bonds (polyalcohols). This argues that hydrogen bonding is an independent effect from molecular size that controls surface diffusion.[19,24] The hydrogen-bonding effect on surface mobility has been attributed to the persistence of hydrogen bonds (in terms of the number of bonds per molecule) as a molecule is moved from the bulk to the surface environment. Assuming that hydrogen bonding controls the barrier for molecular rearrangement, this means that the barrier at the surface is substantially the same as that in the bulk.

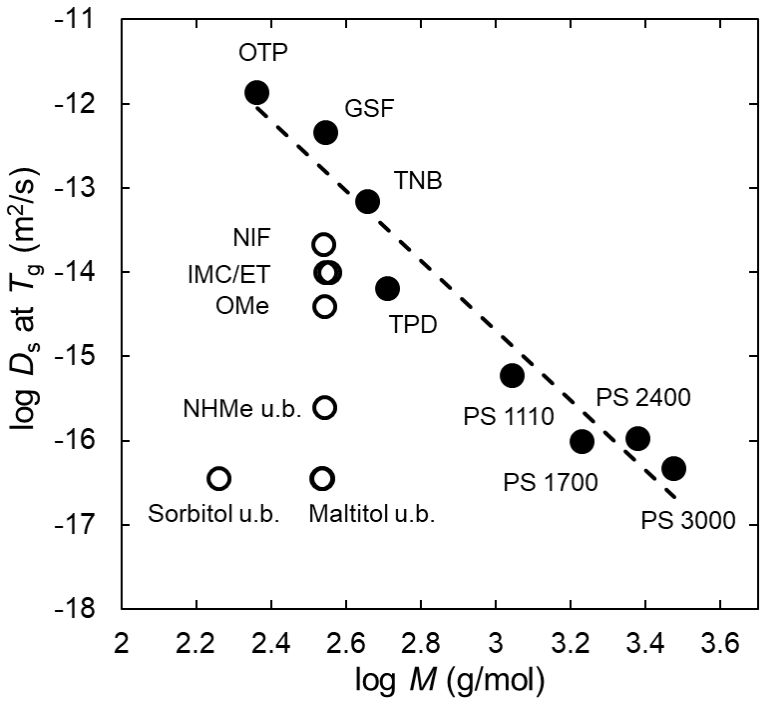

Figure 4. The surface diffusion coefficient, D_s, at T_g as a function of molecular weight. Solid symbols: no intermolecular hydrogen bonds. Open symbols: with intermolecular hydrogen bonds. "u.b." means upper bound.

2.5 Discussion

Motivated by understanding its fast crystallization,[20,21,22,23] this study has measured the surface diffusion in GSF glasses. We find that surface diffusion is remarkably fast in this system, making GSF the second fastest among all molecular glasses studied to date (13 in total). Here we discuss the significance of this result for understanding the crystallization of GSF glasses.

In Figure 5, the surface crystal growth rate u_s of GSF is plotted against its surface diffusion coefficient D_s, along with the literature data on 4 other molecular glasses (OTP, TNB, NIF, and IMC)[13,16] and on amorphous silicon.[36,37] For GSF and all the other molecular glasses, u_s is roughly proportional to D_s.[16] Furthermore, the data points for the different systems approximately cluster together (within one decade in u_s); the overall trend (straight line) is described by the power law $u_s \sim D_s^{0.87}$. It is significant that this trend encompasses 7 different systems, organic and inorganic. It shows that at the same D_s, the rate of surface crystal growth is approximately the same regardless of the molecular details. This strong correlation between u_s and D_s argues that surface diffusion has a controlling role in the process of surface crystal growth.

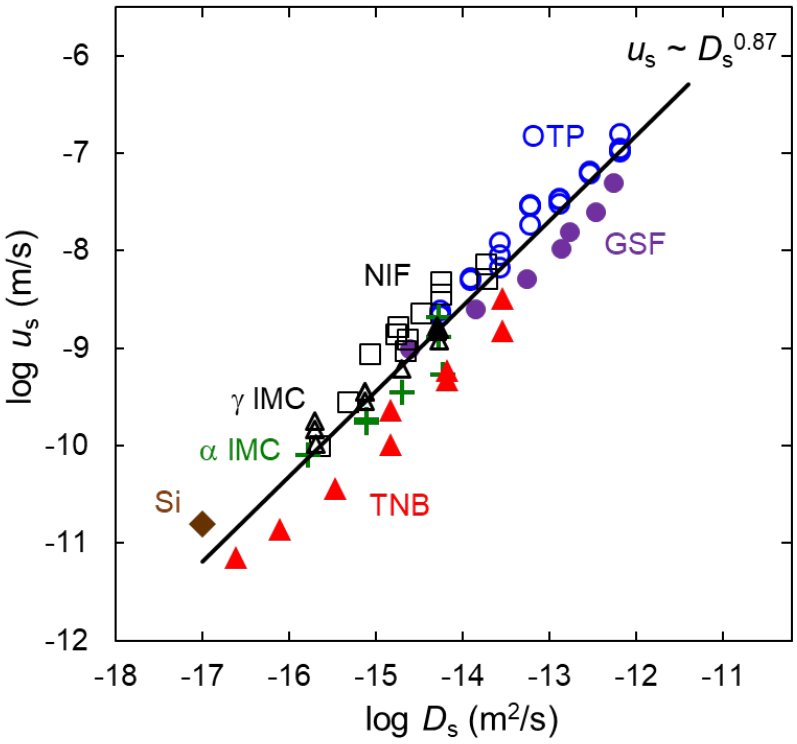

Figure 5. Crystal growth rate on the surface, u_s, plotted against the surface diffusion coefficient, D_s, for molecular glasses and amorphous silicon.

In addition to fast surface crystal growth, a GSF glass is known to grow crystals rapidly *in the bulk* (the so-called GC growth).[21] This growth mode abruptly emerges as a GSF liquid is cooled near its T_g, as also observed in other molecular liquids.[4,5,6] Among its various explanations, the most recent by Powell et al.[10] argues that the GC growth process continuously creates voids and free surfaces through fracture, which in turn enables fast local transformation. Powell et al. based their model on the fact that the overall volume is conserved during crystal growth in a rigid glass. Given the higher density of the crystal than the glass, voids and free surfaces must be created during crystal growth. Small-molecule glasses generally have low fracture resistance and cannot be strained by the amount (several percent) corresponding to the glass-crystal density difference without fracture.[38] This picture seems equally valid for GSF: crystalline GSF is 8 % denser than its glass;[20] as a result, a large amount of void space must be created if the overall volume of the system is fixed during crystallization. Zhu et al. observed that crystal growth is accelerated along artificially created cracks in a GSF glass.[20] This suggests that if cracks are created during GC growth, local transformation could be accelerated through high surface mobility, leading to fast bulk crystal growth.

2.6 Conclusion

Surface diffusion coefficients of amorphous griseofulvin (GSF) have been measured by the surface-grating decay method. Similar to other molecular systems, the flattening of surface grating occurs by viscous flow at high temperatures and by surface diffusion at low temperatures, with the transition occurring at T_g + 12 K for 1000 nm wavelength gratings. The surface diffusion of GSF is vastly faster than bulk diffusion, by a factor of 10^8 at T_g. The surface diffusion in GSF is faster than in any other molecular glass except for the small aromatic hydrocarbon *o*-terphenyl. The new

result on GSF fits well with the trend formed by molecular glasses free of intermolecular hydrogen bonds where surface diffusion systematically slows down with increasing molecular size. This indicates that when not participating in hydrogen bonds, the polar functional groups in GSF (ether and carbonyl) have similar influence on surface diffusion as the non-polar hydrocarbon groups, while the formation of hydrogen bonds imposes a strong inhibitory effect. Thus, molecular size and hydrogen bonding are two independent factors that control surface diffusion. Whether other molecular attributes (e.g., shape and rigidity) influences surface diffusion warrants future studies.

We find a nearly linear relation between the surface crystal growth rate and the surface diffusion coefficient of GSF and all other molecular glasses studied to date. This strongly supports the notion that surface diffusion has a controlling role in surface crystallization. Our results on GSF are consistent with the proposal of Powell et al. that the fast crystal growth *in the bulk* of molecular glasses ("GC growth") is also enabled by surface mobility through the constant creation of voids and free surfaces as the growth front advances. This mechanism of glass crystallization could be tested by *in situ* microscopy. With its large volume change (8 %), GSF could be a suitable system for this purpose.

2.7 Acknowledgments

We thank the NSF for supporting this work through DMR-1206724 and the UW-MRSEC (DMR-1720415).

2.8 References

[1] Wilson, H. W. On the velocity of solidification and viscosity of super-cooled liquids. *Philosophical Magazine* **1900,** *50,* 238-250.

[2] Frenkel, J. Note on a relation between the speed of crystallization and viscosity, *Physikalische Zeitschrift der Sowjetunion*, **1932**, *1*, 498-500.

[3] Greet, R. J.; Turnbull, D. Glass transition in *o*-terphenyl. *The Journal of Chemical Physics* **1967,** *46*, 1243-1251.

[4] Hikima, T.; Adachi, Y.; Hanaya, M.; Oguni, M. Determination of potentially homogeneous-nucleation-based crystallization in *o*-terphernyl and an interpretation of the nucleation-enhancement mechanism. *Phys. Rev. B* **1995,** *52*, 3900-3908.

[5] Ishida, H.; Wu, T. A.; Yu, L. A. Sudden rise of crystal growth rate of nifedipine near Tg without and with polyvinylpyrrolidone. *Journal of Pharmaceutical Sciences* **2007,** *96*, 1131-1138.

[6] Sun, Y.; Xi, H. M.; Chen, S.; Ediger, M. D.; Yu, L. Crystallization near glass transition: transition from diffusion-controlled to diffusionless crystal growth studied with seven polymorphs. *J. Phys. Chem. B* **2008,** *112*, 5594-5601.

[7] Konishi, T.; Tanaka, H. Possible origin of enhanced crystal growth in a glass. *Phys. Rev. B* **2007,** *76*, 220201.

[8] Stevenson, J. D.; Wolynes, P. G. The ultimate fate of supercooled liquids. *The Journal of Physical Chemistry A* **2011,** *115*, 3713-3719.

[9] Caroli, C.; Lemaître, A. Ultrafast spherulitic crystal growth as a stress-induced phenomenon specific of fragile glass-formers. *The Journal of Chemical Physics* **2012,** *137*, 114506.

[10] Powell, C. T.; Xi, H.; Sun, Y.; Gunn, E.; Chen, Y.; Ediger, M. D.; Yu, L. Fast crystal growth in *o*-terphenyl glasses: a possible role for fracture and surface mobility. *The Journal of Physical Chemistry B* **2015,** *119*, 10124-10130.

[11] Wu, T.; Yu, L. Surface crystallization of indomethacin below Tg. *Pharmaceutical Research* **2006,** *23*, 2350-2355.

[12] Sun, Y.; Zhu, L.; Kearns, K. L.; Ediger, M. D.; Yu, L. Glasses crystallize rapidly at free surfaces by growing crystals upward. *Proceedings of the National Academy of Sciences* **2011,** *108*, 5990-5995.

[13] Hasebe, M.; Musumeci, D.; Powell, C. T.; Cai, T.; Gunn, E.; Zhu, L.; Yu, L. Fast surface crystal growth on molecular glasses and its termination by the onset of fluidity. *The Journal of Physical Chemistry B* **2014,** *118*, 7638-7646.

[14] Zhu, L.; Brian, C. W.; Swallen, S. F.; Straus, P. T.; Ediger, M. D.; Yu, L. Surface self-diffusion of an organic glass. *Physical Review Letters* **2011,** *106*, 256103.

[15] Zhang, W.; Brian, C. W.; Yu, L. Fast surface diffusion of amorphous *o*-terphenyl and its competition with viscous flow in surface evolution. *The Journal of Physical Chemistry B* **2015,** *119*, 5071-5078.

[16] Ruan, S.; Zhang, W.; Sun, Y.; Ediger, M. D.; Yu, L. Surface diffusion and surface crystal growth of tris-naphthyl benzene glasses. *The Journal of Chemical Physics* **2016,** *145*, 064503.

[17] Zhang, W.; Yu, L. Surface diffusion of polymer glasses. *Macromolecules* **2016,** *49*, 731-735.

[18] Brian, C. W.; Yu, L. Surface self-diffusion of organic glasses. *The Journal of Physical Chemistry A* **2013,** *117*, 13303-13309.

[19] Chen, Y.; Zhu, M.; Laventure, A.; Lebel, O.; Ediger, M. D.; Yu, L. Influence of hydrogen bonding on the surface diffusion of molecular glasses: comparison of three triazines. *The Journal of Physical Chemistry B* **2017**, *121*, 7221-7227

[20] Zhu, L.; Jona, J.; Nagapudi, K.; Wu, T. Fast surface crystallization of amorphous griseofulvin below Tg. *Pharmaceutical Research* **2010,** *27*, 1558-1567.

[21] Shi, Q.; Cai, T. Fast crystal growth of amorphous griseofulvin: relations between bulk and surface growth modes. *Crystal Growth & Design* **2016,** *16*, 3279-3286.

[22] Shi, Q.; Zhang, C.; Su, Y.; Zhang, J.; Zhou, D.; Cai, T. Acceleration of crystal growth of amorphous griseofulvin by low-concentration poly(ethylene oxide): aspects of crystallization kinetics and molecular mobility. *Molecular pharmaceutics* **2017,** *14*, 2262-2272.

[23] Willart, J. F.; Dudognon, E.; Mahieu, A.; Eddleston, M.; Jones, W.; Descamps, M. The role of cracks in the crystal nucleation process of amorphous griseofulvin. *The European Physical Journal Special Topics* **2017,** *226*, 837-847.

[24] Chen, Y.; Zhang, W.; Yu, L. Hydrogen bonding slows down surface diffusion of molecular glasses. *The Journal of Physical Chemistry B* **2016,** *120*, 8007-8015.

[25] Mullins, W. W. Theory of thermal grooving. *J. Appl. Phys.* **1957,** *28*, 333-339.

[26] Mullins, W. W. Flattening of a nearly plane solid surface due to capillarity. *J. Appl. Phys.* **1959,** *30*, 77-83.

[27] Advanced Chemistry Development (ACD/Labs) Software, v11.02, ACD/Labs, Ontario, Canada, 2016.

[28] Jakubczyk, D.; Derkachov, G.; Duc, T. D.; Kolwas, K.; Kolwas, M. Coefficients of evaporation and gas phase diffusion of low-volatility organic solvents in nitrogen from interferometric study of evaporating droplets. *The Journal of Physical Chemistry A* **2010,** *114*, 3483-3488.

[29] Mapes, M. K.; Swallen, S. F.; Ediger, M. D. Self-diffusion of supercooled o-terphenyl near the glass transition temperature. *The Journal of Physical Chemistry B* **2006,** *110*, 507-511.

[30] Swallen, S. F.; Traynor, K.; McMahon, R. J.; Ediger, M. D.; Mates, T. E. Self-diffusion of supercooled tris-naphthylbenzene. *The Journal of Physical Chemistry B* **2009,** *113*, 4600-4608.

[31] Hiemenz, P. C.; Lodge, T. P. *Polymer Chemistry*, 2nd ed.; CRC Press: New York, 2007.

[32] Urakawa, O.; Swallen, S. F.; Ediger, M. D.; von Meerwall, E. D. Self-diffusion and viscosity of low molecular weight polystyrene over a wide temperature range. *Macromolecules* **2004,** *37*, 1558-1564.

[33] Zhang, Y.; Potter, R.; Zhang, W.; Fakhraai, Z. Using tobacco mosaic virus to probe enhanced surface diffusion of molecular glasses. *Soft Matter* **2016,** *12*, 9115-9120.

[34] Yang, Z.; Fujii, Y.; Lee, F. K.; Lam, C.-H.; Tsui, O. K. C. Glass transition dynamics and surface layer mobility in unentangled polystyrene films. *Science* **2010,** *328*, 1676-1679.

[35] Chai, Y.; Salez, T.; McGraw, J. D.; Benzaquen, M.; Dalnoki-Veress, K.; Raphaël, E.; Forrest, J. A. A direct quantitative measure of surface mobility in a glassy polymer. *Science* **2014,** *343*, 994-999.

[36] Sallese, J. M.; Ils, A.; Bouvet, D.; Fazan, P.; Merritt, C. Modeling of the depletion of the amorphous-silicon surface during hemispherical grained silicon formation. *J. Appl. Phys.* **2000,** *88*, 5751-5755.

[37] Sakai, A.; Tatsumi, T.; Ishida, K. Growth kinetics of Si hemispherical grains on clean amorphous-Si surfaces. *Journal of Vacuum Science & Technology A: Vacuum, Surfaces, and Films* **1993,** *11*, 2950-2953.

[38] Powell, C. T.; Chen, Y.; Yu, L. Fracture of molecular glasses under tension and increasing their fracture resistance with polymer additives. *Journal of Non-Crystalline Solids* **2015,** *429*, 122-128.

Chapter 3. Crystal Nucleation Rates in Glass-Forming Molecular Liquids: D-Sorbitol, D-Arabitol, D-Xylitol, and Glycerol

As published in ***The Journal of Chemical Physics***

149, 054503 (2018)

Chengbin Huang[1], Zhenxuan Chen[1], Yue Gui[1], Chenyang Shi[2], Geoff G. Z. Zhang[2,*], Lian Yu[1,3,*]

[1] School of Pharmacy, University of Wisconsin-Madison, Madison, WI, 53705, USA

[2] Drug Product Development, Research and Development, AbbVie Inc., North Chicago, IL, 60064, USA

[3] Department of Chemistry, University of Wisconsin-Madison, Madison, WI, 53705, USA

3.1 Abstract

The rate of crystal nucleation has been measured in four glass-forming molecular liquids: D-sorbitol, D-arabitol, D-xylitol and glycerol. These polyalcohols have similar rates of crystal growth when compared at the same temperature relative to T_g (the glass transition temperature), peaking near 1.4 T_g, while the nucleation rates J are vastly different. In D-sorbitol and D-arabitol, J reaches a maximum of ~ 10^8 $m^{-3}\cdot s^{-1}$ near 1.1 T_g, whereas $J < 10^{-2}$ $m^{-3}\cdot s^{-1}$ in D-xylitol and < 1 $m^{-3}\cdot s^{-1}$ in glycerol based on no nucleation in large samples after long waits. This confirms the fundamentally different mechanisms for nucleation and growth. Near T_g, both nucleation and growth slow down with a similar temperature dependence, suggesting a similar kinetic barrier for the two processes. This temperature dependence is significantly weaker than that of viscosity η, approximately following $\eta^{-0.75}$. This indicates that viscosity is a poor representative of the kinetic barrier for nucleation, and a better choice is the crystal growth rate. Under the latter assumption, the classical nucleation theory (CNT) describes our data reasonably well, yielding σ = 0.013 J/m^2 for D-sorbitol and 0.026 J/m^2 for D-arabitol, where σ is the critical nucleus/liquid interfacial free energy. There is no strong indication that the CNT fails as the length scale for corporative rearrangement exceeds the size of the critical nucleus, as recently suggested for lithium disilicate.

3.2 Introduction

Crystallization is a process of nucleation and growth. During nucleation, a viable nucleus is formed that can grow to macroscopic size.[1,2,3,4] Nucleation and growth can have very different kinetics; for example, nucleation in silicate liquids reaches its peak rate at a lower temperature than growth.[2,5] This makes it important to study nucleation as an independent process from growth. The nucleation process has a strong influence on the microstructure of metals, the formation of ice in the environment, and the glass-forming ability of liquids.

Despite a long history of research, the current understanding of crystal nucleation remains limited on both experimental and theoretical fronts. Experimentally, it is not trivial to establish that a given nucleation process is homogeneous (a volume process unaided by foreign particles or surfaces). Homogeneous nucleation rates have been reported and approximately agreed upon for only a small number of systems: water,[6] pure metals,[7,8] and silicates.[2] This is in contrast to the vast body of data on crystal growth rates, enabling the discovery of systematic trends for prediction.[9,10,11,12] It is the goal of this work to measure homogeneous nucleation rates in a class of materials that have not been characterized previously: glass-forming molecular liquids. These materials are increasingly used in biomedical and electronic applications, motivating a deeper understanding of their crystallization, since crystallization is detrimental to their performance.

On the theoretical side, the classical nucleation theory (CNT)[1,2,4] provides the foundation for understanding nucleation and is also recognized for its limitations. According to the CNT, nucleation rate is given by

$$J = k_J \exp(-W_c/kT) \qquad (1)$$

where $W_c = \frac{16\pi}{3}\frac{\sigma^3}{\Delta G_V^2}$ is the thermodynamic barrier for creating a critical nucleus, with σ being the crystal nucleus/liquid interfacial free energy and ΔG_v the free-energy difference between the crystal and the liquid, and k_J is a kinetic factor specifying the attempt frequency at which molecules join the nucleus. At present, there are serious questions concerning both factors in eq. (1). In the W_c function, σ is generally unknown with enough precision from independent measurements[13] or simulations,[14,15] while a small change in σ can change J by orders of magnitude.[16] This makes eq. (1) effectively a fitting model, not a predictive one. For the kinetic factor k_J, it is common to assume that the kinetic barrier for nucleation is similar to that for diffusion or viscous flow in the bulk liquid. But it is questionable whether a *bulk* property can accurately describe the kinetics of *an*

interfacial process (nucleation). Recent work has also shown that seemingly equivalent measures of fluidity can decouple at low temperatures; for example, the diffusion coefficient D and the viscosity η satisfy the Stokes-Einstein relation at high temperatures but do not at low temperatures.[17,18] Another approach to evaluating k_J is to use the "lag time for nucleation" to calculate an effective diffusivity relevant for the nucleation process.[2] This method, however, requires careful extraction of the intrinsic lag time from the experimental induction time, accounting for the influence of thermal history from nuclei formation to detection as macroscopic crystals.[2,19] In this study, we propose that the widely available crystal growth rate could be used to estimate the kinetic factor for nucleation.

The particular systems of this study (Scheme 1) belong in the family of polyalcohols, which are well-characterized glassformers widely used in food, drugs, and biotechnologies. D-xylitol and D-sorbitol are sweeteners in "sugar-free" chewing gums where crystallization can cause the gum to harden. Despite the similarity of their structures, polyalcohols have very different tendencies to crystallize. Glycerol, for example, is a good glass-former, while D-mannitol crystallizes rapidly. Comparison of these systems will help understand the molecular factors controlling nucleation and growth. Finally, each of these systems is composed of a single chemical component and the complications do not arise from the possibility of compositional change between the critical nucleus and the mature crystal.[2]

We report that the nucleation rates are vastly different in the four polyalcohols studied, even though their crystal growth rates are quite similar. The crystal growth rates of the four liquids cluster together when compared at the same temperature relative to T_g, whereas their nucleation rates span at least 10 orders of magnitude. In D-sorbitol and D-arabitol, the nucleation rate J reaches a maximum of $\sim 10^8\ m^{-3}\cdot s^{-1}$ near 1.1 T_g, whereas $J < 10^{-2}\ m^{-3}\cdot s^{-1}$ in D-xylitol. The measured

J value is independent of sample volume, consistent of homogeneous nucleation. We find that nucleation slows down at low temperatures at a similar pace as crystal growth, indicating a similar kinetic barrier for both processes. This kinetic barrier is significantly lower (by 25%) than that for viscous flow. The CNT describes our data reasonably well especially if the kinetic barrier is evaluated using the crystal growth rate, not viscosity. Additionally, there is no indication that the CNT fails as the length scale for corporative rearrangement exceeds the size of the critical nucleus, as suggested for lithium disilicate.

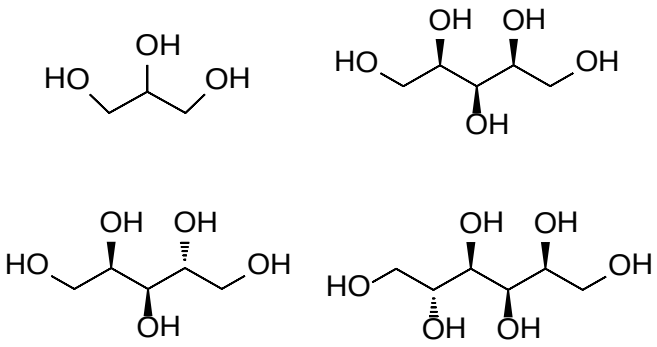

Scheme 1. Molecular structures of the polyalcohols studied.

Table 1. Physical properties of the polyalcohols studied

Polyalcohol	T_g (K)	T_m (K)	ΔH_m (kJ/mol)	Ref.
Glycerol	189	291	18.3	20,21
D-xylitol	250	366	37.3 (0.7)	This work
D-arabitol	260	376	39.9 (0.2)	This work
D-sorbitol	269	353	26.7	22

Note: T_g is the onset temperature during heating at 10 K/min, following cooling at 10 K/min. The literature values on D-xylitol[23,24,25,26] and D-arabitol[23,24,25] are broadly consistent with our values. For D-sorbitol, the values in Ref. 22 are roughly consistent with those in Ref. 27. In addition, the literature values on L-arabitol[23,24,28] agree with our values on D-arabitol, as expected.

3.3 Experimental Section

D-sorbitol and D-arabitol (purity ≥ 99 % for both) from Sigma-Aldrich (St. Louis, MO), D-xylitol (purity ≥ 99 %) from Sigma-Aldrich and Alfa Aesar (Haverhill, MA), glycerol (purity ≥ 99.5 %) from Fisher Chemicals (Fair Lawn, NJ) and Alfa Aesar. The as-received glycerol was dried in vacuum at 383 K before use (this reduced the water content to be less than 0.2 wt % based on Karl Fischer titration). Some physical properties of these polyalcohols are shown in Table 1.

The polyalcohols were used both as-received and after purification to assess the effect of impurity on nucleation rates. The same substance from multiple sources also provided a check on the effect of impurity. For D-xylitol, D-arabitol and D-sorbitol, a purification procedure was performed as follows: dissolve 1 g of the material in 10 mL of water, filter the solution through a 0.2-micron syringe nylon filter, and dry the solution in vacuum at 383 K for two days. The resulting material contained less than 0.5 wt % water based on Karl Fischer titration. We observed no significant effect of the source material and the purification procedure on the observed nucleation rates.

To measure the nucleation rate in D-arabitol or D-sorbitol, 10-20 mg crystal powder was placed on a round coverslip (diameter = 15 mm) and held at 413 K for 6 h in the liquid state to remove air bubbles. The clear melt was covered by another coverslip. The thickness of the liquid film was calculated from its mass and lateral area, and fell in the range 40-80 μm for a standard measurement. The sample thickness was confirmed not to affect the observed nucleation rate (by varying the thickness from 40 to 400 μm, see below). For the slow-crystallizing liquids glycerol and D-xylitol, larger samples were used (2 g of liquid sealed in a glass tube, 8 mm in diameter). To measure the nucleation rate, each sample was stored at a chosen temperature (stable within ± 1 K) in a desiccator. Crystals were observed and counted through an Olympus BX53 polarized light

microscope equipped with a digital camera. Crystal growth rate was measured by tracking the size of a crystal over time; each reported rate is the average of 9-12 measurements in three separate samples.

Crystal polymorphs were identified by X-ray diffraction (Bruker D8 Advance diffractometer with a Cu Kα source) and Raman microscopy (Thermo Scientific DXR with a 532 nm laser). Differential scanning calorimetry was performed with a TA Q2000 in a crimped aluminum pan under 50 mL/min N_2 purge. Modulated DSC was used to measure the heat capacity under the following conditions: heating at 2 K/min, sinusoidal temperature modulation with an amplitude of 0.5 K and a period of 60 s. The error of this measurement is ~ 5 % based on calibration against a sapphire standard.

3.4 Results

Methods for Measuring Nucleation Rates. In this work, two methods were used to measure nucleation rates. The *one-stage method* was used when both nucleation and growth were relatively fast. A sample is allowed to crystallize for some time t_0 at which individual crystals are observable, as shown in Figure 1a. Note the different sizes of the crystals. Since the crystals grow at a constant rate u (0.6 nm/s), an early-nucleating crystal has longer time to grow to a larger size. The birth time of each crystal is calculated from its current size (radius, r):

$$t = t_0 - r/u$$

where t_0 is the current time (time of observation).

The ability to date the birth of each crystal allows the determination of the number of nucleation events per unit volume as a function of time (Figure 1b). This plot shows an induction period noted in other work[2] and a steady state where the nuclei density increases linearly with time. In this study,

we focus on the steady-state nucleation rate J, given by the slope of the plot in Figure 1b ($J = 5.2 \times 10^6$ $m^{-3} \cdot s^{-1}$ at 297 K). It is worth noting that in the foregoing calculation, u is the growth rate of the observable crystal and is assumed to be the same for the (invisible) crystal nucleus. If the nucleus growth rate differs from that of the mature crystal, a constant shift is added to the calculated birth times without affecting the calculation of the steady-state nucleation rate.

The method described above requires relatively fast growth of crystals to observable sizes, and is unsuitable when crystal growth is slow. A *two-stage method* has been employed for this situation.[29] Here, nuclei are allowed to form at a low temperature and the temperature is raised to grow these nuclei to visible size to be counted. The growth temperature is chosen so that pre-formed nuclei can grow quickly but no new nuclei form during the time of development. This method has been employed to measure J in silicates.[2]

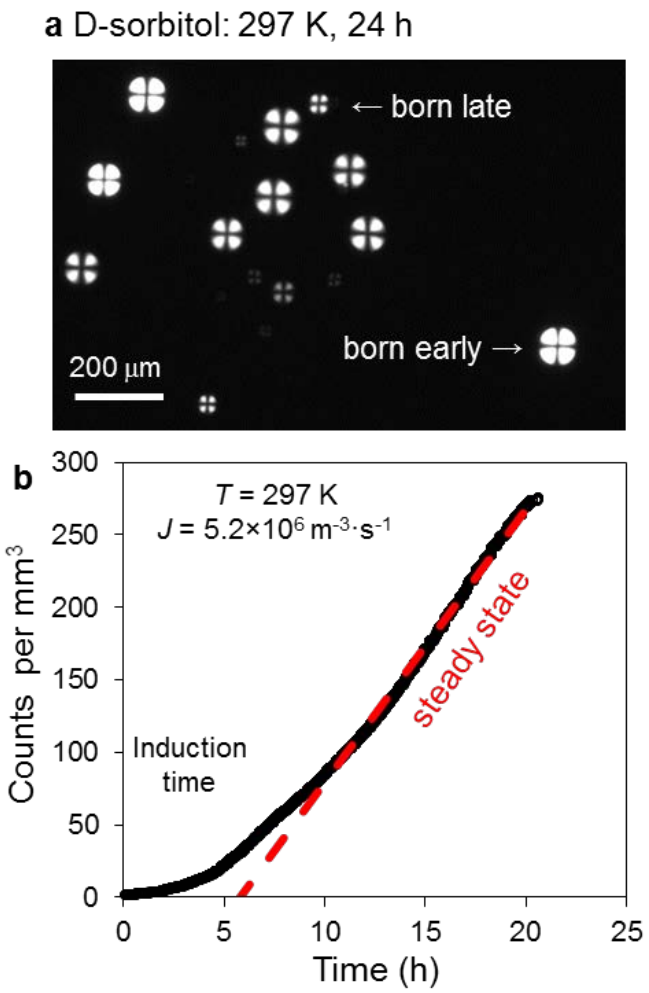

Figure 1. (a) A sample of D-sorbitol after crystallizing for 24 h at 297 K. Note the different crystal sizes. Since the crystals grow at the same rate (0.6 nm/s), the larger ones were born earlier, and the smaller ones born later. This enables the determination of the number of crystal nuclei formed per unit volume as a function of time (b). The slope of this plot is the nucleation rate.

Figure 2a shows the typical data collected by the two-stage method. The D-arabitol samples spent different times at 278 K but the same time (10 min) at 313 K. Note the sample that spent longer time at 278 K (16 h) developed more crystals than the sample that spent shorter time (4 h), but both contained crystals of similar size. Furthermore, before heating to 313 K, no crystals were visible, and without the time at 278 K, no crystals were observed at 313 K up to 30 min. All these results confirm that the crystals (seen in Figure 2a) nucleated at 278 K and grew at 313 K. This allows the determination of the density of nuclei formed at 278 K as a function of nucleation time (Figure 2b). As in Figure 1b, an induction period is evident, followed by a steady state nucleation whose rate is $J = 3.7 \times 10^{7}$ $m^{-3} \cdot s^{-1}$.

In this work, we find that the one-stage and two-stage methods yield consistent results; for example, for D-sorbitol at 308 K, $J = 1.6 \times 10^{6}$ $m^{-3} \cdot s^{-1}$ by the one-stage method and $J = 2.0 \times 10^{6}$ $m^{-3} \cdot s^{-1}$ by the two-stage method.

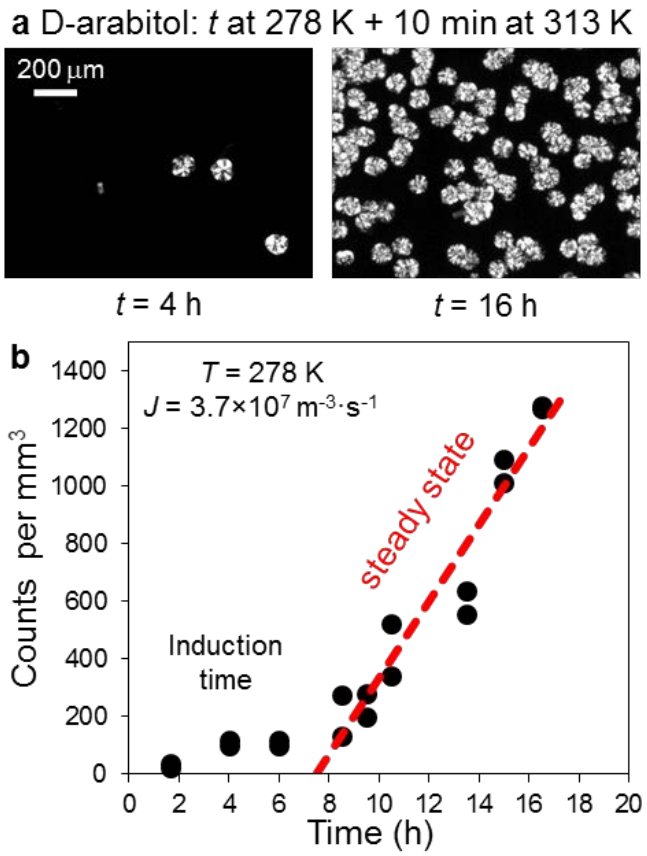

Figure 2. (a) Crystals observed after D-arabitol spent different times at 278 K (4 or 16 h) to nucleate followed by 10 min at 313 K to grow. Before heating to 313 K, no crystals were visible. (b) Nuclei density as a function of nucleation time at 278 K.

Homogeneous Nucleation. It is important to establish whether the observed nucleation is a volume process ("homogeneous") or aided by contact with foreign surfaces ("heterogeneous"). Here we demonstrate that the nucleation rates measured correspond to the volume nucleation. To evaluate whether nucleation occurred on substrate surfaces, liquid films of D-sorbitol with different thicknesses were allowed to crystallize at 297 K for the same time (17 h), and the samples were examined through the microscope covering the same lateral field of view (Figure 3a; the field of view is 1.4 mm^2). In this way, the numbers of crystals formed in different volumes can be directly compared, with each volume proportional to the film thickness. (The crystals were sparse enough so that they did not overlap.) A volume process requires that the number of crystals formed within a given time increases linearly with the film thickness, which is observed in Figure 3b.

To evaluate the possibility of heterogeneous nucleation, materials from different sources were compared (they came from different batches of preparation and might differ in the level of impurity and foreign particles). We observed no significant effect of source materials on measured nucleation rates. Furthermore, we checked the effect of filtration of an as-received material through a 0.2-micron filter. This also had insignificant effect on the observed nucleation rates; for example, $\log J$ ($m^{-3} \cdot s^{-1}$) = 7.1 for D-sorbitol at 297 K and 6.9 after filtration. Finally, we note that the existence of a steady state (Figures 1b and 2b) is consistent with volume nucleation but inconsistent with nucleation on active sites provided by foreign particles. In the latter case, nucleation rate is expected to be fast initially but plateaus afterwards. All the evidence above argues that our nucleation rates are not significantly affected by chemical purity or presence of foreign particles, and can be interpreted as rates of homogeneous nucleation.

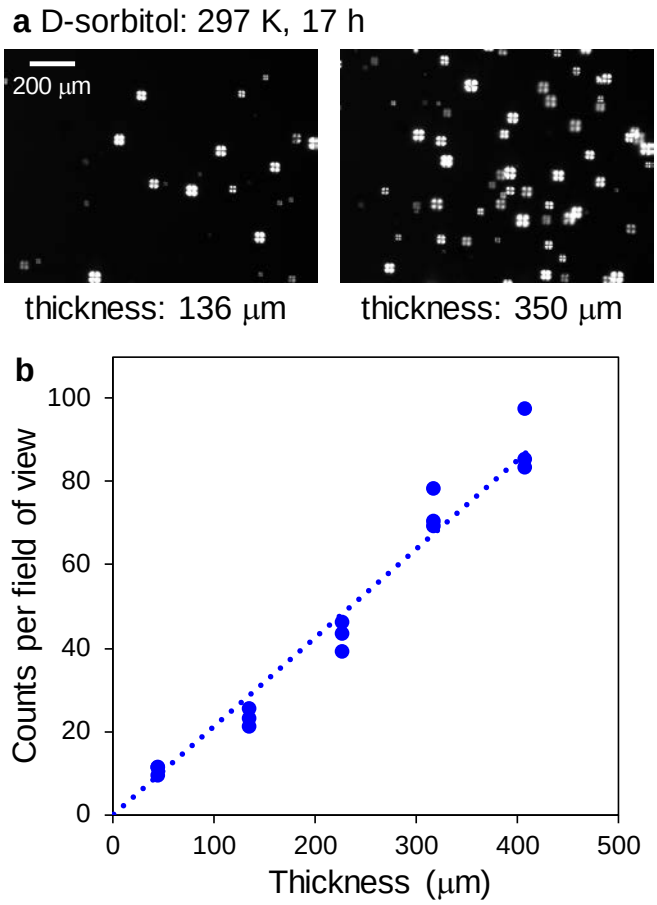

Figure 3. (a) Crystals formed at 297 K for 17 h in D-sorbitol films of two thicknesses and the same lateral field of view. The thicker sample has more crystals. (b) The number of crystals per field of view plotted as a function of film thickness. The linear increase indicates a volume nucleation process.

D-sorbitol. Liquid D-sorbitol spontaneously crystallizes near the ambient temperature, yielding the so-called polymorph E (T_m = 353 K).[22,30] Figure 4 shows the rate of crystal nucleation J and growth u in liquid D-sorbitol. The nucleation rate spans 3 orders of magnitude and is maximal near 288 K (T_g + 19 K). This temperature is well below that for the fastest crystal growth (Figure 4b), which is near 333 K (T_g + 64 K). The different kinetics for nucleation and growth is similar to that observed for silicates.[2,5] The curve in Figure 4a is the CNT fitting of the data (see below).

D-sorbitol is polymorphic.[27] Apart from polymorph E, it can crystallize as γ (T_m = 373 K),[31] ε (T_m unknown, prepared by evaporating an EtOH-water solution),[32] and α (T_m = 359 K, prepared by annealing E).[27] We performed limited experiments to investigate if other polymorphs also nucleated but could not be observed because their growth was too slow. Given that E has the lowest melting point (353 K) of known polymorphs, this possibility was tested by heating a nucleated sample above 353 K. At this temperature, polymorph E is melted but other higher-melting polymorphs. (γ and α, if nucleated, can grow to be observed. In fact, the commercial γ polymorph is obtained by seeding at a high temperature,[33] while γ-seeding at a low temperature leads to the cross-nucleation and growth of polymorph E.[34]) For this experiment, D-sorbitol (*ca.* 60 mg) was nucleated into polymorph E at 295 K for two days, and then the sample was heated at 363 K for 5 min. No crystals were observed after heating. This indicates that as polymorph E nucleated at 295 K, the higher-melting polymorphs nucleated at a much slower rate, with $J < 10^2$ $m^{-3}\cdot s^{-1}$ based on no nucleation in the known volume, compared to $J = 4 \times 10^6$ $m^{-3}\cdot s^{-1}$ for polymorph E.

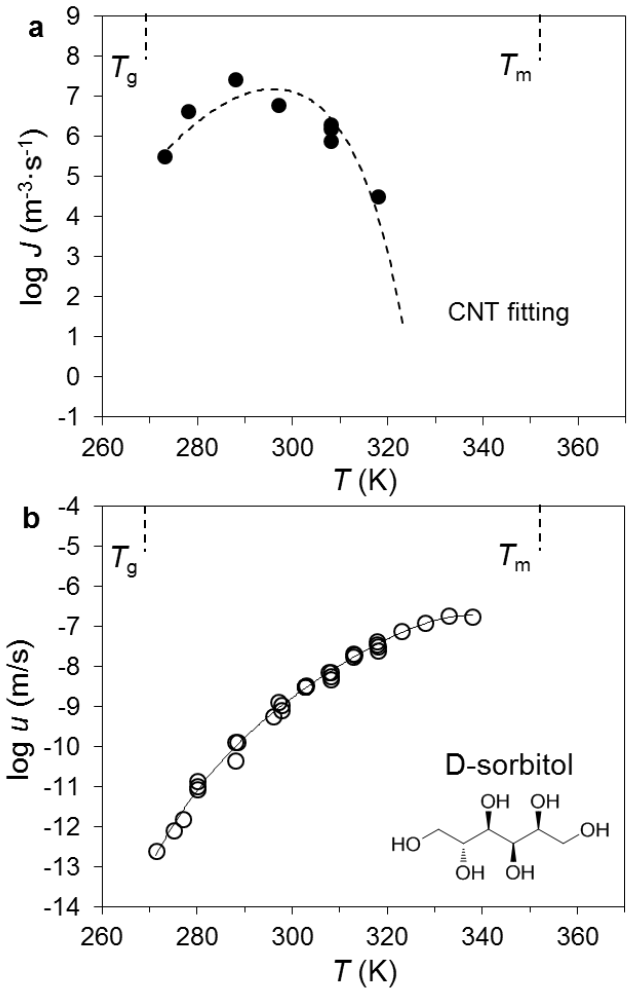

Figure 4. The rate of crystal nucleation (a) and growth (b) in liquid D-sorbitol vs. temperature. The curve in (a) is the CNT fitting of the data (discussed below); the curve in (b) is guide to the eye. The crystal growth rates are from this work and Ref. 22 and 30.

D-arabitol. Similar to D-sorbitol, liquid D-arabitol spontaneously crystallizes near the ambient temperature. Figure 5 shows its rate of crystal nucleation and growth. These results correspond to the known crystal structure of D-arabitol[35] (T_m = 376 K; Cambridge Structural Database Ref. Code: VOZMAY), but as we discuss later, a second polymorph can also nucleate at a lower rate. As in the case of D-sorbitol, the nucleation rate reaches a maximum at 288 K (T_g + 28 K), well below the temperature for fastest growth, 363 K (T_g + 103 K).

Interestingly, the crystallization of D-arabitol can yield two polymorphs. In addition to Form I,[35] a minor polymorph (Form II) crystallizes simultaneously. Form II has lower melting point (T_m = 356 K) and distinct Raman spectrum, XRD pattern, and crystal growth rate (Figure S1). This polymorph appears to correspond to a second polymorph of D-arabitol reported by Diogo *et al*.[23] Furthermore these two polymorphs of D-arabitol seem to have their counterparts in L-arabitol,[28,36] as expected. This study concerns only Form I, which nucleates faster in the temperature range studied.

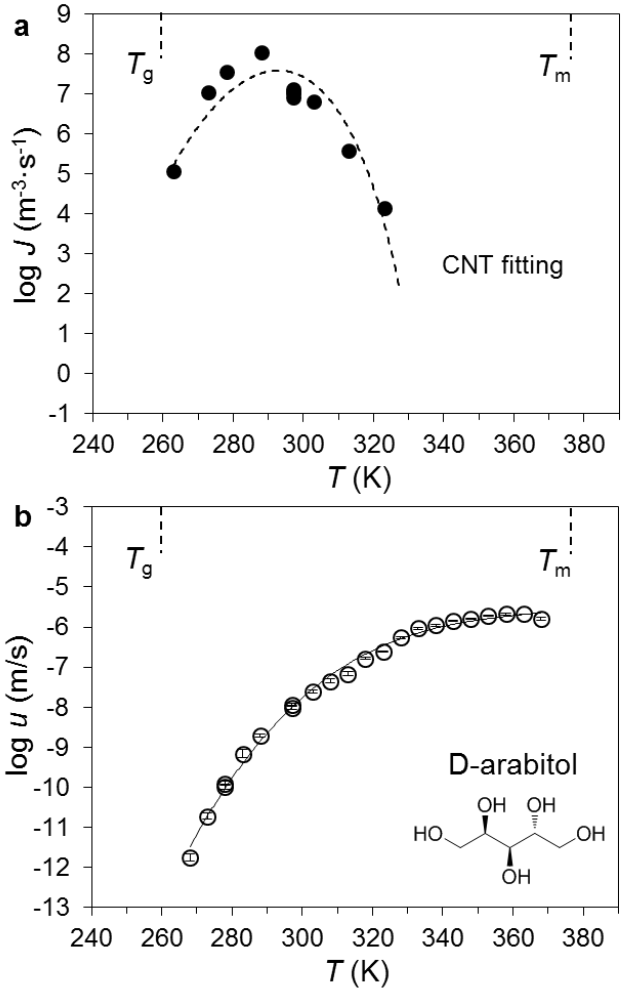

Figure 5. The rate of crystal nucleation (a) and growth (b) in liquid D-arabitol vs. temperature. The data are for polymorph I; a minor polymorph was also observed (see *Supporting Information*). The curve in (a) is the CNT fitting of the data (discussed below); the curve in (b) is guide to the eye.

D-xylitol. Nucleation is much slower in D-xylitol than in D-sorbitol and D-arabitol. Performing the same experiments but with 1000-times larger samples, no nucleation was observed up to 6 months. In these experiments, the sample was held at several temperatures near T_g (short dashes in Figure 6a), and heated to 313 K where growth rate is sufficiently fast. Since no crystals were observed, an upper bound was obtained for J at 10^{-2} $m^{-3} \cdot s^{-1}$ (Figure 6a; this calculation assumes no induction time for nucleation). This places the J value for D-xylitol at least 10 orders of magnitude below the peak values for D-arabitol and D-sorbitol. The curve in Figure 6a is a hypothetical profile produced by the CNT consistent with the experimental upper bound.

In contrast to its slow nucleation, crystal growth rate of D-xylitol is “normal” relative to the other polyalcohols, with a maximum rate near 350 K (T_g + 100 K). The crystal growth rates were measured by seeding liquid D-xylitol with the as-received crystal polymorph (T_m = 366 K, Cambridge Structural Database Ref. Code: XYLTOL).

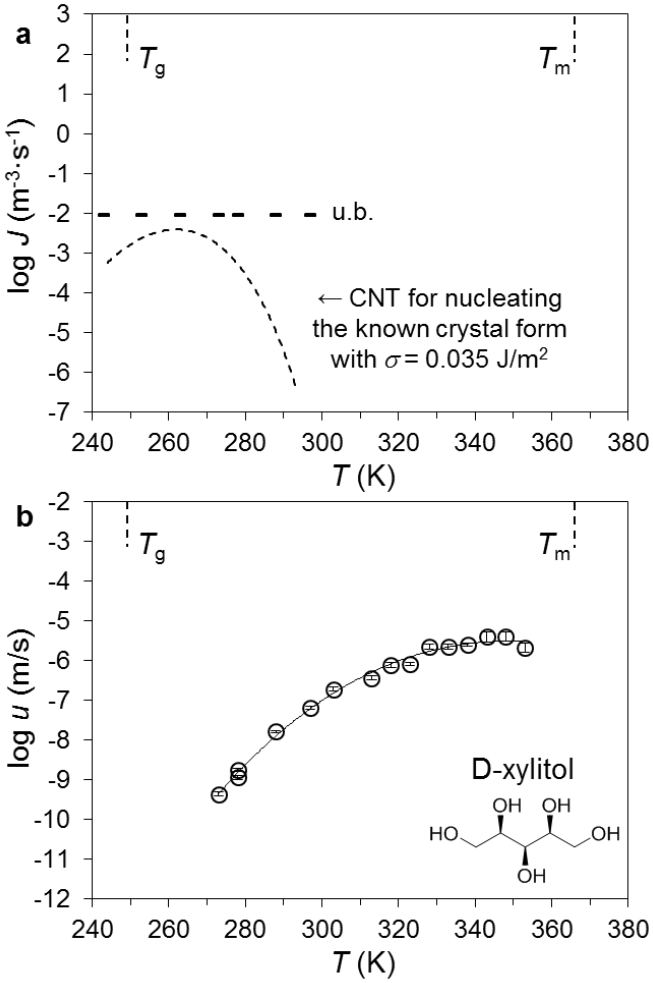

Figure 6. The upper bound for the rate of crystal nucleation (a) and the rate of crystal growth (b) in liquid D-xylitol vs. temperature. The curve in (a) is the CNT result with $\sigma = 0.035$ J/m^2 consistent with the experimental upper bound (see below); the curve in (b) is guide to the eye.

Glycerol. Similar to D-xylitol, nucleation was very slow in glycerol. As with D-xylitol, glycerol liquid was held at several temperatures near T_g (short dashes in Figure 7a), and heated to 278 K where growth rate is fast. No nucleation was observed in 3 days in a large sample of 10 g. Again, the absence of crystallization places an upper bound for J at 1 $m^{-3} \cdot s^{-1}$ (Figure 7a; this calculation assumes no induction time for nucleation).

In contrast to its slow crystal nucleation, the crystal growth rate is easily measured in glycerol. In Figure 7b, the rate of crystal growth (Ref. 29) is shown along with limited measurements from this work. The growth rate shows a maximum near 270 K (T_g + 81 K). (For our growth-rate measurements, glycerol was nucleated by dipping a glass tube containing glycerol in liquid nitrogen and the subsequent growth rate was recorded.)

It is worth noting that our result of slow nucleation in glycerol disagrees with Tammann and Jenckel,[29] who reported much faster nucleation. From their nuclei counts, we have calculated the J values (assuming no induction time) and plotted them in Figure 7a. Their maximal rate is one million times faster than our upper bound. One feature of these data, however, is a strong volume dependence of J: with a reduction of sample volume by a factor of 4, the J value decreases by a factor of 10. This suggests that the nucleation process measured is likely not a homogeneous process. The authors indicated residual moisture in glycerol as a possible cause for the variation of J.[29]

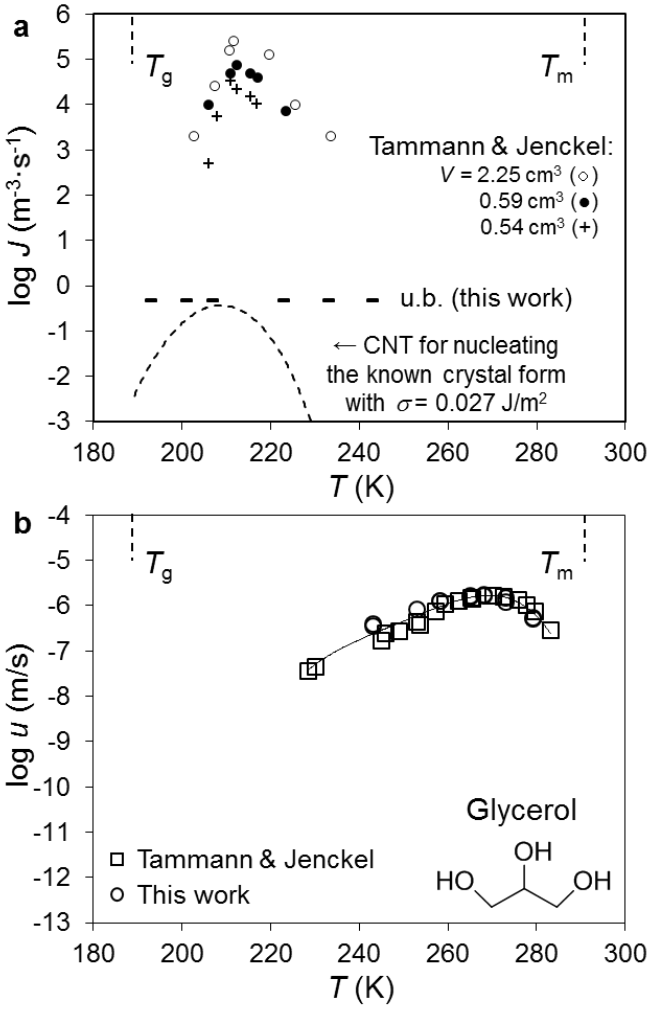

Figure 7. The upper bound rate of crystal nucleation (a) and the rate of growth (b) in liquid glycerol vs. temperature. The J values from Tammann and Jenckel[29] are reproduced in (a). The curve in (a) is the CNT result with σ = 0.027 J/m^2 (see below); the curve in (b) is guide to the eye.

Different Kinetics of Nucleation and Growth. A key result of this work is that the four liquids studied have similar crystal growth rates when compared at the same temperature relative to T_g, but very different nucleation rates. Figure 8 shows the two rates are plotted against T/T_g. In this format, the crystal growth rates nearly collapse to a "master curve" (Figure 8a), clustering within one decade at the same T/T_g. In contrast, the nucleation rates span a much larger range of at least 10 decades (Figure 8b). It is also seen that the growth rate reaches a maximum near 1.4 T_g, while the nucleation rate peaks near 1.1 T_g for the two systems for which there are data.

The literature data on inorganic silicates also suggest a wider variation of nucleation rates relative to crystal growth rates. For example, both nucleation and growth rates are reported for $Li_2O{\cdot}2SiO_2$,[37,38] $CaO{\cdot}2SiO_2$,[39] $Na_2O{\cdot}2CaO{\cdot}3SiO_2$,[40] and $2BaO{\cdot}TiO_2{\cdot}2SiO_2$;[41] the nucleation rates span 10 decades, while the growth rates are within 2.5 decades.

In Figure 9, we plot the rates of nucleation and growth against viscosity to assess whether these processes track bulk dynamics at low temperatures. For D-sorbitol, the viscosity is from Ref. 42; for D-arabitol and D-xylitol, it is calculated from the structural relaxation time τ_α (Ref. 43,44) using the relation: $\log \eta$ (Pa·s) = $\log \tau_\alpha$ (s) + C, where C = 8.7. The latter equation is valid for D-sorbitol;[42,45] it is also consistent with the Maxwell model for liquid relaxation. For additional comparison, Figure 9 also includes the literature data on lithium disilicate.[37,38]

For the polyalcohols, the growth rates cluster together when plotted against viscosity. This is expected from their collapse in Figure 8 when plotted against T/T_g. The growth rates decrease with increasing viscosity approximately following $\eta^{-0.75}$ (straight line) for nearly all available data, over ~10 decades of change in η; deviation occurs only at the very high temperatures (near the crystal melting point) where growth rate is limited by the thermodynamic driving force. The "decoupling" of crystal growth rate and viscosity from the simple relation $u \propto \eta^{-1}$ is known for other systems,[10]

indicating that viscosity is a poor representative of the kinetic barrier for crystal growth at low temperatures. For the nucleation rates, the slowdown with cooling occurs at higher viscosities relative to the growth rate. This is well understood in the framework of the CNT: the activation barrier is higher for creating a critical nucleus in a liquid than adding molecules to an existing crystal. From the limited nucleation data at high viscosities, we note that *nucleation slows down at approximately the same pace as growth* (straight line in Figure 9b). This similarity argues that both processes are kinetically controlled at low temperatures, and have a similar kinetic barrier. This kinetic barrier is lower (by ~ 25%) than that for viscous flow, given the power-law relation. Thus, for the polyalcohols studied, viscosity would be a poor representative for the kinetic factor for nucleation (k_J in eq. 1), while the crystal growth rate could better serve this purpose.

The literature data on lithium disilicate appear to present a similar picture. Relative to the polyalcohols, this system has faster nucleation and growth when compared at the same viscosity. This difference aside, we see that the crystal growth rate in lithium disilicate is well described by $u \propto \eta^{-0.75}$. There is some local departure from the relation, but the overall trend is in agreement over a wide range of viscosity (11 decades). This conclusion is consistent with that of Nascimento and Zanotto who performed a more sophisticated analysis, obtaining $u_{kin} \propto \eta^{-0.81}$, where u_{kin} is the value of u corrected for the driving force for crystallization.[46] Similar to the polyalcohols, the nucleation rate of lithium disilicate reaches its maximum at a higher viscosity than the growth rate; at even higher viscosities, nucleation slows down with cooling. The literature data (from many groups) show considerable scatter at high viscosities, but the overall trend seems parallel to that for the growth rate (straight line). Thus for this inorganic system, it is also reasonable to conclude that nucleation and growth have roughly the same kinetic barrier. Given the scatter in the nucleation data, this conclusion is not particularly strong. It also differs from that of Fokin *et al*.[47]

who compared the effective diffusion coefficients for nucleation and growth, D_J and D_u. In their study, D_J is calculated from the "lag time for nucleation", not the steady-state nucleation rate at low temperatures, and D_u from the crystal growth rate. They find a stronger temperature dependence for D_J (by ~ 30%). Given that both approaches are valid for evaluating the kinetic factors for nucleation, each with its own assumptions, this discrepancy calls for further work to develop a consistent picture. Fokin *et al*. attribute the difference between D_J and D_u to the different compositions of the critical nucleus and the macroscopic crystal. This complexity does not arise in the single-component systems studied here. It is possible that the assumption of similar kinetic factor for nucleation and growth could be more accurate for single-component liquids than multi-component systems like lithium disilicate.

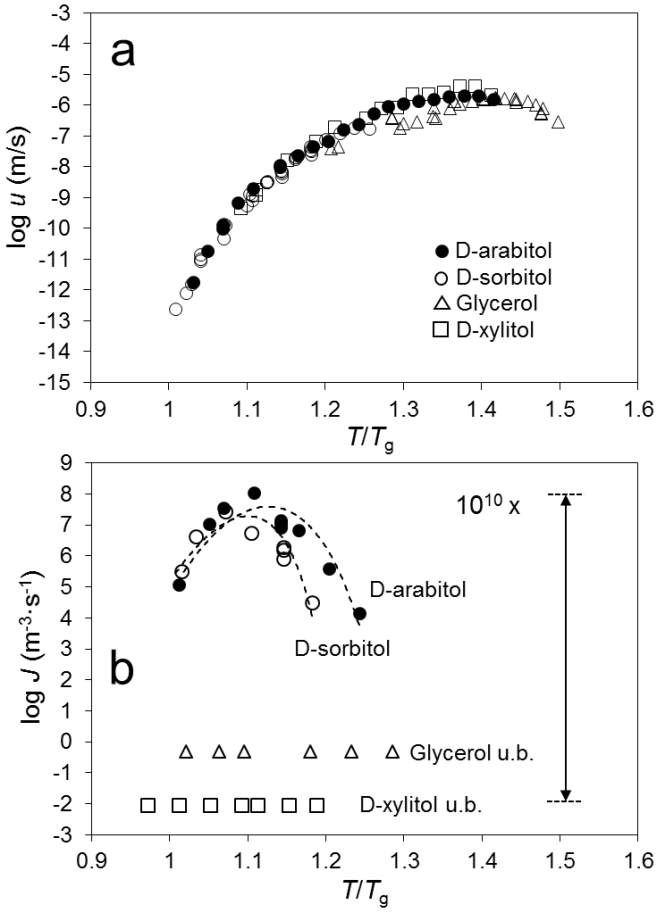

Figure 8. Comparison of the rates of crystal growth (a) and nucleation (b) in the four polyalcohols studied. Temperature has been scaled by T_g. "u.b." means upper bound. The curves in (b) are the CNT fits (discussed below).

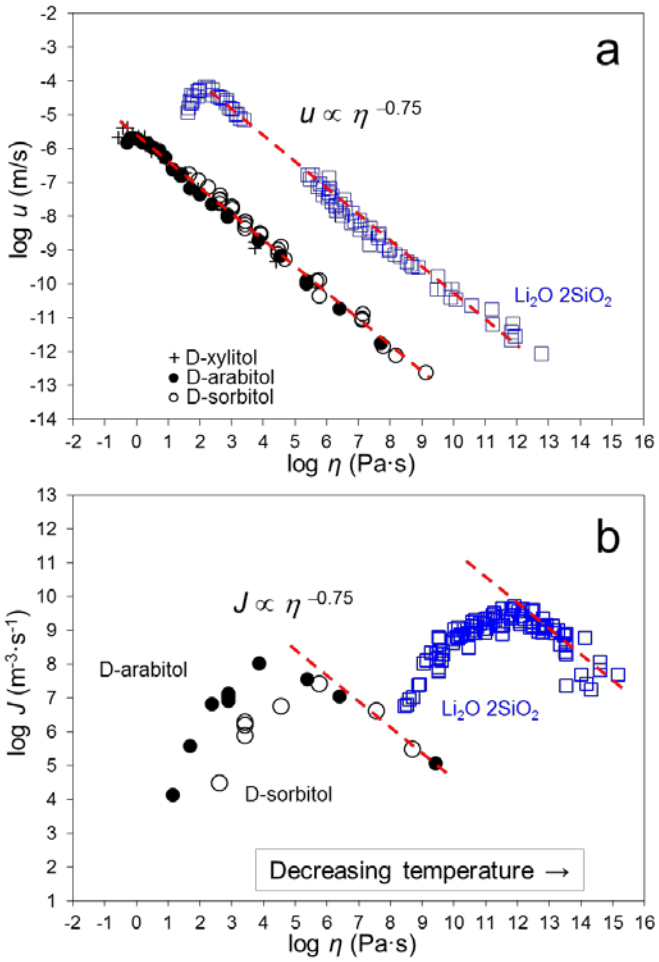

Figure 9. Rates of crystal growth (a) and nucleation (b) plotted against viscosity for polyalcohols and lithium disilicate. The data trends at low temperatures are approximately described by $u \propto \eta^{-0.75}$ and $J \propto \eta^{-0.75}$ (lines). Glycerol is excluded from the u plot for the small temperature range over which u was measured and a possible influence from water contamination.[29] The lithium silicate data are from the compilations in Ref. 37,38, and data from different sources are not distinguished.

3.5 Discussion

This study has investigated the rate of crystal nucleation in four glass-forming polyalcohols (glycerol, D-xylitol, D-arabitol and D-sorbitol). These polyalcohols have similar rates of crystal growth when compared at the same temperature scaled by T_g, but very different crystal nucleation rates (Figure 8). In this section, we discuss these results in the framework of the CNT.

To implement the CNT, a suitable kinetic factor (k_J in eq. 1) is required. It is common to express k_J as a function of some measure of liquid dynamics:

$$k_J = f_D D \qquad (2)$$

$$k_J = f_\eta/\eta \qquad (3)$$

$$k_J = f_\tau/\tau_\alpha \qquad (4)$$

where D is the diffusion coefficient, η is the viscosity, τ_α is the structural relaxation time, and f_D, f_η and f_τ are temperature-insensitive constants. (Detailed CNT equations provide explicit expressions for the temperature-insensitive constants, but we set aside these details in this work.) Since D is unavailable for the polyalcohols, the available η and τ_α are possible candidates for evaluating k_J.[42,43,44,45] We note that η and τ_α should be essentially equivalent for this purpose since they are approximately proportional to each other.

In addition, motivated by the finding (Figure 9) that nucleation and growth rates decrease at a similar pace at low temperatures, we shall evaluate another way to calculate k_J

$$k_J = f_u u \qquad (5)$$

where u is the crystal growth rate at low temperatures (or more rigorously u_{kin}), and f_u is a temperature-insensitive constant. Eq. 5 is not a standard choice in implementing the CNT, but the notion is embedded in the theories of crystal growth,[10] where the kinetic factor for growth k_u is

written in the same form as k_J (*e.g.* proportional to D). The results in Figure 9 suggest that crystal growth rate could provide a more accurate estimate of k_J than viscosity.

Following the literature procedure,[2] we test the CNT by plotting a "kinetically scaled" nucleation rate against $1/(T\Delta G_v^2)$. For example, if η gives an accurate description of k_J (eq. 3), the function ln ($J\eta$) is plotted, and if the CNT holds, the resulting plot should be linear, with its slope yielding the interfacial free energy σ. Likewise, $J\tau_\alpha$ and J/u are plotted for other choices for k_J. Figures 10 and 11 show these plots. The ΔG_v values needed for these plots are calculated using standard thermodynamic equations and calorimetric data (see *Supporting Information*).

Figures 10 and 11 show that all the reduced nucleation rates are approximately linear on $1/(T\Delta G_v^2)$, indicating a reasonable performance of the CNT implemented with all the kinetic factors (eqs. 3-5). In addition, we find that among these choices, *the linearity is the best for the (J/u) plot*. This is seen by comparing the R^2 values and inspecting the curvature of each plot. We interpret this to mean that of the three choices, crystal growth rate gives the most accurate description of the kinetic factor for nucleation (eq. 5), consistent with our conclusion above in connection with Figure 9. With this choice, the CNT gives a reasonable description of our data. From the slopes of lines in Figures 10a and 11a, we obtain σ = 0.013 J/m^2 for D-sorbitol and 0.026 J/m^2 for D-arabitol; from the intercepts, log f_u (m^{-4}) = 20.5 for D-sorbitol and log f_u (m^{-4}) = 22.7 for D-arabitol. The curves in Figures 4a and 5a are calculated from these parameters using eq. 1. The σ values obtained are reasonable considering the typical liquid/vapor interfacial energies of organic liquids (~0.05 J/m^2).

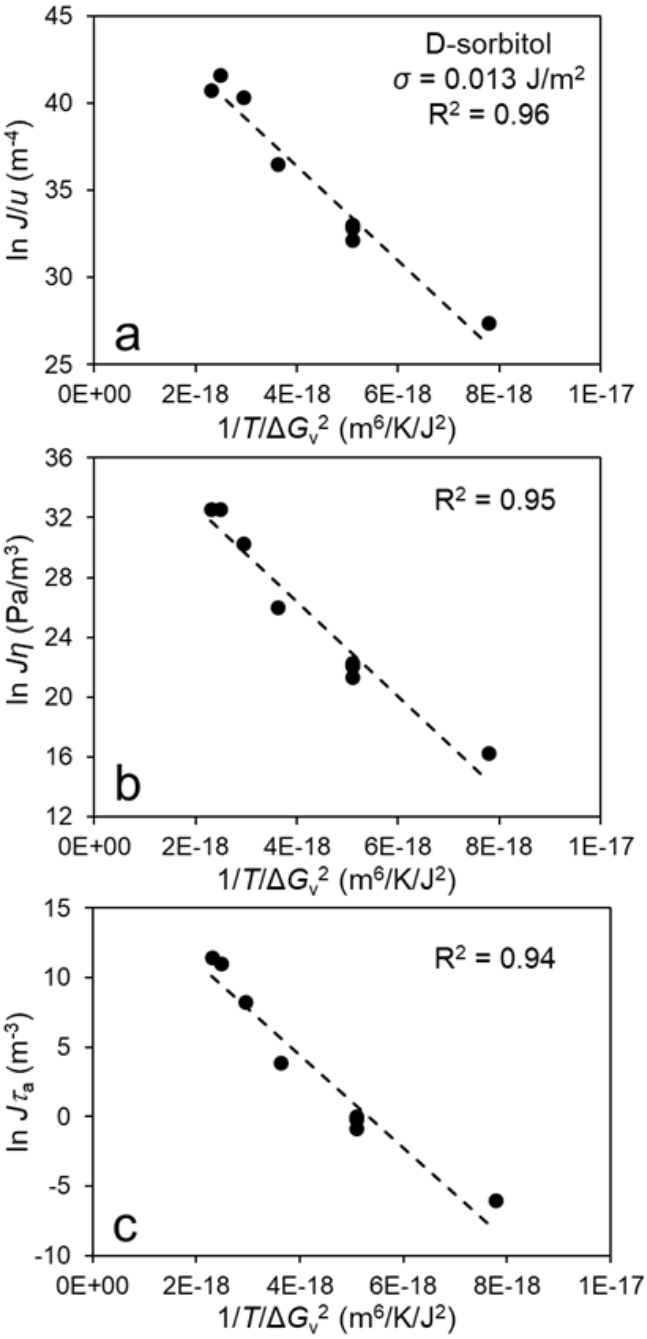

Figure 10. CNT test for D-sorbitol. ln (J/u), ln ($J\eta$), and ln ($J\tau_\alpha$) are plotted against $1/(T\Delta G_v^2)$. A straight line is expected if the CNT holds with a constant σ. The best linearity is seen for the J/u plot (a), suggesting the kinetic factor for nucleation is best described as being proportional to u.

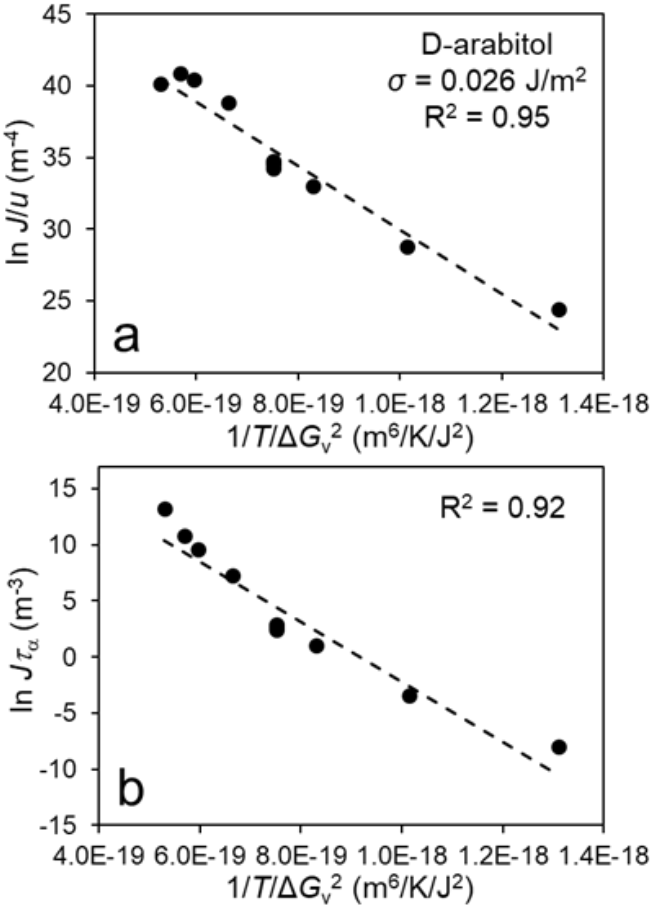

Figure 11. CNT test for D-arabitol. ln (J/u) and ln ($J\tau_\alpha$) are plotted against $1/(T\Delta G_v^2)$. A straight line is expected if the CNT holds with a constant σ. Better linearity is seen for the J/u plot (a), suggesting the kinetic factor for nucleation is better described as being proportional to u.

According to the CNT, the diameter of the critical nucleus is $d_c = \frac{4\sigma}{\Delta G_v}$. For D-sorbitol, we obtain d_c = 1.3 to 2.6 nm for the temperature range studied. This corresponds to 6 – 45 molecules per critical nucleus (the molecular diameter of D-sorbitol is ~ 0.6 nm). Similarly, for D-arabitol, we obtain d_c = 1.2 to 2.2 nm for the temperature range studied, corresponding to 6 – 31 molecules per critical nucleus (the molecular diameter of D-arabitol is ~ 0.5 nm). In the case of lithium disilicate, the critical nucleus inferred from the CNT analysis contains approximately 20 structural units.[37] As noted by other workers,[2] the small number of molecules in a critical nucleus questions the validity of using the bulk free-energy difference ΔG_v to represent the free-energy difference between a crystal nucleus and the surrounding liquid.

In summary, the CNT provides a reasonable description of our nucleation rates if the kinetic factor k_J is chosen to scale as u. The CNT's performance is slightly worse if k_J is chosen to scale as η or τ_α. This suggests that the kinetic barrier for nucleation is more accurately described as similar to the barrier for crystal growth than to the barrier for viscous flow. Given the widely available crystal growth rate data, this potentially offers a general way to analyze nucleation rates. This is not to say that the crystal growth rate is a perfect representative of the kinetic factor for nucleation. In principle, molecular mobility at a nucleus/liquid interface cannot be identical with that at a crystal/liquid interface. Nevertheless, if the two prove to be sufficiently similar, it is of significant practical value to use easily-measured growth rates to represent the kinetic factor for nucleation.

Turnbull noted that for pure metals, the ratio $\alpha = \sigma_g/\Delta H_m$ is approximately 0.5, where $\sigma_g = \sigma_g V^{2/3} N_A^{1/3}$ is the molar free energy of the crystal nucleus/liquid interface, with V being the specific volume and N_A Avogadro's number, and ΔH_m is the enthalpy of fusion.[48] Thomas and Staveley reported that for molecular liquids, $\alpha \approx 1/3$.[49] From our results, we obtain α = 0.10 for D-sorbitol

and 0.13 for D-arabitol, which are smaller than those of Thomas and Staveley. This difference is not understood at present. One possible reason is that the σ values from this studyy are evaluated near T_g at which the density difference between the crystal and the liquid is reduced relative to the systems studied by Thomas and Staveley near crystal melting points.

Given that the CNT can describe the nucleation rates in D-sorbitol and D-arabitol, we apply it to D-xylitol. For this system, only upper bounds have been obtained for J. Using its crystal growth rate to describe the kinetic factor k_J and assuming $f_u = 10^{22.7}$ m^{-4} (the value for D-arabitol), we obtain $\sigma > 0.035$ J/m^2 (we have assumed that the known crystal form of xylitol crystallizes). In Figure 6, the CNT result on D-xylitol is shown with $\sigma = 0.035$ J/m^2. For glycerol, the same analysis yielded $\sigma > 0.027$ J/m^2 (again assuming the known crystal form crystallizes). For this analysis, the limited growth-rate data is extended to lower temperatures, assuming $u \propto \tau_\alpha$.[50] In Figure 7, the CNT result on glycerol is shown with $\sigma = 0.027$ J/m^2. It is worth noting that all these σ values are quite similar, but in the framework of the CNT, enough to cause more than 10-orders-of-magnitude changes in nucleation rates (to illustrate this point, for D-xylitol, changing σ by 0.002 J/m^2 alters the predicted J by a factor of 100). This confirms the difficulty to make first-principle predictions by CNT because highly precise interfacial free energies are needed.

Dependence on Crystal Structure. It is worth noting that the nucleation rates are similar in D-sorbitol and D-arabitol when compared at the same viscosity (Figure 9), but the driving forces for the two processes differ significantly. For D-sorbitol, the nucleating polymorph is a low-crystallinity, metastable phase called polymorph E; its melting point is ~20 K below that of the stable form (γ). For D-arabitol, the nucleating polymorph studied is the stable form (Form I). At the temperatures of maximal nucleation rates, the driving force ΔG_v for nucleating D-sorbitol

polymorph E is approximately half that for nucleating D-arabitol Form I (3.4×10^7 J/m^3 vs. 7.3×10^7 J/m^3; Figure S1). According to the CNT, for D-sorbitol's polymorph E to nucleate at a similar rate as D-arabitol's Form I, its σ value must be smaller, by a factor of $(7.3/3.4)^{2/3} \sim 2$, which is in agreement with the σ values obtained from CNT fitting (0.013 J/m^2 for D-sorbitol and 0.026 J/m^2 for D-arabitol). This example shows that the observed rate of nucleation depends strongly on whether a viable crystal structure exists to which the liquid can crystallize. If the metastable polymorph E did not exist, the apparent nucleation rate in D-sorbitol would have been much slower (given the small driving force ΔG_v). In fact, our limited work indicates that the γ polymorph of D-sorbitol nucleates at least 4 orders of magnitude slower than polymorph E, despite a larger driving force. The absence of fast-nucleating crystal structures could explain the slow nucleation of D-xylitol and glycerol.

The analysis above suggests that the nucleation rate of a given molecular liquid have much to do with its crystal-structure landscape, in particular, whether a fast-nucleating polymorph exists, even if it grows at a similar rate as other polymorphs. Thus, one approach to understanding the glass-forming ability of molecular liquids is to examine the crystal-structure landscape and evaluate the propensity for each polymorph to nucleate. There has been significant progress in the computational prediction of crystal structures and polymorphs.[51,52] This capability could be combined with the evaluation of the crystal/liquid interfacial free energy to predict whether a given polymorph will nucleate quickly,[15] thus providing an assessment of the glass-forming ability from the molecular structure alone.

Size of Critical Nucleus and Length Scale for Cooperative Rearrangement. Recently, Gupta *et al.*[37] investigated why the CNT appears to describe the nucleation rate in lithium disilicate at

high temperatures but not at low temperatures. They argue that the failure of the CNT is related to the dynamic heterogeneity in deeply cooled liquid. This idea builds on the proposal of Stevenson and Wolynes[53] that the mechanism of crystallization changes as the size of the cooperatively rearranging region (CRR) increases and eventually exceeds the size of the critical nucleus. Gupta *et al.* suggest that the failure of the CNT for lithium disilicate coincides with the intersection of the two length scales. Here we test their idea using the data on D-sorbitol. For this system, the CNT appears to hold over the full range of temperature studied (Figure 10a). In Figure 12 we plot the length scale of dynamic heterogeneity ξ in D-sorbitol obtained by different methods: 3.6 nm at 261 K (by DSC),[20] 2.5 nm at 275 K (ssNMR),[54] and 1.5 nm at 267 K (Boson peak).[55] This length scale should be an upper bound for and is often equated with the size of the CRR. The experimental ξ values are quite scattered, a result of different methods and assumptions employed. Qiu and Ediger argue that ssNMR provides the most direct measurement of ξ.[54] These experimental values are in broad agreement with theoretical predictions; for example, 2.3 nm at 275 K by Qiu and Ediger[54] and 2.7 nm at 268 K by Capaccioli *et al*.[56] As temperature increases, ξ is expected to decrease, approaching the molecular diameter (0.6 nm). This expectation is illustrated in Figure 12 using one of the theoretical predictions (an entropy-fluctuation model by Ediger).[54]

Figure 12 also plots the diameter of the critical nucleus (d_c) calculated from the nucleation rates and the CNT. The d_c curve decreases with cooling and at the temperatures studied (273 – 318 K), d_c is either comparable to or smaller than the experimental values of ξ. According to Gupta *et al.*, the CNT should fail under these circumstances. Our data, however, show no such failure. Thus, for this system, there is no obvious indication that the CNT fails as a result of an increasing length scale of cooperative rearrangement. It would be interesting to measure the nucleation rate in D-sorbitol down to even lower temperatures to see if the CNT continues to hold.

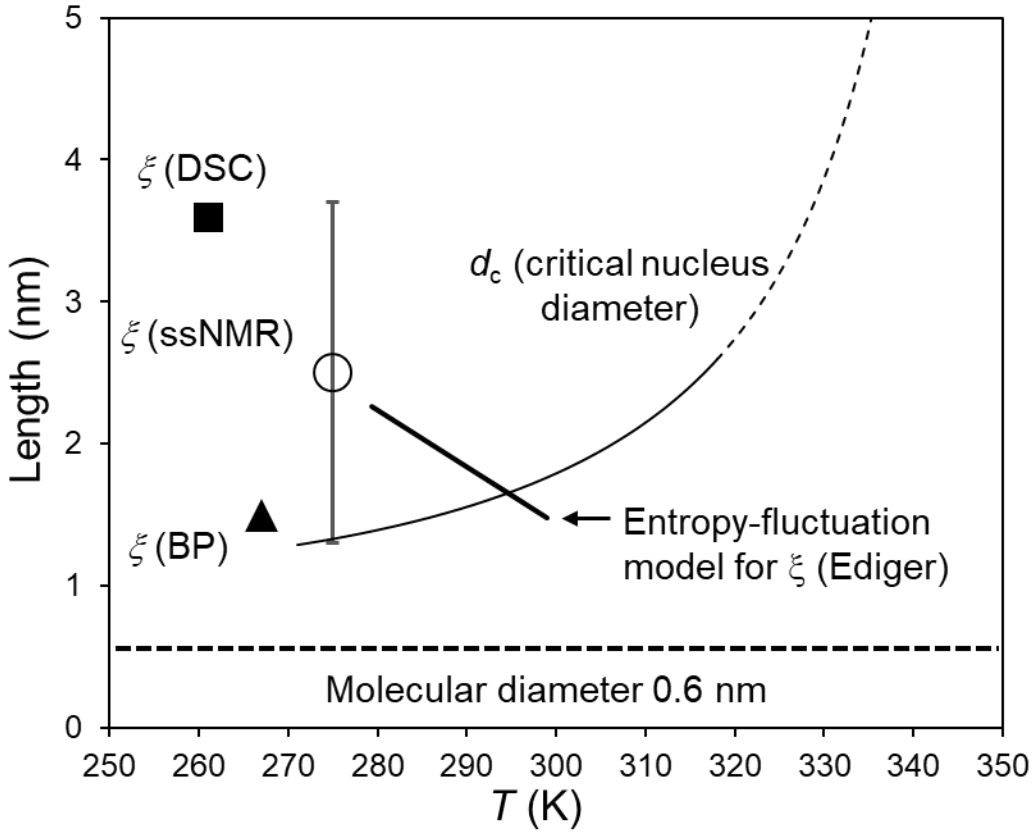

Figure 12. Comparison of the diameter of the critical nucleus d_c in D-sorbitol and the length scale of dynamic heterogeneity ξ obtained by different methods.[20,54,55] d_c is calculated from the nucleation rates and the CNT; the solid portion of the d_c curve corresponds to the experimental temperature range and the dashed portion to CNT extrapolation to higher temperatures. A theoretical prediction of ξ is included[54] to illustrate to the expected temperature dependence of ξ. The molecular diameter of D-sorbitol (0.6 nm) is indicated.

3.6 Conclusion

This study has measured the crystal nucleation rates in four structurally similar glass-forming liquids: D-sorbitol, D-arabitol, D-xylitol, and glycerol. The measurements were made using the one-stage and two-stage methods, yielding consistent results. Similar rates of nucleation were observed in D-sorbitol and D-arabitol, but the rates were too slow to measure in glycerol and D-xylitol. For these four systems, the nucleation rates span a wide range (by at least 10 orders of magnitude), but their crystal growth rates are similar when compared at the same T_g-scaled temperature. Our results indicate a similar kinetic barrier for crystal nucleation and growth, but this barrier is lower than that for the viscous flow of the bulk liquid. The CNT describes our data reasonably well if the kinetic barrier for nucleation is taken to be the same as that for growth. The theory seems to hold down to the lowest temperature of our study, showing no sign of failure as the length scale for corporative rearrangement exceeds the size of the critical nucleus.

Near and below T_g, molecular glasses are known to exhibit a fast mode of crystal growth (the so-called “glass-to-crystal” or GC growth mode).[57,58] This growth mode is apparently unlimited by bulk dynamics in the liquid state, and has been given a number of explanations, including homogeneous nucleation,[58] shrinking critical-nucleus size to below the dynamic length scale,[53] and micro-fracture and surface mobility. [59] The phenomenon has been observed in many molecular glass-formers (though not the ones studied here). It would be of interest to learn whether there is a fast “glass-to-crystal” nucleation mode in molecular glasses.

3.7 Acknowledgments

We thank AbbVie for supporting this work and the Zeeh Pharmaceutical Experiment Station for experimental assistance. We thank Yixu Zong for translating Ref. 29 from German and John Perepezko and Mark Ediger for helpful discussions.

3.8 References

[1] D. Turnbull, and J. C. Fisher, The Journal of Chemical Physics **17**, 71 (1949).

[2] V. M. Fokin, E. D. Zanotto, N. S. Yuritsyn, and J. W. P. Schmelzer, Journal of Non-Crystalline Solids **352**, 2681 (2006).

[3] K. F. Kelton, Solid State Physics **45** (1991) 75.

[4] G. C. Sosso, J. Chen, S. J. Cox, M. Fitzner, P. Pedevilla, A. Zen, and A. Michaelides, Chemical Reviews **116**, 7078 (2016).

[5] M. L. F. Nascimento, and E. D. Zanotto, The Journal of Chemical Physics **133**, 174701 (2010).

[6] H. Laksmono, T. A. McQueen, J. A. Sellberg, N. D. Loh, C. Huang, D. Schlesinger, R. G. Sierra, C. Y. Hampton, D. Nordlund, M. Beye, A. V. Martin, A. Barty, M. M. Seibert, M. Messerschmidt, G. J. Williams, S. Boutet, K. Amann-Winkel, T. Loerting, L. G. M. Pettersson, M. J. Bogan, and A. Nilsson, The Journal of Physical Chemistry Letters **6**, 2826 (2015).

[7] D. Turnbull, The Journal of Chemical Physics **20**, 411 (1952).

[8] J. Bokeloh, R. E. Rozas, J. Horbach, and G. Wilde, Physical Review Letters **107**, 145701 (2011).

[9] D. Turnbull, The Journal of Physical Chemistry **66**, 609 (1962).

[10] M. D. Ediger, P. Harrowell, and L. Yu, The Journal of Chemical Physics **128**, 034709 (2008).

[11] J. Orava, and A. L. Greer, The Journal of Chemical Physics **140**, 214504 (2014) .

[12] C. Huang, S. Ruan, T. Cai, and L. Yu, The Journal of Physical Chemistry B **121**, 9463 (2017).

[13] C. L. Jackson, and G. B. McKenna, The Journal of Chemical Physics **93**, 9002 (1990).

[14] B. B. Laird, and R. L. Davidchack, The Journal of Physical Chemistry B **109**, 17802 (2005).

[15] J. Gerges, and F. Affouard, The Journal of Physical Chemistry B **119**, 10768 (2015).

[16] D. Turnbull, Contemporary Physics **10**, (1969) 473.

[17] M. K. Mapes, S. F. Swallen, and M. D. Ediger, The Journal of Physical Chemistry B **110**, 507 (2006).

[18] S. F. Swallen, K. Traynor, R. J. McMahon, M. D. Ediger, and T. E. Mates, The Journal of Physical Chemistry B **113**, 4600 (2009).

[19] J. Deubener, M. Montazerian, S. Krüger, O. Peitl, E.D. Zanotto, Journal of Non-Crystalline Solids **474**, 1 (2017).

[20] E. Hempel, G. Hempel, A. Hensel, C. Schick, and E. Donth, The Journal of Physical Chemistry B **104**, 2460 (2000).

[21] G. E. Gibson, and W. F. Giauque, Journal of the American Chemical Society **45**, 93 (1923).

[22] L. Yu, Crystal Growth & Design **3**, 967 (2003).

[23] H. P. Diogo, S. S. Pinto, and J. J. Moura Ramos, Carbohydrate Research **342**, 961 (2007).

[24] L. Carpentier, S. Desprez, and M. Descamps, Journal of Thermal Analysis and Calorimetry **73**, 577 (2003).

[25] G. Barone, G. D. Gatta, D. Ferro, and V. Piacente, Journal of the Chemical Society, Faraday Transactions **86**, 75 (1990).

[26] R. A. Talja, and Y. H. Roos, Thermochimica Acta **380**, 109 (2001).

[27] A. Nezzal, L. Aerts, M. Verspaille, G. Henderickx, and A. Redl, Journal of Crystal Growth **311**, 3863 (2009).

[28] L. Carpentier, K. Filali Rharrassi, P. Derollez, and Y. Guinet, Thermochimica Acta **556**, 63 (2013).

[29] G. Tammann, and E. Jenckel, Zeitschrift für anorganische und allgemeine Chemie **193**, 76 (1930).

[30] T. Wu, and L. Yu, The Journal of Physical Chemistry B **110**, 15694 (2006).

[31] M. Rukiah, J. Lefebvre, O. Hernandez, W. Beek, and M. Serpelloni, Journal of Applied Crystallography **37**, 766 (2004).

[32] A. Schouten, J. A. Kanters, J. Kroon, S. Comini, P. Looten, and M. Mathlouthi, Carbohydrate Research **312**, 131 (1998).

[33] J. Sztatisz, S. Gal, L. Fodor, and E. Pungor, Journal of thermal analysis **12** 351 (1977).

[34] L. Yu, Journal of the American Chemical Society **125** 6380 (2003).

[35] J. Kopf, M. Morf, B. Zimmer, and P. Köll, Carbohydrate Research **218**, 9 (1991).

[36] M. Descamps, and E. Dudognon, Journal of Pharmaceutical Sciences **103**, 2615 (2014).

37 P. K. Gupta, D. R. Cassar, and E. D. Zanotto, The Journal of Chemical Physics 145, 211920 (2016).

[38] M. L. F. Nascimento, V. M. Fokin, E. D. Zanotto, and A. S. Abyzov, The Journal of Chemical Physics **135**, 194703 (2011).

[39] L. Gránásy, T. Wang, and P. F. James, The Journal of Chemical Physics **108**, 7317 (1998).

[40] O. V. Potapov, V. M. Fokin, V. L. Ugolkov, L. Ya. Suslova, and V. N. Filipovich, Glass Physics and Chemistry **26**, 27 (2000).

[41] A. A. Cabral, V. M. Fokin, E. D. Zanotto, and C. R. Chinaglia, Journal of Non-Crystalline Solids **330**, 174 (2003).

[42] A. Nakheli, A. Eljazouli, M. Elmorabit, E. Ballouki, J. Fornazero, and J. Huck, Journal of Physics: Condensed Matter **11**, 7977 (1999).

[43] L. Carpentier, M. Paluch, and S. Pawlus, The Journal of Physical Chemistry B **115**, 1062 (2011).

[44] R. Wehn, P. Lunkenheimer, and A. Loidl, Journal of Non-Crystalline Solids **353**, 3862 (2007).

[45] A. Minoguchi, K. Kitai, and R. Nozaki, Physical Review E **68**, 031501 (2003).

[46] M. L. F. Nascimento, and E. D. Zanotto, The Journal of Chemical Physics **133**, 174701 (2010).

[47] V. M. Fokin, J. W. P. Schmelzer, M. L. F. Nascimento, and E. D. Zanotto, E. D., J. Chem. Phys. 126 234507 (2007).

[48] D. Turnbull, J. Appl. Phys. **21**, 1022 (1950).

[49] D. G. Thomas, and L. A. K. Staveley, Journal of the Chemical Society **0**, 4569 (1952).

[50] N. Menon, K. P. O'Brien, P. K. Dixon, L. Wu, S. R. Nagel, B. D. Williams, J. P. Carini, Journal of Non-Crystalline Solids **141**, 61 (1992).

[51] S. L. Price, Chem. Soc. Rev. **43,** 2098 (2014).

[52] A. M. Reilly *et al.*, Acta Crystallogr., Sect. B **72**, 439 (2016).

[53] J. D. Stevenson, and P. G. Wolynes, The Journal of Physical Chemistry A **115**, 3713 (2011).

[54] X. Qiu, and M. D. Ediger, The Journal of Physical Chemistry B **107**, 459 (2003).

[55] L. Hong, P. D. Gujrati, V. N. Novikov, and A. P. Sokolov, The Journal of Chemical Physics **131**, 194511 (2009).

[56] S. Capaccioli, G. Ruocco, and F. Zamponi, The Journal of Physical Chemistry B **112** (2008) 10652.

[57] R. J. Greet, and D. Turnbull, The Journal of Chemical Physics **46**, 1243 (1967).

[58] T. Hikima, Y. Adachi, M. Hanaya, and M. Oguni, Phys. Rev. B **52**, 3900 (1995).

[59] C. T. Powell, H. Xi, Y. Sun, E. Gunn, Y. Chen, M. D. Ediger, and L. Yu, The Journal of Physical Chemistry B **119**, 10124 (2015).

3.9 Supporting Information

Nucleation rate, growth rate, and other relevant physical properties of the polyalcohols studied

Table S1. D-sorbitol.

Steady-state crystal nucleation rate	T (K)	log J ($m^{-3}s^{-1}$)
	273	5.5 (0.3)
	278	6.6 (0.3)
	288	7.4 (0.3)
	297	6.8 (0.3)
	308	6.1 (0.3)
	318	4.5 (0.3)
Crystal growth rate	T (K)	log u (m/s) (this work)
	288	-10.34 (0.02)
	296	-9.26 (0.04)
	308	-8.24 (0.01)
	318	-7.67 (0.01)
	Polynomial fitting of growth rates from this and previous works (Ref. 1 and 2): $\log u$ (m/s) = $-0.0011332T^2 + 0.77634T - 139.7$, 271 K < T < 338 K	
Thermodynamic properties for calculating ΔG_v	T_m (K) = 353, ΔH_m (kJ/mol) = 26.7, ΔC_p (liq.–cryst., J/mol/K) = $694.8-1.785T$, T = 271 – 353 K V_{sp} (crystal, cm^3/g) = $1.458*10^{-7}T^2 + 1.394*10^{-5}T + 0.66013$, T = 260 – 301 K (Ref. 3)	
Viscosity	$\log \eta$ (Pa s) = $-4.4321 + 682.08/(T - 221)$, T = 268 – 413 K (Ref. 4)	
Structural relaxation time	$\tau_\alpha = 1/(2\pi f_m)$, where $\log f_m$ (Hz) = $12.7 – 572/(T - 229)$, T = 263 – 344 K (Ref. 5)	

Table S2. D-arabitol.

Steady-state crystal nucleation rate	T (K)	log J ($m^{-3}s^{-1}$)
	263	5.1 (0.3)
	273	7.0 (0.3)
	278	7.6 (0.3)
	288	8.0 (0.3)
	297	7.0 (0.3)
	303	6.8 (0.3)
	313	5.6 (0.3)
	323	4.1 (0.3)
Crystal growth rate	T (K)	log u (m/s)
	268	-11.75 (0.09)
	273	-10.72 (0.07)
	278	-9.95 (0.05)
	283	-9.16 (0.10)
	288	-8.71 (0.05)
	297	-7.98 (0.03)
	303	-7.62 (0.04)
	308	-7.35 (0.05)
	313	-7.16 (0.04)
	318	-6.78 (0.03)
	323	-6.61 (0.01)
	328	-6.26 (0.02)
	333	-6.04 (0.02)
	338	-5.96 (0.02)
	343	-5.85 (0.02)
	348	-5.80 (0.01)
	353	-5.71 (0.01)
	358	-5.67 (0.03)
	363	-5.68 (0.01)
	368	-5.80 (0.03)
	Polynomial fitting of growth rates: $\log u$ (m/s) = $0.0000067522T^3 - 0.0071578T^2 + 2.5476T - 310.15$, 268 K < T < 363 K	
Thermodynamic properties for calculating ΔG_v	T_m (K) = 376, ΔH_m (kJ/mol) = 39.9 (0.2), ΔC_p (liq.–cryst., J/mol/K) = $-4.15*10^{-3}T^2 + 2.56T - 210$, T = 268 – 363 K ρ (crystal, g/cm^3) [a] = 1.493 at T = 295 K (Ref. 6)	
Structural relaxation time	$\log \tau_\alpha = -11.98 + 935/(T-231)$, T = 265 – 313 K (Ref. 7)	

Note: [a] ρ of D-arabitol crystal is consistent with 1.489 g/cm^3 for L-arabitol crystal at room temperature[8].

Table S3. D-xylitol.

Crystal growth rate	T (K)	log u (m/s)
	273	-9.35 (0.04)
	278	-8.84 (0.05)
	288	-7.78 (0.04)
	297	-7.18 (0.04)
	303	-6.72 (0.05)
	313	-6.43 (0.05)
	318	-6.11 (0.07)
	323	-6.08 (0.03)
	328	-5.64 (0.06)
	333	-5.64 (0.06)
	338	-5.58 (0.04)
	343	-5.39 (0.12)
	348	-5.39 (0.11)
	353	-5.67 (0.10)
	Polynomial fitting of growth rates: $\log u$ (m/s) = $-0.00066136T^2 + 0.46215T - 86.17$, 273 K < T < 348 K	
Structural relaxation time	$\tau_\alpha = 6.4*10^{-14} \exp[1290/(T-210)]$, T = 250 – 400 K (Ref. 9)	

Table S4. Glycerol.

Crystal growth rate	T (K)	log u (m/s) (this work)
	243	-6.41 (0.03)
	253	-6.06 (0.02)
	258	-5.88 (0.01)
	265	-5.78 (0.01)
	268	-5.76 (0.01)
	273	-5.87 (0.04)
	279	-6.27 (0.02)
Structural relaxation time	$\tau_\alpha = 1/(2\pi f_m)$, where $f_m = 7.4*10^{13} \exp[-2240/(T-130)]$, T = 184 – 355 K (Ref. 10)	

Calculation of ΔG_v (thermodynamic driving force for crystallization)
ΔG_v is calculated with the following equations:

$$\Delta G_V = (\Delta H_V - T\Delta S_V)$$

$$\Delta H_V = \Delta H_m + \int_{T_m}^{T} (C_{pl} - C_{pc})dT$$

$$\Delta S_V = \Delta S_m + \int_{T_m}^{T} (C_{pl} - C_{pc})dlnT$$

where ΔH_v and ΔS_v are enthalpy and entropy differences between the crystal and the liquid, ΔH_m and ΔS_m are the heat of fusion and the entropy of fusion, and (C_{pl} - C_{pc}) is the heat capacity difference between the liquid and the crystal. The fusion data are from this work and the literature (Table 1 in the main text);[1,11] heat capacities are from this work by temperature modulated DSC (Tables S1 and S2) except for glycerol whose data are from Ref. 11. To convert the per-mole value of ΔG_v to the per-volume value, crystal densities are used, given in Tables S1 and S2 for D-sorbitol and D-arabitol; ρ (crystal) = 1.515 g/cm^3 for D-xylitol at room temperature,[12] and 1.402 g/cm^3 for glycerol at 143 K.[13] The calculated ΔG_v values are shown in Figure S1.

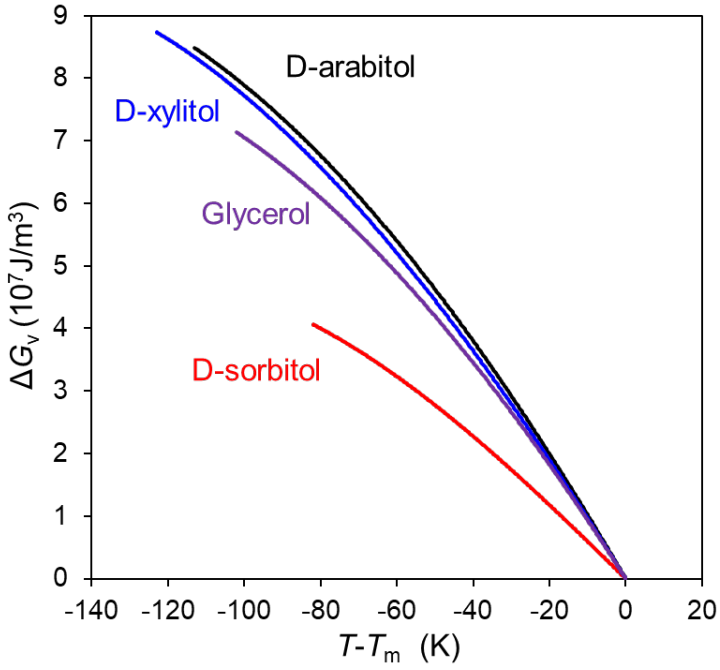

Figure S1. Calculated ΔG_v values for D-sorbitol, D-arabitol, D-xylitol and glycerol as a function of temperature relative to T_m.

Polymorphs of D-arabitol

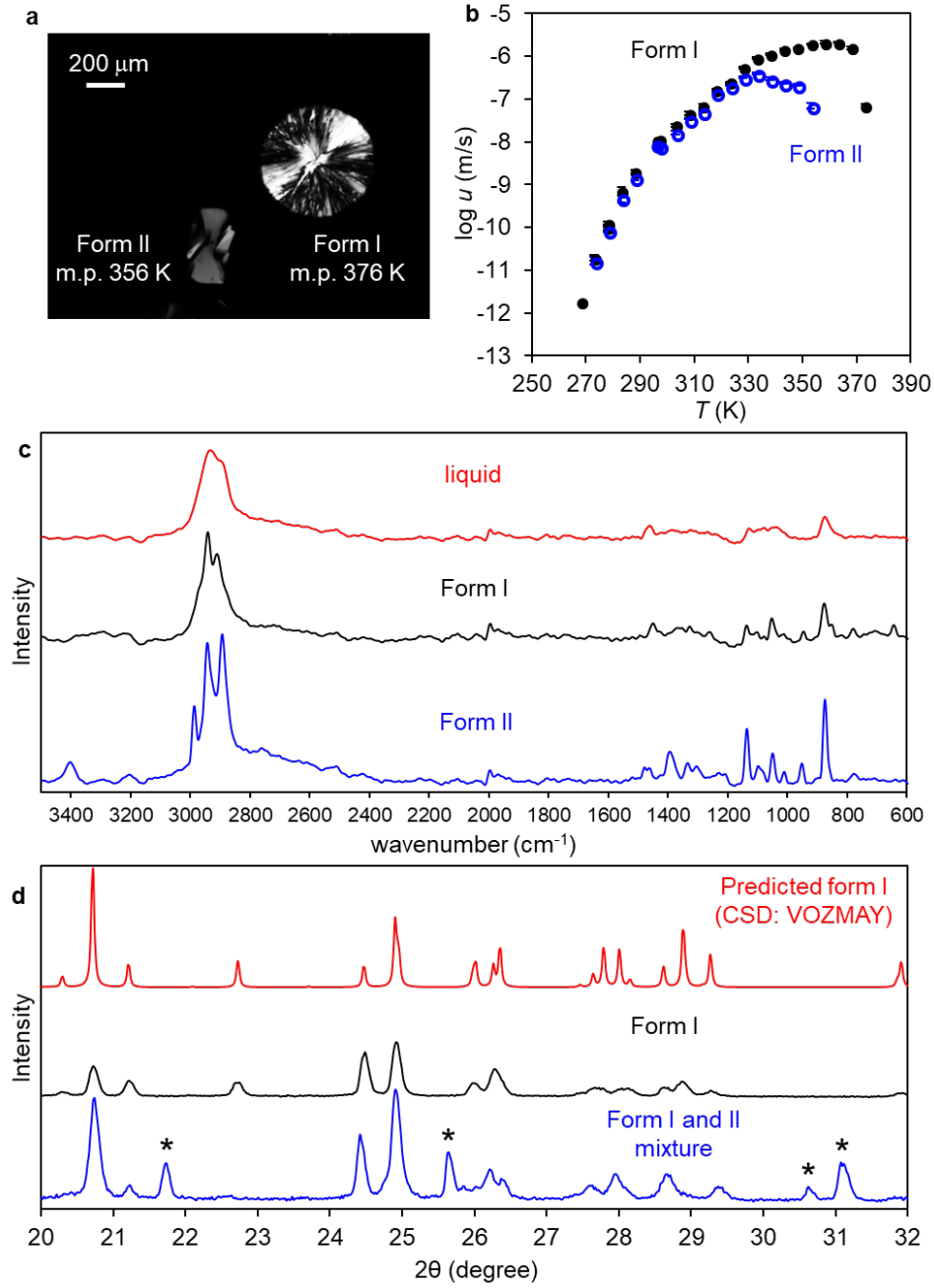

Figure S2. Comparison of two polymorphs of D-arabitol. (a) Crystal morphologies. (b) Crystal growth rates. (c) Raman spectra. (d) XRD patterns (* indicates peaks unique to Form II).

References

[1] L. Yu, Crystal Growth & Design **3**, 967 (2003).

[2] T. Wu, and L. Yu, The Journal of Physical Chemistry B **110**, 15694 (2006).

[3] M. Naoki, K. Ujita, and S. Kashima, The Journal of Physical Chemistry **97**, 12356 (1993).

[4] A. Nakheli, A. Eljazouli, M. Elmorabit, E. Ballouki, J. Fornazero, and J. Huck, Journal of Physics: Condensed Matter **11**, 7977 (1999).

[5] A. Minoguchi, K. Kitai, and R. Nozaki, Physical Review E **68**, 031501 (2003).

[6] J. Kopf, M. Morf, B. Zimmer, and P. Köll, Carbohydrate Research **218**, 9 (1991).

[7] L. Carpentier, M. Paluch, and S. Pawlus, The Journal of Physical Chemistry B 115, 1062 (2011).

[8] P. Derollez, Y. Guinet, F. Affouard, F. Danède, L. Carpentier, and A. Hédoux, Acta Crystallographica Section B **68**, 407 (2012)

[9] R. Wehn, P. Lunkenheimer, and A. Loidl, Journal of Non-Crystalline Solids **353**, 3862 (2007).

[10] N. Menon, K. P. O'Brien, P. K. Dixon, L. Wu, S. R. Nagel, B. D. Williams, J. P. Carini, Journal of Non-Crystalline Solids **141**, 61 (1992).

[11] G. E. Gibson, and W. F. Giauque, Journal of the American Chemical Society **45**, 93 (1923).

[12] H. S. Kim, and C. A. Jeffrey, Acta Crystallographica Section B **25**, 2607 (1969).

[13] K. Takahiro, N. Genki, S. Takato, O. Ryosuke, H. Wataru, and K. Masahiro, Bulletin of the Chemical Society of Japan **86**, 351 (2013).

Chapter 4. Effect of Low-Concentration Polymers on Crystal Growth in Molecular Glasses: A Controlling Role for Polymer Segmental Mobility Relative to Host Dynamics

As published in ***The Journal of Physical Chemistry B***

2017, vol. 121 (8), page 1963–1971

Chengbin Huang [1], C. Travis Powell [2], Ye Sun [2], Ting Cai [3], Lian Yu [1,2,*]

[1] School of Pharmacy, University of Wisconsin-Madison, Madison, Wisconsin 53705, United States.

[2] Department of Chemistry, University of Wisconsin-Madison, Madison, Wisconsin 53705, United States.

[3] State Key Laboratory of Natural Medicines, Jiangsu Key Laboratory of Drug Discovery for Metabolic Diseases, Department of Pharmaceutics, College of Pharmacy, China Pharmaceutical University, Nanjing 210009, China

4.1 Abstract

Low-concentration polymers can strongly influence crystal growth in small-molecule glasses, a phenomenon important for improving physical stability against crystallization. We measured the velocity of crystal growth in two molecular glasses, nifedipine (NIF) and *o*-terphenyl (OTP), each doped with 4 or 5 different polymers. For each polymer, the concentration was fixed at 1 wt % and a wide range of molecular weights was tested. We find that a polymer additive can strongly alter the rate of crystal growth, from a 10-fold reduction to a 10-fold increase. For a given polymer, increasing molecular weight slows down crystal growth and the effect saturates around DP = 100, where DP is the degree of polymerization. For all the systems studied, the polymer effect on crystal growth rate forms a master curve in the variable $(T_{g\ polymer} - T_{g\ host})/T_{cryst}$, where T_g is the glass transition temperature and T_{cryst} is the crystallization temperature. These results support the view that a polymer's effect on crystal growth is controlled by its segmental mobility relative to the host-molecule dynamics. In the proposed model, crystal growth rejects impurities and creates local polymer-rich regions, which must be traversed by host molecules to sustain crystal growth at rates determined by polymer segmental mobility. Our results do not support the view that host-polymer hydrogen bonding plays a controlling role in crystal growth inhibition.

4.2 Introduction

Glasses are amorphous solids formed by cooling liquids, drying solutions and condensing vapors while preventing crystallization. Glasses combine the mechanical strength of crystals and the spatial uniformity of liquids with numerous applications ranging from optics to structural materials. While better known glasses are inorganic, polymeric and metallic, there is increasing interest in organic glasses of relatively low molecular weight ("molecular glasses") for applications in pharmaceutics,[1] bio-preservation[2] and electronics.[3] In all their applications,

amorphous materials must resist crystallization. While this requirement is easily met by some glasses, others – notably molecular glasses – readily crystallize,[4,5,6,7,8,9,10] making the inhibition of crystallization a major task in developing these materials.

Crystallization has two elemental steps – nucleation and growth, which have different kinetics. In the context of controlling crystallization in molecular glasses, an important phenomenon is the strong inhibitory effect of polymers on the process of crystal growth.[11,12,13,14,15,16] For example, at only 1 wt %, polyvinylpyrrolidone can slow crystal growth in nifedipine by a factor of 10,[14,15] suggesting the potential to use polymers as a general method to stabilize organic glasses. At present, it is still unclear how to select the best polymer for this purpose and more important, how a polymer interferes with the process of crystal growth. Some propose that host-polymer hydrogen bonding plays a controlling role,[12,13,16] while others suggest that the polymer's segmental mobility is important.[15] A deeper understanding in this area is relevant for producing stable amorphous materials and controlling crystallization using low-concentration additives.

In this study, we systematically investigated the effect of several polymers with different molecular weights on crystal growth in the glasses of nifedipine (NIF) and *o*-terphenyl (OTP). NIF and OTP are model molecular glass-formers, which show relatively fast crystal growth in the glassy state.[4,11] The utilized polymers were polybutadiene (PB), polyisoprene (PI), poly(ethylene glycol/oxide) (PEG/PEO), polystyrene (PS), poly(4-tert-butylstyrene) (PtBS) and polyvinylpyrrolidone (PVP). At the molecular weight and concentration (1 wt %) used, they are all miscible with the host molecules and except for the highest molecular weight used, are present in the dilute state (the polymer concentration is below the contact concentration c^*).[17,18,19,20,21] For each polymer, the molecular weight covered a wide range to provide a critical assessment of the polymer attributes that control the effect on crystallization.

We find that at 1 wt %, the polymer additive can strongly alter the rate of crystal growth in the glasses of NIF and OTP, from a 10-fold reduction to a 10-fold increase. For a given polymer, increasing molecular weight systematically slows down crystal growth and the effect saturates around DP = 100, where DP is the degree of polymerization. For all the systems studied, the polymer effect on crystal growth rate forms a master curve in the variable $(T_{g\ polymer} - T_{g\ host})/T_{cryst}$, where T_g is the glass transition temperature and T_{cryst} is the crystallization temperature. These results support the view that the polymer's segmental mobility relative to host-molecule dynamics controls its effect on crystal growth. Our results do not support the view that host-polymer hydrogen bonding controls crystal growth inhibition. We suggest a tentative model for the polymer effect on crystal growth on the basis of fracture, surface diffusion, and host-polymer segregation on the surface.

4.3 Experimental Section

Nifedipine (NIF) and *o*-terphenyl (OTP) were obtained from Sigma-Aldrich (St. Louis, MO) and used as received. Polystyrene (PS), polybutadiene (PB), and polyisoprene (PI) were purchased from Scientific Polymer Products Inc. Polyisoprene (PI) was obtained from Polymer Source Inc. and Sigma-Aldrich. Poly(4-tert-butylstyrene) (PtBS) was purchased from Polymer Source Inc. Poly (ethylene glycol) (PEG) or poly (ethylene oxide) (PEO) was purchased from Sigma-Aldrich. The dimer of vinyl pyrrolidone ("VP dimer") was from Abbott Laboratories. Polyvinylpyrrolidone (PVP) was from ISP Technologies, BASF, and GAF Chemicals. Figure 1 shows the molecular structures of the materials in this study and Table 1 collects the relevant information on the polymers used. Figure 2 shows the T_g of polymers used relative to the T_g of the host molecules. For the systems studied, the presence of 1 wt % polymer generally had only a small effect on the

host T_g (< 1 K). For the oligomers of PB and PI (M < 1000 g/mole), a slightly larger depression of the host T_g was observed, up to 2 K.

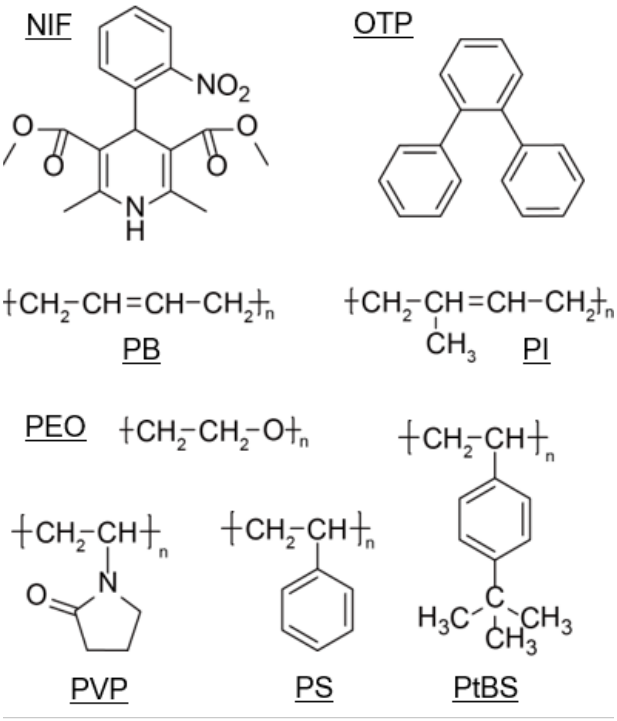

Figure 1. Molecular structures of the materials in this study. NIF: nifedipine; OTP: *o*-terphenyl; PB: polybutadiene; PI: polyisoprene; PEO: poly (ethylene oxide); PVP: polyvinylpyrrolidone; PS: polystyrene; PtBS: poly (t-butyl styrene).

NIF glasses containing polymers were prepared by cryomilling (SPEX CertiPrep 6750 with liquid nitrogen as coolant) followed by melting and cooling. 1 g of 10 wt % polymer-doped NIF glasses were cryomilled first and then diluted to 1 g of 1 wt % polymer-doped NIF glasses. Each sample was milled at 10 Hz for five 2-min cycles, each followed by a 2-min cool down. To make a sample for measuring crystal growth, 2-3 mg of NIF glasses was melted at 453 K on a round coverslip (diameter = 15 mm) for 1 min and then covered by another coverslip to make a sandwich sample. The sample was cooled to room temperature by contact with an aluminum block. Because of its photosensitivity, all NIF samples were shielded from light. To measure the crystal growth rates, the NIF samples were nucleated at 333 K and then stored in a desiccator at 303 K or 313 K maintained with an oven stable within ± 1 K. Faster crystal growth at higher temperatures was observed with a Linkam THMS 600 hot stage (temperature stability ± 0.1 K) in flowing nitrogen.

OTP glasses containing 1 wt % polymer additive were prepared by direct dissolution. The correct amounts of OTP and polymer additive were weighed, mixed and heated in a sealed vial at 353 K for at least 48 h with intermittent shaking to obtain a clear solution. A drop of the OTP solution was pipetted on a coverslip and covered by another coverslip. To initialize crystallization, a piece of OTP crystal was pushed into contact with the edge of the OTP liquid at room temperature. The sample was cooled to 243 K in a Linkam THMS 600 cold stage and crystal growth was observed under nitrogen purge.

Crystal growth rate was measured through an Olympus BH2-UMA polarized light microscope equipped with a digital camera. Each reported growth rate is the average of 9-12 measurements in three separate samples.

Differential Scanning Calorimetry (DSC) measurements were performed in crimped aluminum pans with approximately 4-6 mg materials, using a TA Q2000 differential scanning calorimeter. The samples were cooled and heated at 10 K/min under 50 ml/min N_2 purge to determine the T_g.

Polymorphs of NIF crystals were identified with a Raman microscope (Thermo Scientific DXR Raman microscope; 780 nm laser). The polymorph of NIF crystal matched the known Raman pattern of β NIF,[22] with the following identifying peaks: C−C−O stretch (1215 cm^{-1}), and C=C stretch (1651 cm^{-1}). Only one OTP crystal structure is known (Cambridge Structural Database Ref. Code: TERPHO02) and was observed.

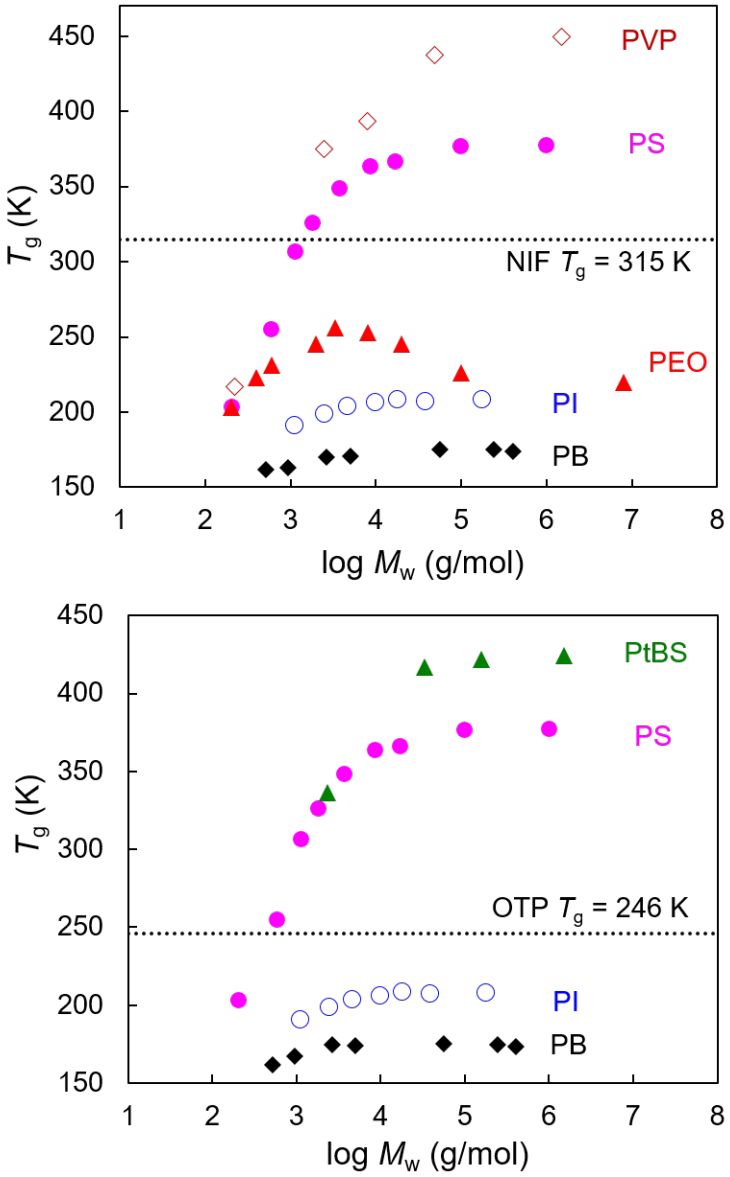

Figure 2. The glass transition temperatures T_g of the polymers used in this work shown as functions of molecular weight. The T_g of the host molecular glass is shown as horizontal line.

Table 1. Properties of the polymers used.

	M_w (g/mol) or range	M_w/M_n	T_g (K)
Polybutadiene	520	1.11	162
(PB)	940	1.08	167
	2640	1.05	175
	5020	1.04	174
	56 K	1.01	175
	242 K	1.06	175
	400 K	1.43	174
Polyisoprene	1100	1.1	191
(PI)	2450	1.02	199
	4600	1.04	204
	9870	1.03	207
	18 K	1.04	209
	38 K	NA	207
	176 K	1.15	208
Poly (ethylene oxide)	200 (190-210)	NA	203
(PEO)	400 (380-420)	NA	223
	600 (570-630)	NA	231
	2000 (1900-2100)	NA	245
	3350 (3000-3700)	NA	256
	8 K (7-9 K)	NA	253
	20 K (16-20 K)	NA	245
	100 K (M_v)	NA	226
	8000 K (M_v)	NA	220
Polystyrene	201	1.02	204
(PS)	580	1.07	255
	1110	1.12	307
	1780	1.09	326
	3680	1.08	349
	8400	1.05	364
	17 K	1.04	367
	97 K	1.01	377
	979 K	1.06	378
Poly (t-butyl styrene)	2350	1.07	336
(PtBS)	33 K	1.04	417
	156 K	1.08	422
	1500 K	1.35	424
Polyvinylpyrrolidone	224 (“VP dimer”)	NA	217
(PVP)	2000-3000 (“K12”)	NA	375
	8000 (“K15”)	NA	393
	44-54 K (“K30”)	NA	437
	1-2 M (“K90”)	NA	449

Note: T_g values of PB from Hintermeyer *et al.*[23]; T_g values of PEO from Faucher *et al.*[24]; T_g values of PVP from Powell *et al.*[15] All other data from this work.

4.4 Results

Before measuring its effect on crystal growth, we confirmed that each polymer used was miscible with the host molecules at the concentration used (1 wt %). This conclusion was based on the systematic change of the mixture's glass transition temperature T_g and melting point T_m with concentration.[15,25,26] Figure 3a illustrates the T_m test for NIF doped with PB 400K: T_m changes from pure NIF, to 1 wt % PB 400K doped NIF, to 10 wt % doped NIF, consistent with full miscibility at 1 wt % between the components.

In addition to the T_g and T_m tests, the dependence of crystal growth rate on polymer concentration was also used to evaluate the state of mixing. For miscible systems, the crystal growth rate u decreases exponentially with the polymer concentration ($\log u$ is linear on c). This is illustrated in Figure 3b for NIF doped with PVP K15.[14,15] In contrast, the corresponding data on NIF doped with PS exhibit plateaus. We interpret these results to mean that PS 17K is miscible with NIF up to ~ 1 wt %, whereas PS 97K is immiscible at 1 wt %. Because of this, PS 97K was not used in crystallization studies, but PS 17K was.

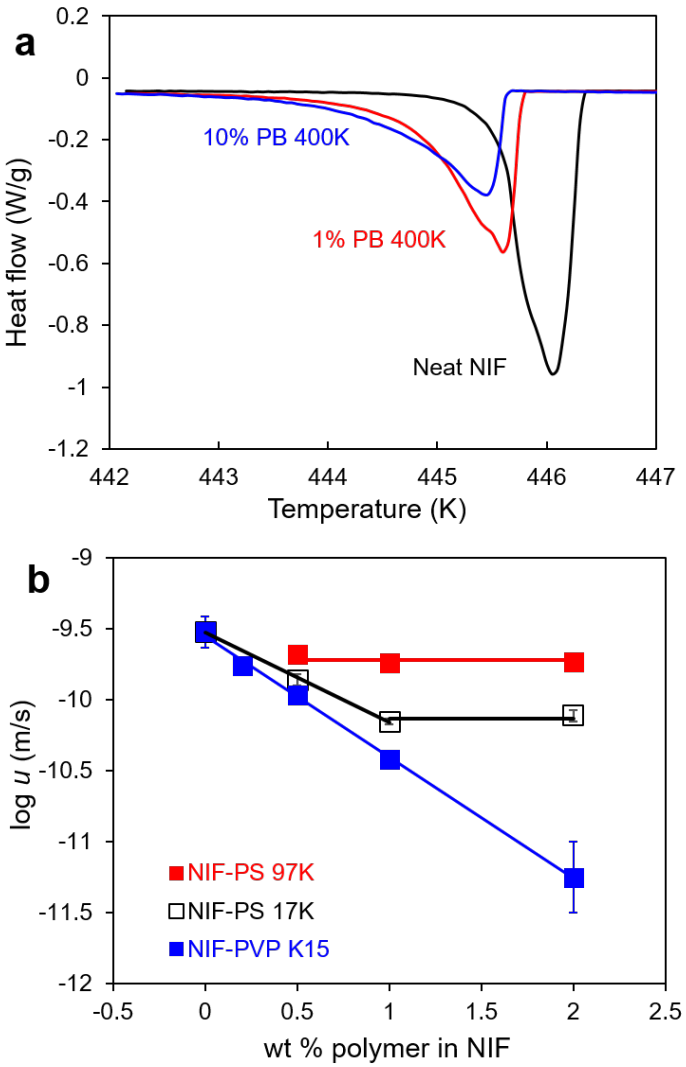

Figure 3. (a) Melting endotherms of NIF crystals in the presence of 1 and 10 wt % PB 400K at a 2 K/min heating rate. The results show that at 1 wt %, the polymer is miscible with NIF. (b) Crystal growth rates of NIF at 303 K in the presence of PS 17K, PS 97K and PVP K15 as functions of polymer concentration. The results indicate that PVP K15 is miscible with NIF, PS 17K is miscible up to ~ 1wt %, and PS 97K is immiscible at 1 wt %.

Figure 4 shows typical data collected in this work. The process of crystal growth was followed in a pure NIF glass at 303 K and in NIF glasses containing 1 wt % PI 1100 and 176 K. These crystals are polycrystalline spherulites and their growth rate is constant in time (Figure 4d). Relative to pure NIF, the presence of 1 wt % PI (a low T_g polymer; see Figure 2) significantly *speeds up* NIF crystal growth. The rate increase depends on the PI molecular weight: by a factor of 20 for PI 1100 and a factor of 5 for and PI 176 K.

Figure 5 summarizes the data collected on the effect of 1 wt % polymer on crystal growth in NIF glasses. Crystal growth rates u are shown for two temperatures of crystallization, T_{cryst} = 303 and 313 K, and plotted as functions of the polymers' molecular weights. The u value for a pure NIF glass is shown as horizontal line. Notice a wide range of effects of a polymer additive on the crystal growth rate: PB, PI and PEO speed up crystal growth, whereas PVP and PS slow down crystal growth. It is noteworthy that at such a low polymer concentration of 1 wt %, the crystal growth rate in an NIF can be increased or decreased by one order of magnitude.

Notice also that the polymer's *molecular weight* has a strong effect on the NIF crystal growth rate. For a given polymer, increasing the molecular weight systematically decreases the crystal growth rate and the effect saturates near M_w = 10 kg/mol. All the polymers tested show virtually the same molecular weight dependence, at both temperatures of crystallization (303 and 313 K).

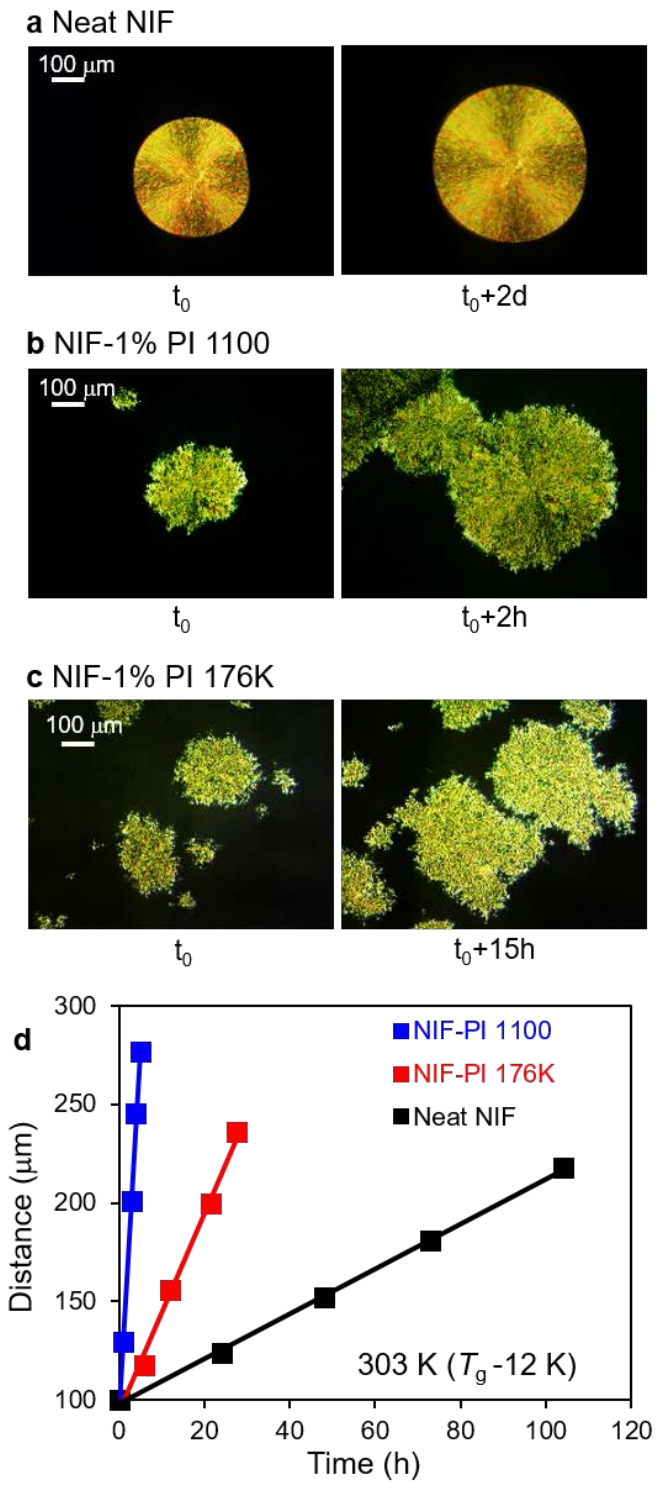

Figure 4. Process of crystal growth at 303 K in an NIF glass (a) and an NIF glass containing PI 1100 (b) and PI 176 K (c). (d) Distance of crystal growth vs. time.

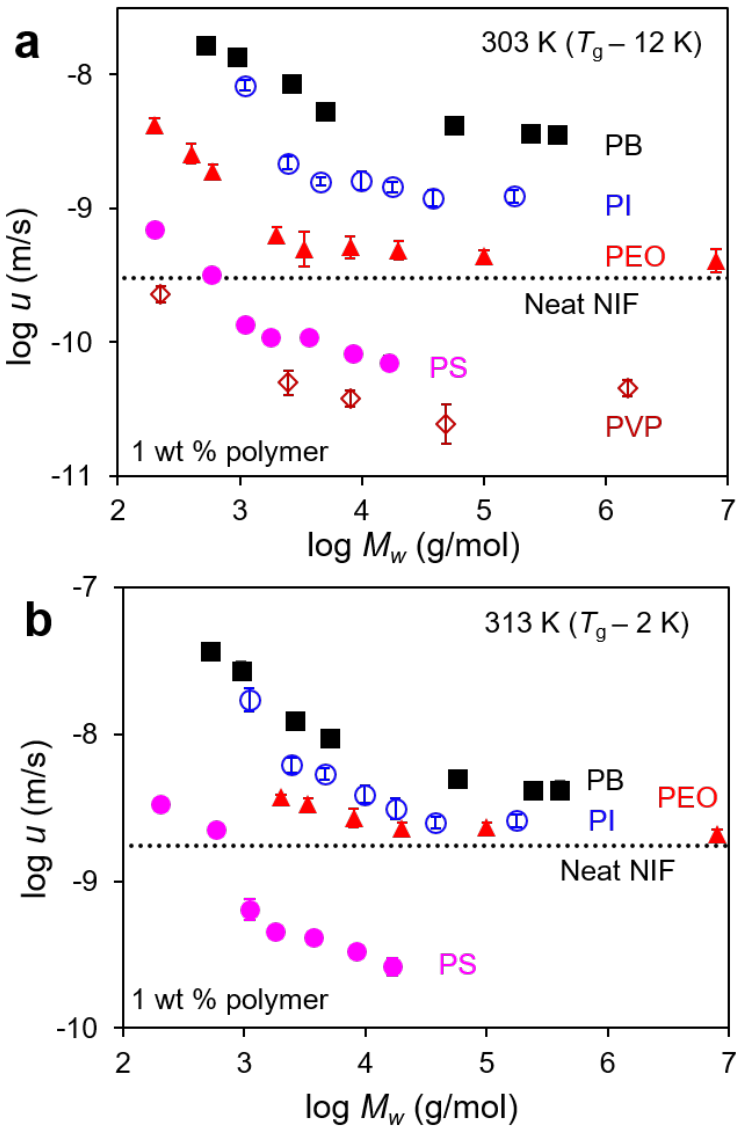

Figure 5. Crystal growth rates in NIF glasses doped with 1 wt % polymers of different structures and molecular weights. (a) 303 K. (b) 313 K. For each temperature, the growth rate in pure NIF glass is shown as horizontal line.

Figure 6 shows typical data collected for polymer-doped OTP glasses. The process of crystal growth was followed in a pure OTP glass at 243 K and in OTP glasses containing 1 wt % PI 1100 and 176 K. As in the case of NIF (Figure 4), the crystals formed are polycrystalline spherulites with constant growth rates (Figure 6d). Relative to pure OTP, the presence of 1 wt % PI 1110 has little effect on crystal growth rate, while 1 wt % PI 176K *slows down* OTP crystal growth.

Figure 7 summarizers the data collected on the effect of 1 wt % polymer on crystal growth in OTP glasses. Crystal growth rates u are plotted as functions of the polymers' molecular weights. The u value for a pure OTP glass is shown as horizontal line. Notice that a polymer additive generally slows down crystal growth in OTP, with the exception of PB whose oligomers speed up crystal growth. For PS and PtBS, the inhibitory effect is very strong on crystal growth, reducing the growth rate by more than one order of magnitude.

As in the case of NIF, the polymer's effect on OTP crystal growth varies with its molecular weight. For a given polymer, increasing the molecular weight decreases the crystal growth rate and the effect saturates near M_w = 10 kg/mol for PB and PI and near 100 kg/mol for PS and PtBS. The overall pattern is similar to that observed for NIF (Figure 5).

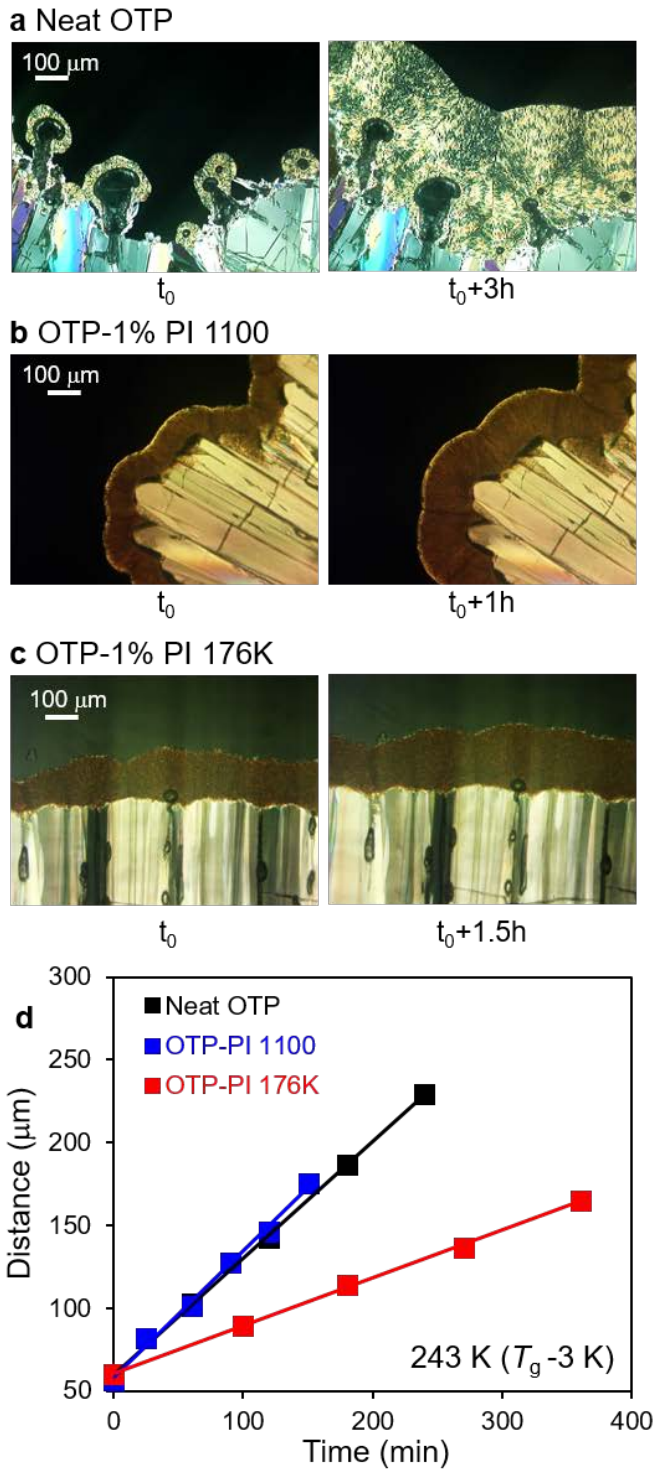

Figure 6. Process of crystal growth at 243 K in a pure OTP glass (a) and an OTP glass doped with PI 1100 (b) and PI 176 K (c). (d) Distance of crystal growth vs. time.

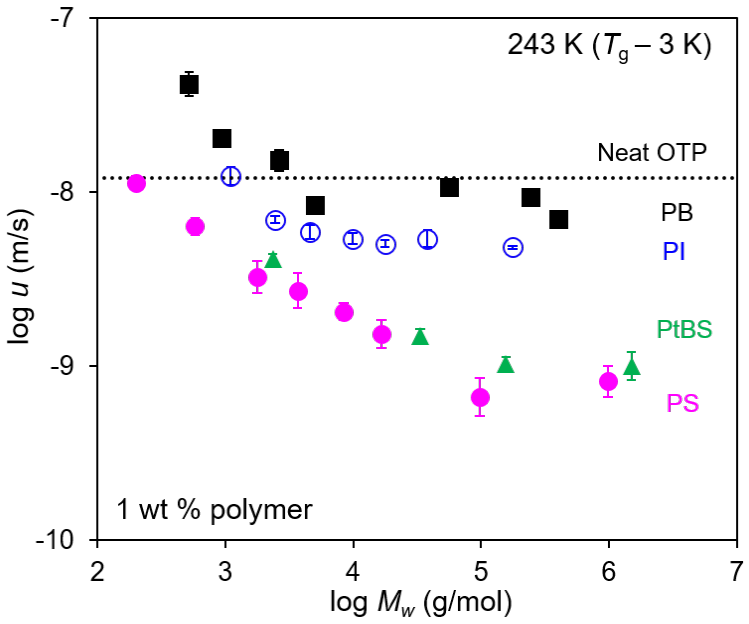

Figure 7. Crystal growth rates in OTP glasses doped with 1 wt % polymers of different structures and molecular weights. The growth rate in pure NIF glass is shown as horizontal line.

The latter point is further demonstrated in Figure 8, where the results on NIF and OTP are plotted together. To emphasize the molecular weight dependence, we normalize each crystal growth rate (u) by u_∞, the growth rate plateau in Figures 5 and 7 reached at high polymer molecular weight. This normalization is equivalent to vertically shifting the data points to coincide at high molecular weights. Figure 8 shows that after this normalization, all the data points cluster together, forming a common trend. For this plot, we have used the degree of polymerization DP (DP = molecular weight of the polymer/molecular weight of the monomer) instead of molecular weight as the x axis because it slightly improves the collapsing of data. The general pattern revealed by Figure 8 is that for the systems studied, increasing the polymer's DP decreases the rate of crystal growth rate and the effect saturates around DP = 100.

Figure 9 shows another instructive way our results can be organized. Here we measure the polymer effect on crystal growth using the ratio u/u_{host}, where u_{host} is the crystal growth rate of the pure molecular glass and u is the value in the presence of a polymer. This ratio is plotted against $(T_{g\ polymer}-T_{g\ host})/T_{cryst}$, where host = NIF or OTP, $T_{g\ polymer}$ and $T_{g\ host}$ are the T_gs of the polymer and the host, respectively, and T_{cryst} is the crystallization temperature. In this format, all the results of this study are organized into a master curve. The points above the horizontal line correspond to the cases where the polymer accelerates the crystal growth of host molecules, and those below to the cases where the polymer has an inhibitory effect. Figure 9 indicates that the polymer effect on crystal growth correlates strongly with the ratio $(T_{g\ polymer}-T_{g\ host})/T_{cryst}$. It is significant that this master curve includes all the systems studied, including two hosts, three temperatures of crystallization, and 4 or 5 polymer additives in each host with wide ranges of molecular weights. As we discuss later, the ratio $(T_{g\ polymer}-T_{g\ host})/T_{cryst}$ measures the polymer's segmental mobility relative to the host dynamics at the temperature of crystallization.

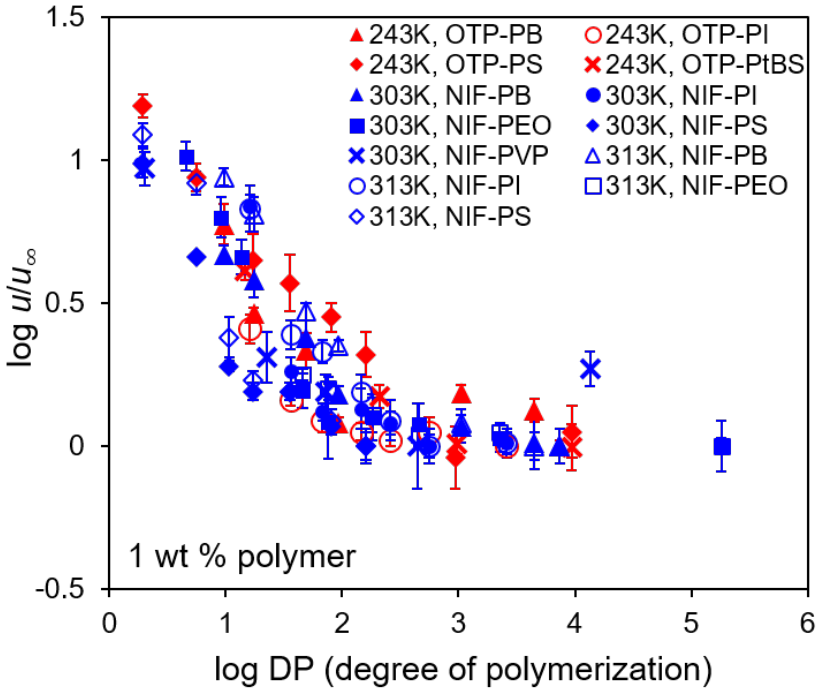

Figure 8. Normalized crystal growth rates in NIF and OTP glasses vs. the polymer's degree of polymerization. Note a similar dependence on DP for all polymers tested in both molecular glasses.

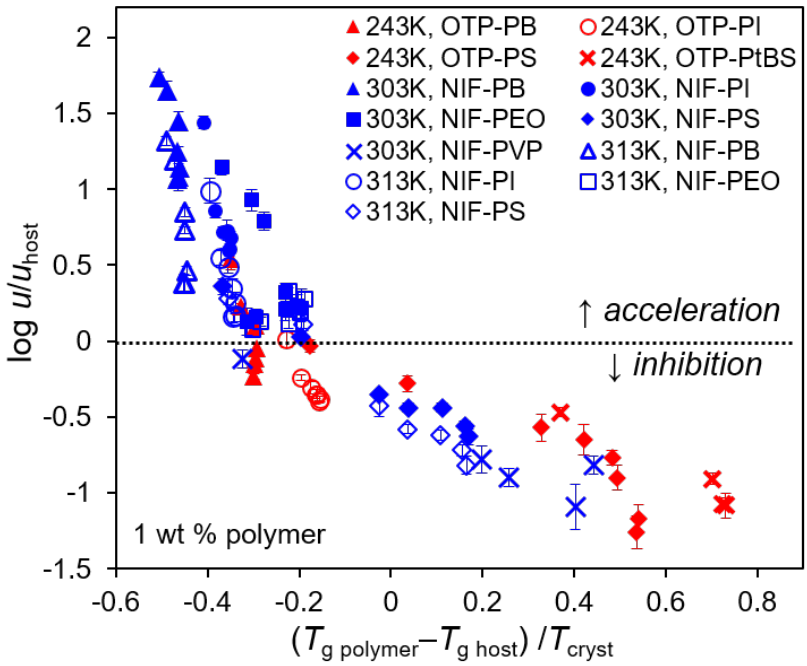

Figure 9. Polymer effect on crystal growth measured by u/u_{host} plotted against $(T_{g\ polymer}–T_{g\ host})/T_{cryst}$, where T_{cryst} is the crystallization temperature. All the results of this study are organized into a master curve in this manner.

We close the Results section with a comment on a peculiar behavior of PS-doped OTP glasses. At some PS fractions, two rates of crystal growth were observed. Figure 10a/b shows this phenomenon for the PS 8400 fraction: in the fast mode, the growth rate u is four times larger than in the slow mode. This phenomenon is observed in the M_w range 2 – 17 kg/mol, but not at lower or high M_w (Figure 10c). In the fast mode, u is insensitive to the PS molecular weight, whereas in the slow mode, it is. At present, the mechanisms for the two crystal growth modes are still unclear. The foregoing analysis (Figures 7-9) has focused on the slow mode in the PS-OTP system.

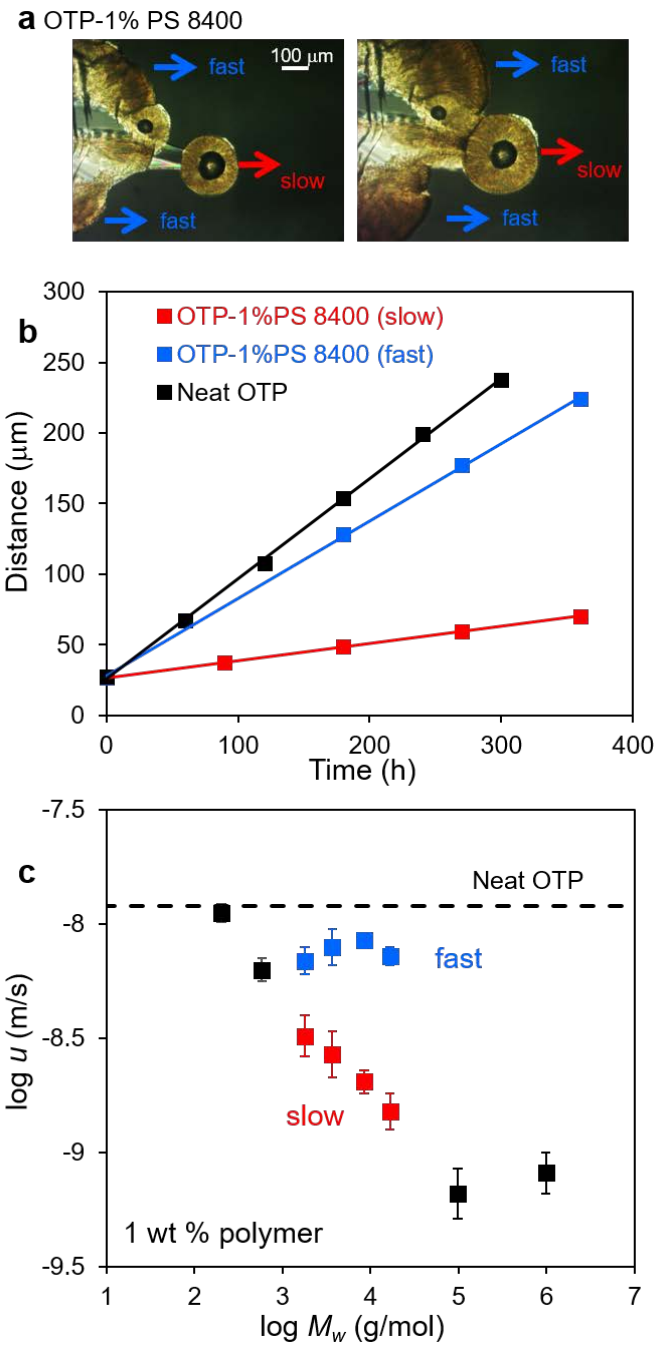

Figure 10. (a) Fast and slow modes of crystal growth in PS-doped OTP at 243 K. (b) Growth distance vs. time for the two growth modes. (c) Crystal growth rate in an OTP glass at 243 K containing 1 wt % PS of different molecular weights. Two rates are observed (fast and slow) for PS 1780, 3680, 8400 and 17K, and only one for other PS fractions.

4.5 Discussion

This study has examined the effect of low-concentration polymers on crystal growth in two molecular glasses (NIF and OTP). At 1 wt %, the polymer can strongly alter the rate of crystal growth, from a 10-fold reduction to a 10-fold increase. For a given polymer, increasing molecular weight slows down crystal growth and the effect saturates around DP = 100 (Figure 8). For all the systems studied, the polymer effect on crystal growth forms a master curve in the variable ($T_{g\ polymer} - T_{g\ host}$)/$T_{cryst}$ (Figure 9). As we discuss here, these findings support the notion that the polymer's segmental mobility relative to the host-molecule mobility controls crystal growth in molecular glasses. We propose a tentative model for this effect.

The fact that a polymer's effect on crystal growth saturates with increasing molecular weight M argues that its center-of-mass diffusion constant D or intrinsic viscosity [η] does not have a rate-limiting role in the process. For our systems, the polymer is in a dilute solution (no entanglement), and both D and [η] are expected to change monotonically with M: D roughly as $M^{-0.5}$ (Ref. 27 and 28) and [η] roughly as $M^{0.5}$ (Ref. 29 and 30). These trends are predicted by standard models.[31] These trends, however, differ from the M dependence of a polymer's effect on crystal growth (Figure 8), where a plateau is reached near DP = 100. It follows that D or [η] does not define the rate-limiting step for crystal growth in host molecular glasses.

The same analysis above also suggests that the *segmental* mobility of polymer chains is a possible limiting factor for crystal growth. It is known that a polymer's segmental mobility in a dilute solution decreases with increasing molecular weight but reaches a plateaus near DP = 100.[32] This dependence is consistent with standard models.[31] This molecular weight dependence of segmental mobility is in excellent agreement with that of a polymer's effect on crystal growth (Figure 8).

A further support for our conclusion is provided by the master curve in Figure 9, showing a strong correlation between a polymer's effect on crystal growth and the ratio $(T_{g\ polymer} - T_{g\ host})/T_{cryst}$. According to Angell,[33] the relaxation time τ of a glass-forming molecular liquid is well described by

$$\log \tau = \log \tau_g + m\,(T_g/T - 1) \qquad (1)$$

where T is a temperature near T_g, τ_g is the relaxation time at T_g (~ 100 s), and m is a fragility index. For the two host liquids, m = 80 for OTP[34] and 83 for NIF.[35] These values are typical of glass-forming molecular liquids, though one should note a sizable variation in the literature values (a 20 % difference is not uncommon for a given system). This variation arises in part from the non-Arrhenius T dependence of τ, making its apparent activation energy sensitive to the choice of T_g. Eq. (1) also describes the *segmental* relaxation time τ_{seg} for a polymer melt with m having broadly similar values: m = 70-120 for PS,[23] 70-90 for PB,[23] 70-140 for PtBS,[36] and 75-85 for PI.[37]

At the crystallization temperature T_{cryst}, the host-polymer mobility difference is given by

$$\log \tau_{seg}/\tau_{host} = m\,(T_{g\ polymer} - T_{g\ host})/T_{cryst} \qquad (2)$$

Thus the ratio $(T_{g\ polymer} - T_{g\ host})/T_{cryst}$ is directly related to τ_{seg}/τ_{host}, and the master curve in Figure 9 indicates a strong correlation between a polymer's effect on crystal growth (measured by u/u_{host}) and the host-polymer mobility difference, where the polymer mobility refers to its segmental mobility. Note that the ratio τ_{seg}/τ_{host} refers to the mobility difference between a neat polymer and a pure host at a common temperature. It might be more relevant to evaluate this property *in the actual polymer solution.* There is no direct experimental data at present on this property for our systems. The self-concentration model[38] predicts that τ_{seg} of a polymer solute is not the same as the solvent dynamics τ_{seg}, but "remembers" its intrinsic mobility in the neat state. This is because for a given polymer segment, the local concentration of polymer segments exceeds

the overall bulk concentration. This is a consequence of chain connectivity. The self-concentration effect means that τ_{seg} of the neat polymer can be used to rank τ_{seg} in a dilute solution.

How does the polymer's segmental mobility control crystal growth in a molecular glass? Here we give a tentative answer with the aid of Figure 11. Our model is based on two recent studies. At the temperatures studied, crystal growth in NIF and OTP glasses is in the so called "glass-to-crystal" or GC mode.[4,5,11] In this process, crystal growth is not limited by the structural relaxation time in the amorphous phase.

Among its various explanations,[4,5,39,40,41,42] the most recent by Powell *et al.*[42] hypothesizes that GC growth involves creation of voids and free surfaces (possibly through fracture) and the surface transport of molecules. Their proposal is based on the observation that volume is conserved during GC growth despite a higher density of the crystal. They reasoned that crystal growth must create voids and free surfaces, which in turn accelerate local transformation. Their proposal is consistent with the fact that the velocities of crystal growth on the free surface and in the bulk have similar temperature dependence. A second result underlying our model is the finding[26] that 1 wt % polystyrene in OTP can strongly inhibit the decay of surface gratings. A corrugated surface grating flattens under the driving force of surface tension, with molecules migrating from the peaks of the grating (regions of high chemical potential) to the valleys (low chemical potential). Zhang et al. suggest that in this process, slow-diffusing polymer molecules are stranded and enriched in regions vacated by host molecules.

As shown in Figure 11, we hypothesize that free surfaces are constantly created during crystal growth, perhaps by fracture. The free surface allows fast transport of molecules to join the crystal. This process is known to create a depletion zone near a crystal,[43] also depicted in Figure 11. We imagine that polymer molecules are rejected by the growing crystal, accumulating near the

crystal/glass interface.[26] Eventually, host molecules must migrate through a polymer-enriched region to reach the crystal. Based on previous work,[44,45,46,47] translational diffusion of small molecules through a polymer matrix is limited by the segmental mobility of polymer chains. If the passage of host molecules through polymer-enriched regions becomes rate-limiting, we would expect a strong correlation between a polymer's effect on crystal growth and its segmental mobility, as observed in this study.

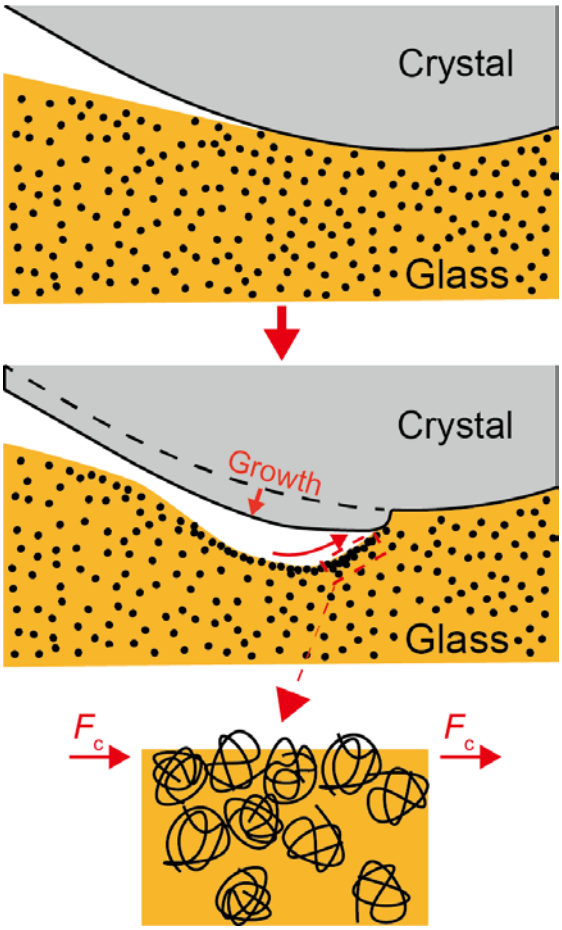

Figure 11. Model for crystal growth in molecular glasses containing dilute polymers (black circles). F_c is crystallization flux.

Does host-polymer hydrogen bonding control crystal growth in molecular glasses? It has been proposed that host-polymer hydrogen bonding has a controlling effect on crystal growth in molecular glasses.[13,16] Here we evaluate this proposal against the results of this work. Of the two host molecules, NIF is a donor and an acceptor of hydrogen bonds, while OTP is neither. Among the utilized polymers, PVP and PEO are acceptors; the rest (PB, PI, PS, and PtBS) are neither donors nor acceptors. The hydrogen-bonding model makes predictions only for NIF-polymer systems. The strength of hydrogen bonding with NIF is PVP (strongest) > PEO > PB ~ PI ~ PS (none). However, the inhibitory effect of a polymer on crystal growth follows the order: PVP > PS > PEO > PI > PB. The latter order is different from the order for host-polymer hydrogen bonding. In particular, PEO forms hydrogen bonds with NIF but *accelerates* its crystal growth; PS forms no hydrogen bonds with NIF but *inhibits* its crystal growth.

A second test of the hydrogen-bonding model is to examine how molecular weight affects a polymer's effect on crystal growth. Since it makes no reference to molecular weight, this model predicts the same effect *independent of the degree of polymerization*. Our results, however, show that the effect of a polymer on crystal growth significantly increases with molecular weight and reaches a plateau near DP = 100. The hydrogen-bonding model therefore does not correctly describe the systems studied. If a single property is to be used to predict crystal growth inhibition, the ratio $(T_{g\ polymer} - T_{g\ host})/T_{cryst}$ performs much better (Figure 9) than host-polymer hydrogen bonding. The hydrogen-bonding model has the further shortcoming that it makes no predictions for systems without hydrogen bonds.

4.6 Conclusion

In this study, we measured the crystal growth rate of amorphous NIF and OTP in the presence of 1 wt % polymer additives with different structures and molecular weights. We found that 1 wt % polymer additives can strongly alter the rate of crystal growth, from a 10-fold reduction to a 10-fold increase. For a given polymer, increasing molecular weight systematically slows down crystal growth and the effect saturates around 10-100 kg/mol (DP ≈ 100). For all the systems studied, the polymer effect on crystal growth rate forms a master curve as a function of $(T_{g\ polymer}-T_{g\ host})/T_{cryst}$. These results argue that center-of-mass diffusion or intrinsic viscosity of polymer chains does not define the rate-limiting step for the crystallization of host molecules, while segmental mobility likely plays this role. This view is consistent with all the host-polymer systems studied and serves as a basis for prediction. On the basis of crystallization-induced fracture and surface diffusion, a tentative model is proposed to explain why a polymer's segmental mobility controls the crystal growth of host molecules.

4.7 Acknowledgments

We thank the NSF (DMR-1234320) for supporting this work and M. D. Ediger for helpful discussions. C.T.P. thanks the NSF for a graduate research fellowship.

4.8 References

[1] Yu, L. Amorphous pharmaceutical solids: preparation, characterization and stabilization. *Adv. Drug Deliv. Rev.* **2001,** *48*, 27-42.

[2] Crowe, J. H.; Carpenter, J. F.; Crowe, L. M. The role of vitrification in anhydrobiosis. *Annu. Rev. Physiol.* **1998,** *60,* 73-103.

[3] Shirota, Y. Photo- and electroactive amorphous molecular materials - molecular design, syntheses, reactions, properties, and applications. *J. Mater. Chem.* **2005,** *15*, 75-93.

[4] Hikima, T.; Adachi, Y.; Hanaya, M.; Oguni, M. Determination of potentially homogeneous-nucleation-based crystallization in o-terphernyl and an interpretation of the nucleation-enhancement mechanism. *Phys. Rev. B* **1995,** *52*, 3900-3908.

[5] Sun, Y.; Xi, H. M.; Chen, S.; Ediger, M. D.; Yu, L. Crystallization near glass transition: transition from diffusion-controlled to diffusionless crystal growth studied with seven polymorphs. *J. Phys. Chem. B* **2008,** *112*, 5594-5601.

[6] Hasebe, M.; Musumeci, D.; Powell, C. T.; Cai, T.; Gunn, E.; Zhu, L.; Yu, L. Fast surface crystal growth on molecular glasses and its termination by the onset of fluidity. *J. Phys. Chem. B* **2014,** *118*, 7638-7646.

[7] Shi, Q.; Cai, T. Fast crystal growth of amorphous griseofulvin: relations between bulk and surface growth modes. *Crystal Growth & Design* **2016,** *16*, 3279-3286.

[8] Sun, Y.; Zhu, L.; Kearns, K. L.; Ediger, M. D.; Yu, L. A. Glasses crystallize rapidly at free surfaces by growing crystals upward. *Proc. Natl. Acad. Sci. U. S. A.* **2011,** *108*, 5990-5995.

[9] Wu, T.; Yu, L. Surface crystallization of indomethacin below T_g. *Pharmaceutical Research* **2006,** *23*, 2350-2355.

[10] Zhu, L.; Wong, L.; Yu, L. Surface-enhanced crystallization of amorphous nifedipine. *Molecular pharmaceutics* **2008,** *5*, 921-926.

[11] Ishida, H.; Wu, T. A.; Yu, L. Sudden rise of crystal growth rate of nifedipine near T_g without and with polyvinylpyrrolidone. *Journal of Pharmaceutical Sciences* **2007,** *96*, 1131-1138.

[12] Kestur, U. S.; Lee, H.; Santiago, D.; Rinaldi, C.; Won, Y. Y.; Taylor, L. S. Effects of the molecular weight and concentration of polymer additives, and temperature on the melt crystallization kinetics of a small drug molecule. *Crystal Growth & Design* **2010,** *10*, 3585-3595.

[13] Kestur, U. S.; Taylor, L. S. Role of polymer chemistry in influencing crystal growth rates from amorphous felodipine. *CrystEngComm* **2010,** *12*, 2390-2397.

[14] Cai, T.; Zhu, L.; Yu, L. Crystallization of organic glasses: effects of polymer additives on bulk and surface crystal growth in amorphous nifedipine. *Pharmaceutical Research* **2011,** *28*, 2458-2466.

[15] Powell, C. T.; Cai, T.; Hasebe, M.; Gunn, E. M.; Gao, P.; Zhang, G.; Gong, Y. C.; Yu, L. Low-concentration polymers inhibit and accelerate crystal growth in organic glasses in correlation with segmental mobility. *J. Phys. Chem. B* **2013,** *117*, 10334-10341.

[16] Kothari, K.; Ragoonanan, V.; Suryanarayanan, R. The role of drug–polymer hydrogen bonding interactions on the molecular mobility and physical stability of nifedipine solid dispersions. *Molecular pharmaceutics* **2015,** *12*, 162-170.

[17] Hiemenz, P. C.; Lodge, T. P. *Polymer Chemistry*, 2nd ed.; CRC Press: New York, 2007.

[18] Roovers, J.; Martin, J. E. The hard-sphere model for linear and regular star polybutadienes. *Journal of Polymer Science Part B: Polymer Physics* **1989,** *27*, 2513-2524.

[19] Davidson, N. S.; Fetters, L. J.; Funk, W. G.; Hadjichristidis, N.; Graessley, W. W. Measurement of chain dimensions in dilute polymer solutions: a light scattering and viscometric study of linear polyisoprene in cyclohexane. *Macromolecules* **1987,** *20*, 2614-2619.

[20] Devanand, K.; Selser, J. C. Asymptotic behavior and long-range interactions in aqueous solutions of poly(ethylene oxide). *Macromolecules* **1991,** *24*, 5943-5947.

[21] Huber, K.; Bantle, S.; Lutz, P.; Burchard, W. Hydrodynamic and thermodynamic behavior of short-chain polystyrene in toluene and cyclohexane at 34.5.degree.C. *Macromolecules* **1985,** *18,* 1461-1467.

[22] Chan, K. L. A.; Fleming, O. S.; Kazarian, S. G.; Vassou, D.; Chryssikos, G. D.; Gionis, V. Polymorphism and devitrification of nifedipine under controlled humidity: a combined FT-Raman, IR and Raman microscopic investigation. *Journal of Raman Spectroscopy* **2004,** *35,* 353-359.

[23] Hintermeyer, J.; Herrmann, A.; Kahlau, R.; Goiceanu, C.; Rossler, E. A. Molecular weight dependence of glassy dynamics in linear polymers revisited. *Macromolecules* **2008,** *41,* 9335-9344.

[24] Faucher, J. A.; Koleske, J. V.; Santee, E. R.; Stratta, J. J.; Wilson, C. W. Glass transitions of ethylene oxide polymers. *J. Appl. Phys.* **1966,** *37,* 3962-3964.

[25] Sun, Y.; Tao, J.; Zhang, G. G. Z.; Yu, L. Solubilities of crystalline drugs in polymers: an improved analytical method and comparison of solubilities of indomethacin and nifedipine in PVP, PVP/VA, and PVAc. *Journal of Pharmaceutical Sciences* **2010,** *99,* 4023-4031.

[26] Zhang, W.; Teerakapibal, R.; Yu, L. Surface mobility of amorphous *o*-terphenyl: a strong inhibitory effect of low-concentration polystyrene. *The Journal of Physical Chemistry B* **2016,** *120,* 6842-6847.

[27] King, T. A.; Knox, A.; Lee, W. I.; McAdam, J. D. G. Polymer translational diffusion. 1. Dilute theta solutions, polystyrene in cyclohexane. *Polymer* **1973,** *14,* 151-155.

[28] Adam, M.; Delsanti, M. Dynamical properties of polymer-solutions in good solvent by Rayleigh-scattering experiments. *Macromolecules* **1977,** *10,* 1229-1237.

[29] Colby, R. H.; Fetters, L. J.; Graessley, W. W. Melt viscosity molecular-weight relationship for linear-polymers. *Macromolecules* **1987,** *20,* 2226-2237.

[30] Abe, F.; Einaga, Y.; Yamakawa, H. Excluded-volume effects on the intrinsic-viscosity of oligomers and polymers of styrene and isobutylene. *Macromolecules* **1993,** *26,* 1891-1897.

[31] Rubinstein, M.; Colby, R. H. *Polymer Physics*; OUP Oxford: 2003.

[32] Horinaka, J.; Aoki, H.; Ito, S.; Yamamoto, M. Molecular weight effect on local motion of polystyrene studied by the fluorescence depolarization method. *Polymer Journal* **1999,** *31*, 172-176.

[33] Angell, C. A. Formation of glasses from liquids and biopolymers. *Science* **1995,** *267,* 1924-1935

[34] Richert, R. On the dielectric susceptibility spectra of supercooled *o*-terphenyl. *J. Chem. Phys*. **2005**, *123*, 154502/1–154502/3.

[35] Goresy, T. E.; Böhmer, R. Dielectric relaxation processes in solid and supercooled liquid solutions of acetaminophen and nifedipine. *J. Phys.: Condens. Matter* **2007**, *19*, 205134/1–205134/9.

[36] Kunal, K.; Robertson, C. G.; Pawlus, S.; Hahn, S. F.; Sokolov, A. P. Role of chemical structure in fragility of polymers: a qualitative picture. *Macromolecules* **2008,** *41*, 7232-7238.

[37] Abou Elfadl, A.; Kahlau, R.; Herrmann, A.; Novikov, V. N.; Rössler, E. A. From Rouse to fully established entanglement dynamics: a study of polyisoprene by dielectric spectroscopy. *Macromolecules* **2010,** *43,* 3340-3351.

[38] Lodge, T. P.; McLeish, T. C. B. Self-concentrations and effective glass transition temperatures in polymer blends. *Macromolecules* **2000,** *33* (14), 5278-5284.

[39] Konishi, T.; Tanaka, H. Possible origin of enhanced crystal growth in a glass. *Phys. Rev. B* **2007,** *76*, 220201.

[40] Stevenson, J. D.; Wolynes, P. G. The ultimate fate of supercooled liquids. *The Journal of Physical Chemistry A* **2011,** *115*, 3713-3719.

[41] Caroli, C.; Lemaître, A. Ultrafast spherulitic crystal growth as a stress-induced phenomenon specific of fragile glass-formers. *The Journal of Chemical Physics* **2012,** *137*, 114506.

[42] Powell, C. T.; Xi, H.; Sun, Y.; Gunn, E.; Chen, Y.; Ediger, M. D.; Yu, L. Fast crystal growth in *o*-terphenyl glasses: a possible role for fracture and surface mobility. *The Journal of Physical Chemistry B* **2015,** *119*, 10124-10130.

[43] Hasebe, M.; Musumeci, D.; Yu, L. Fast surface crystallization of molecular glasses: creation of depletion zones by surface diffusion and crystallization flux. *The Journal of Physical Chemistry B* **2015,** *119*, 3304-3311.

[44] Cicerone, M. T.; Blackburn, F. R.; Ediger, M. D. Anomalous diffusion of probe molecules in polystyrene: evidence for spatially heterogeneous segmental dynamics. *Macromolecules* **1995,** *28*, 8224-8232.

[45] Zhang, S.; Dou, S.; Colby, R. H.; Runt, J. Glass transition and ionic conduction in plasticized and doped ionomers. *Journal of Non-Crystalline Solids* **2005,** *351*, 2825-2830.

[46] Klein, R. J.; Runt, J. Plasticized single-ion polymer conductors: conductivity, local and segmental dynamics, and interaction parameters. *The Journal of Physical Chemistry B* **2007,** *111*, 13188-13193.

[47] Borodin, O.; Smith, G. D. Mechanism of ion transport in amorphous poly(ethylene oxide)/LiTFSI from molecular dynamics simulations. *Macromolecules* **2006,** *39*, 1620-1629.

Chapter 5. Effect of Polymer Additives on Crystal Nucleation in A Glass-Forming Molecular Liquid: D-Sorbitol Containing Polyvinylpyrrolidone

To be submitted to J. Phys. Chem. B

Chengbin Huang[1], Chenyang Shi[2], Geoff G. Z. Zhang[2], Lian Yu[1,3,*]

[1] School of Pharmacy, University of Wisconsin-Madison, Madison, WI, 53705, USA

[2] Drug Product Development, Research and Development, AbbVie Inc., North Chicago, IL, 60064, USA

[3] Department of Chemistry, University of Wisconsin-Madison, Madison, WI, 53705, USA

5.1 Abstract

The rate of crystal nucleation in liquid D-sorbitol has been measured in the presence of polyvinylpyrrolidone (PVP) of different concentrations and molecular weights, and compared with the rate of crystal growth measured under the same conditions. The presence of PVP can significantly reduce the rate of nucleation. At the temperatures studied (near the temperature of maximal nucleation rate in pure sorbitol), 10 wt % PVP K30 can reduce the rate of nucleation by a factor of 40, and the effect increases with polymer concentration and with falling temperature. At a fixed polymer concentration (10 % wt), the polymer's inhibition effect becomes stronger with increasing molecular weight. Under the same conditions of this study, the polymer additive shows a similar effect on the rate of crystal growth, suggesting a similar kinetic inhibition of nucleation and growth by the polymer additives. These results can be explained by the reduction of molecular mobility in the presence of the polymer. They do not support the view that polymer-host hydrogen bonding is the controlling factor since PVP of different molecular weights form the same number of hydrogen bonds per monomer but have very different effects on nucleation and growth at the same weight fraction.

5.2 Introduction

There is considerable interest in understanding the crystallization in supercooled molecular liquids and glasses. These materials have important applications in organic electronics, bio-preservation, and pharmaceutics. Amorphous drugs are useful for the delivery of poorly soluble drugs, taking advantage of their higher solubility than the corresponding crystals. A central issue in developing amorphous materials is to prevent crystallization, since crystallization negates all their advantages over crystalline materials. Many molecular glasses readily crystallize,[1,2,3,4,5] making the understanding of crystallization a major task in developing these materials.

Crystallization consists of nucleation and growth. In the nucleation step, a viable nucleus forms, followed by the growth to macroscopic size. Given their very different kinetics, nucleation and growth must be studied independently. At present, the understanding is further advanced on crystal growth in glass-forming molecular liquids[6,7,8] than on nucleation.[9] It has been shown that crystal growth in molecular glasses can be substantially faster relative to the process in the liquid state owing to crystallization-induced fracture and fast surface diffusion.[10] In contrast, quantitative measurements of nucleation rates have been conducted only recently. These measurements have found a greater variation between systems in nucleation rate relative to growth rate.

Most amorphous materials contain multiple chemical components. Amorphous drugs, for example, are often formulated with polymers to inhibit crystallization and improve wetting by water. It is important to understand how a polymer additive influences nucleation and growth in a molecular glass. Here, again, the polymer effect is better understood on crystal growth than on nucleation. Recent work has shown that polymers can effectively inhibit crystal growth in molecular glasses. [11,12,13,14,15,16,17] For a dilute polymer additive that is melt-miscible with the host molecules, the segmental mobility of the polymer chain plays an important role in controlling the effect on crystal growth.[17] The goal of this work is to expand the current understanding to include the polymer effect on crystal nucleation. This would help produce stable amorphous materials by controlling crystallization using polymer additives.

In this study, the rate of crystal nucleation is measured in D-sorbitol, a well-studied molecular glass-former, that contains polyvinylpyrrolidone (PVP) of different concentrations and molecular weights. For comparison, the effect of the polymer on crystal growth rate is also assessed under the same conditions. We find that PVP can significantly reduce the rate of nucleation. At the temperatures studied (near the temperature of maximal nucleation rate in pure sorbitol), 10 wt %

PVP K30 can reduce the rate of nucleation by a factor of 40. The polymer effect increases with increasing polymer concentration and with falling temperature. At a fixed concentration, the polymer effect is stronger at higher molecular weight. Interestingly, the polymer's effect on crystal growth rate runs approximately in parallel with that on nucleation rate, suggesting a similar kinetic inhibition of both processes at the temperatures studied. These results can be explained by the elevated viscosity in the presence of polymer solutes.

5.3 Experimental Section

D-sorbitol (purity ≥ 99%) was purchased from Sigma-Aldrich (St. Louis, MO) and used as received. The dimer of vinyl pyrrolidone ("VP dimer") was from AbbVie Inc. Polyvinylpyrrolidone (PVP) of different molecular weights was purchased from commercial sources: PVP K12 (Kollidon 12PF) and PVP K30 (Kollidon 30) from BASF; PVP K15 from ISP Technologies (Texas City, TX); PVP K90 from GAF Chemicals. Table 1 shows molecular structures and some physical properties of the materials utilized.

A D-sorbitol solution containing PVP was prepared by cryomilling (SPEX CertiPrep 6750 with liquid nitrogen as coolant) followed by melting. A 1 g mixture of D-sorbitol and 10 wt % PVP was prepared first by cryomilling. This mixture was diluted if necessary (*e.g.* to 2 wt % PVP), also by cryomilling. Each sample was cryomilled at 10 Hz for five 2-min cycles, each followed by a 2-min cooldown. To make a sample for measuring the rates of crystal nucleation and growth, 30-50 mg of a D-sorbitol/PVP mixture was melted at 413 K on a coverslip for 12 h to remove air bubbles; the clear melt was covered by another coverslip to make a sandwich. The thickness of the liquid film was calculated from its mass, its density, and its lateral area (defined by the area of the coverslip). The sample thickness was confirmed not to affect the observed rates of nucleation and growth (by varying thickness from 40 to 400 μm). The sample was cooled and stored in a

desiccator at target temperatures maintained with ovens (±1 K). To obtain nucleation rates, crystals were observed and counted through a polarized light microscope (Olympus BX53) equipped with a digital camera. Crystal growth rate was measured by tracking the size of a crystal front over time; each reported rate is the average of 9-12 measurements in three separate samples.

Differential Scanning Calorimetry (DSC) measurements were performed in crimped aluminum pans with approximately 5-10 mg materials, using a TA Q2000 differential scanning calorimeter. The samples were melted in pans at 413 K for 12 h to remove air bubble, and cooled and heated at 10 K/min under 50 ml/min N_2 purge to determine the T_g.

5.4 Results

Polymer-Host miscibility. To interpret a polymer's effect on the rates of crystal nucleation and growth, it is important to determine whether it is miscible with the host molecules. Given that the isomer of D-sorbitol, D-mannitol, is continuously miscible with PVP,[18] miscibility is likely observed between PVP and D-sorbitol. Limited experiments were performed to verify miscibility at the concentrations studied (up to 10 wt %). For this purpose, the mixture's glass transition temperature T_g was measured as a function of PVP concentration, and a gradual change of T_g would be an indication of miscibility. Figure 1 shows the results of this T_g test for D-sorbitol containing PVP K90 (the highest molecular-weight fraction used). Note the systematic increase of T_g with the concentration of PVP. The increase of T_g is expected because of the high T_g of PVP (T_g = 449 K for PVP K90) relative to D-sorbitol (T_g = 269 K). The data in Figure 1 cover the PVP concentration range 0 – 20 wt %, ensuring that miscibility exists at all the concentrations used in this study (≤ 10 wt %).

Table 1. Molecular structures and properties of the materials used in this study.

	Molecular structure	M_w (g/mol)	T_g (K)
D-sorbitol	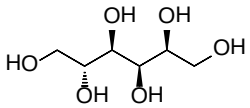	182.2	269
VP dimer	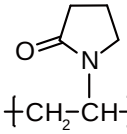	224	217
PVP K12		2000-3000	375
PVP K15		8000	393
PVP K30		44-54 K	437
PVP K90		1-2 M	449

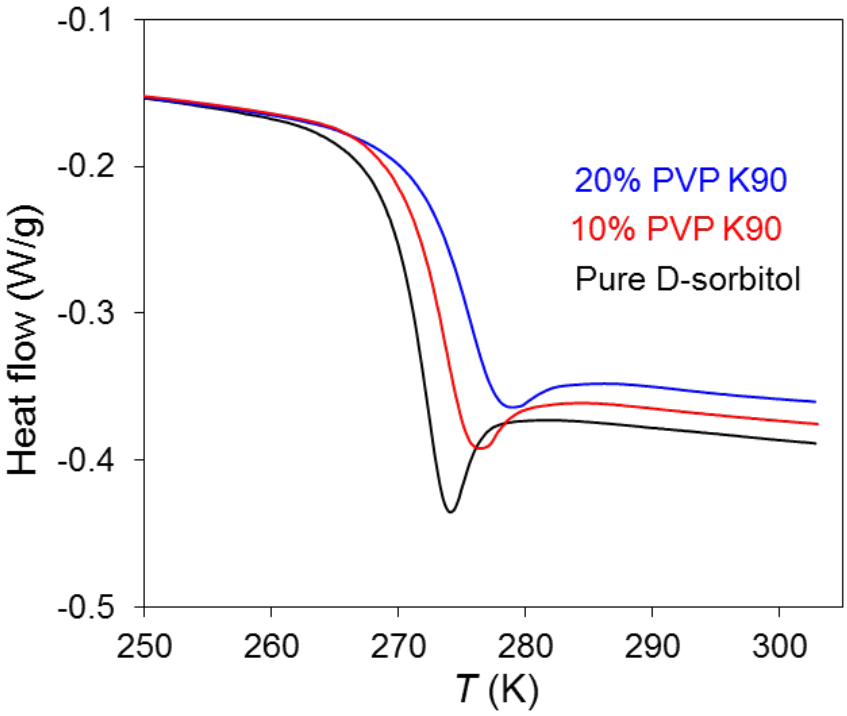

Figure 1. DSC traces of the glass transition in PVP K90 doped D-sorbitol to test the miscibility of the components.

Crystal Nucleation Rates. In this work, the *one-stage method* was used to measure the crystal nucleation rates at the temperatures where crystal growth is relatively fast. The D-sorbitol liquids containing PVP of different molecular weights or concentrations are allowed to nucleate and grow for some time t_0 at which individual crystals are observable. The typical data for D-sorbitol liquid containing 10% PVP K30 is shown in Figure 2a. It is worth noting that the crystals have different sizes. Since the crystal grows at a constant rate u of 0.2 μm/h, an early-born crystal nucleus has longer time to grow to a larger size. The birth time of each crystal is calculated from its current size (radius, r):

$$t = t_0 - r/u$$

where t_0 is the current time (time of observation).

The ability to date the birth of each crystal allows the determination of the number of nucleation events per unit volume as a function of time (Figure 2b). An induction period noted in other work,[19] a steady state where the nuclei density per unit volume increases linearly with time, and a deviation period from the steady state because of the less remaining liquid are shown in the plot. In this study, we focus on the polymer effect on the steady-state nucleation rate J, given by the slope of the plot in Figure 2b ($J = 1.9 \times 10^5$ $m^{-3} \cdot s^{-1}$ at 297 K). It is worth noting that in the calculation of birth time, u is the growth rate of the observable crystal and is assumed to be the same for the (invisible) crystal nucleus. If the nucleus growth rate differs from that of the mature crystal, a constant shift is added to the calculated birth times without affecting the calculation of the steady-state nucleation rate.

The one-stage method above requires relatively fast growth rate of crystals to be observable, and is unsuitable when crystal growth is slow. A *two-stage method* has been employed for this situation,[20] and applied to measure J in pure D-sorbitol and D-arabitol previously.[9] Here, PVP

doped D-sorbitol liquids are allowed to nucleate at a low temperature and then heated to a high temperature to grow the nuclei to visible size to be counted. The growth temperature is chosen so that pre-formed nuclei can grow quickly but no new nuclei form during the time of development.

The typical data collected by the *two-stage method* is shown in Figure 3. The D-sorbitol liquid containing 10 wt % PVP K30 spent different times at 288 K but the same time (5 h) at 313 K. It is obvious that the sample spending longer time at 288 K (504 h) developed more crystals than the sample with shorter time (67 h), while both contained crystals of similar size (*ca.* 90 μm). Furthermore, before heating to 313 K, no crystals were visible, and without the time at 288 K, no crystals were observed at 313 K up to 10 h. All these results confirm that the crystals (seen in Figure 3a) nucleated at 288 K and grew at 313 K. This allows the determination of the density of nuclei formed at 288 K as a function of nucleation time (Figure 3b). As in Figure 2b, an induction period is evident, followed by a steady state nucleation whose rate is $J = 6.7 \times 10^5$ $m^{-3} \cdot s^{-1}$. No deviation period from the steady state is shown in this two-stage method, which might result from the slow crystal growth inside sorbitol-PVP liquids during the nucleation step at 288 K.

Crystal Growth Rates. In addition to the crystal nucleation, the rates of crystal growth are determined by tracking the size of a crystal front over time. Figure 4 shows the typical data collected in this work. The process of crystal growth was recorded in a pure D-sorbitol liquid and in a D-sorbitol liquid containing 10 wt % PVP K30. These crystals are polycrystalline spherulites, and the crystal growth rate is constant in time (Figure 2b). Relative to pure D-sorbitol, the presence of 10 wt % PVP K30 significantly slows down D-sorbitol crystal growth by a factor of 10 at 297 K. This polymer effect is consistent with the previous observations a miscible high-T_g polymer can effectively inhibit crystal growth in a molecular liquid.[15,17]

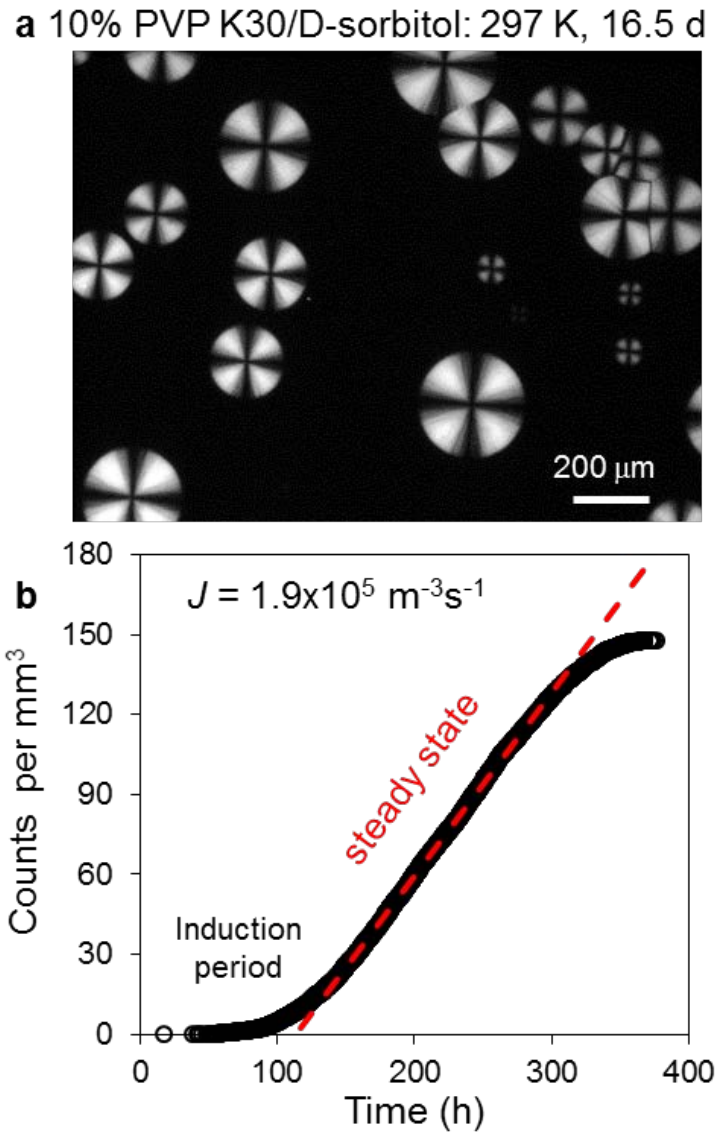

Figure 2. (a) A sample of D-sorbitol containing 10 wt % PVP K30 after crystallizing for 16.5 days at 297 K. Note the different crystal sizes. Since the crystals grow at a constant rate of 0.2 µm/h, the larger ones were born earlier, and the smaller ones born later. This enables the determination of the number of crystal nuclei formed per unit volume as a function of time (b). The slope of this plot is the nucleation rate of 1.9×10^5 $m^{-3} \cdot s^{-1}$.

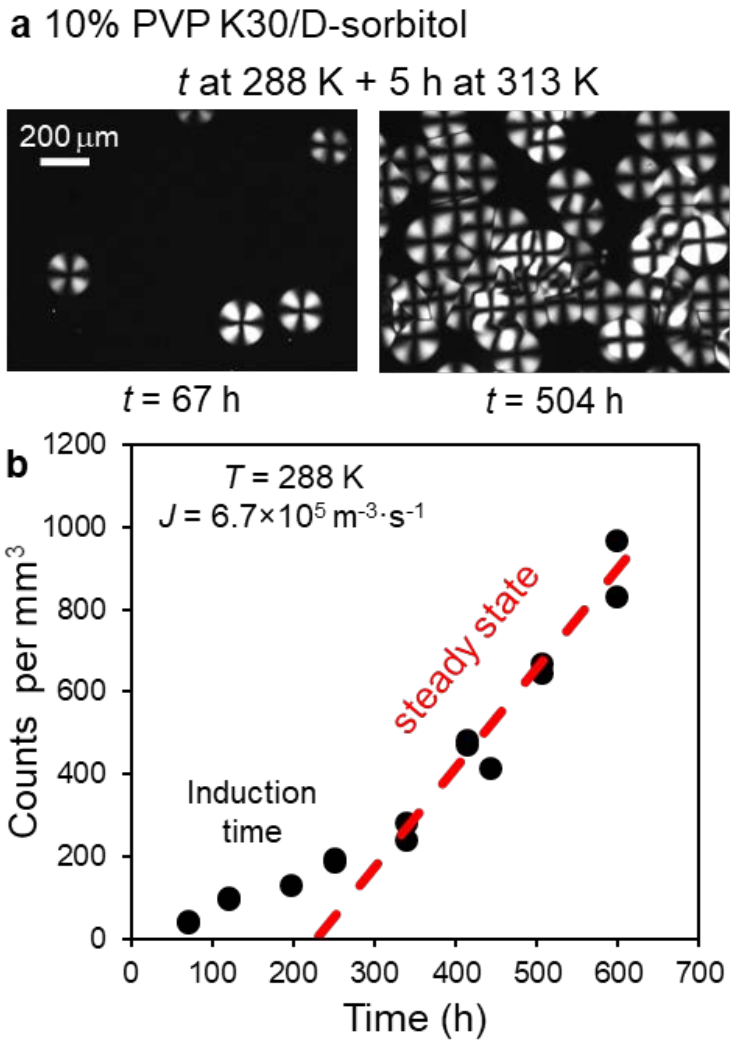

Figure 3. (a) Crystals observed after 10 wt % PVP K30 doped D-sorbitol liquids spent different times at 288 K (67 or 504 h) to nucleate followed by 5 h at 313 K to grow. (b) Nuclei density as a function of nucleation time at 288 K. The slope of this plot is the nucleation rate of 6.7×10^5 $m^{-3} \cdot s^{-1}$.

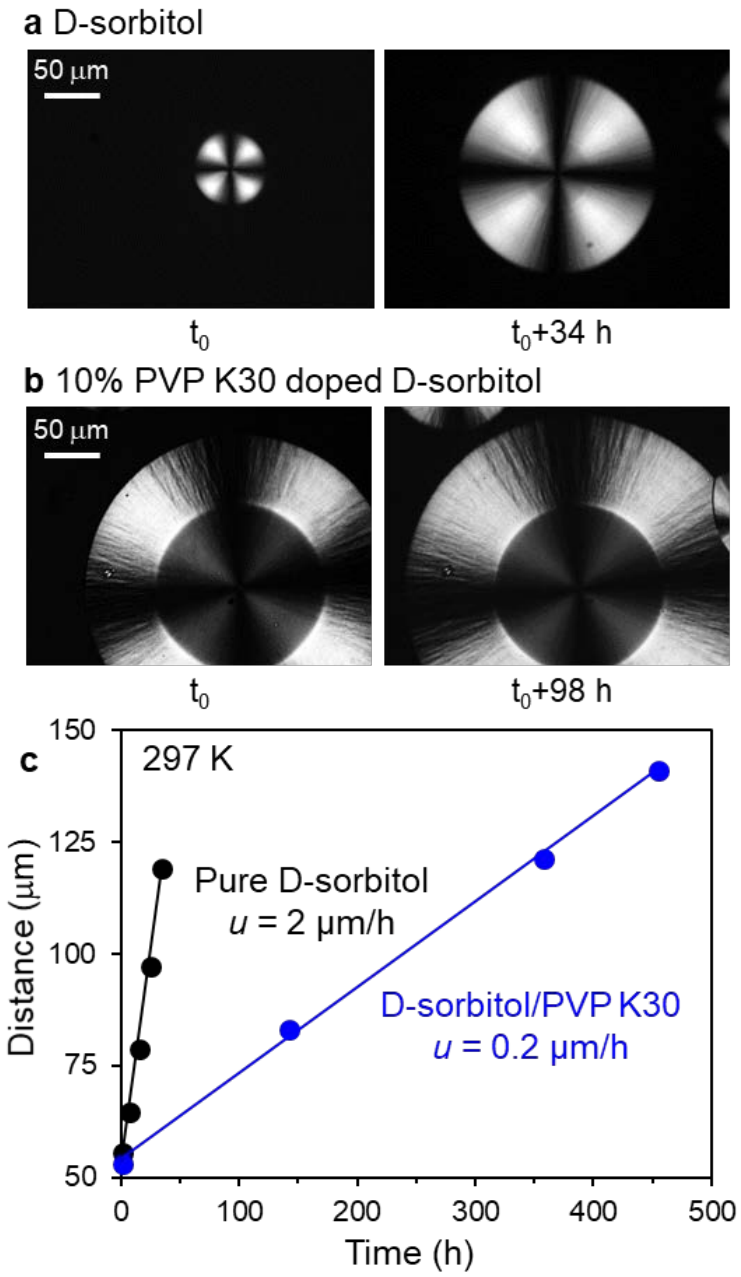

Figure 4. Process of crystal growth at 297 K in (a) D-sorbitol and (b) D-sorbitol containing 10 wt % PVP K30. Regions of different brightness correspond to crystals grown at different temperatures. (c) Distance of crystal growth vs time. The slope is the growth rate of 2 μm/h for pure D-sorbitol and 0.2 μm/h for D-sorbitol containing 10% PVP K30.

Effect of Polymer Concentration on Crystal Nucleation and Growth. Figure 5 summarizes the data collected on the effect of PVP K30 of different concentrations (2, 5 and 10 wt %) on the rates of crystal nucleation and growth in D-sorbitol liquids. The effect of PVP was evaluated at several temperatures near the temperature at which nucleation is the fastest in pure D-sorbitol (see black circles in Figure 5a). At the 10 wt % PVP concentration, nucleation rate J was measured at all but one temperature at which the pure liquid was investigated (the very lowest temperature was skipped because of long experimental time). For this system, the J vs temperature curve as the same shape as that for the pure system. The temperature of maximal nucleation rate T_{max} is approximately 288 K. The presence of the polymer, however, decreases the rate of nucleation at every temperature investigated. At 288 K, the inhibitory effect is a factor of 40 and this effect increases with falling temperature (see below). In addition to 10 wt %, other PVP concentrations were investigated but at more limited temperatures (all above T_{max}). The results (Figure 5a) show that with increasing PVP concentration, J decreases.

Figure 5b shows the effect of PVP on the rates of crystal growth in D-sorbitol. For comparison with the nucleation rates, the crystal growth rates were measured at approximately the same temperatures. These results indicate that the rate of crystal growth systematically decreases with increasing PVP concentration. Note that at most of the temperatures studied, the J and u have the opposite temperature dependence.

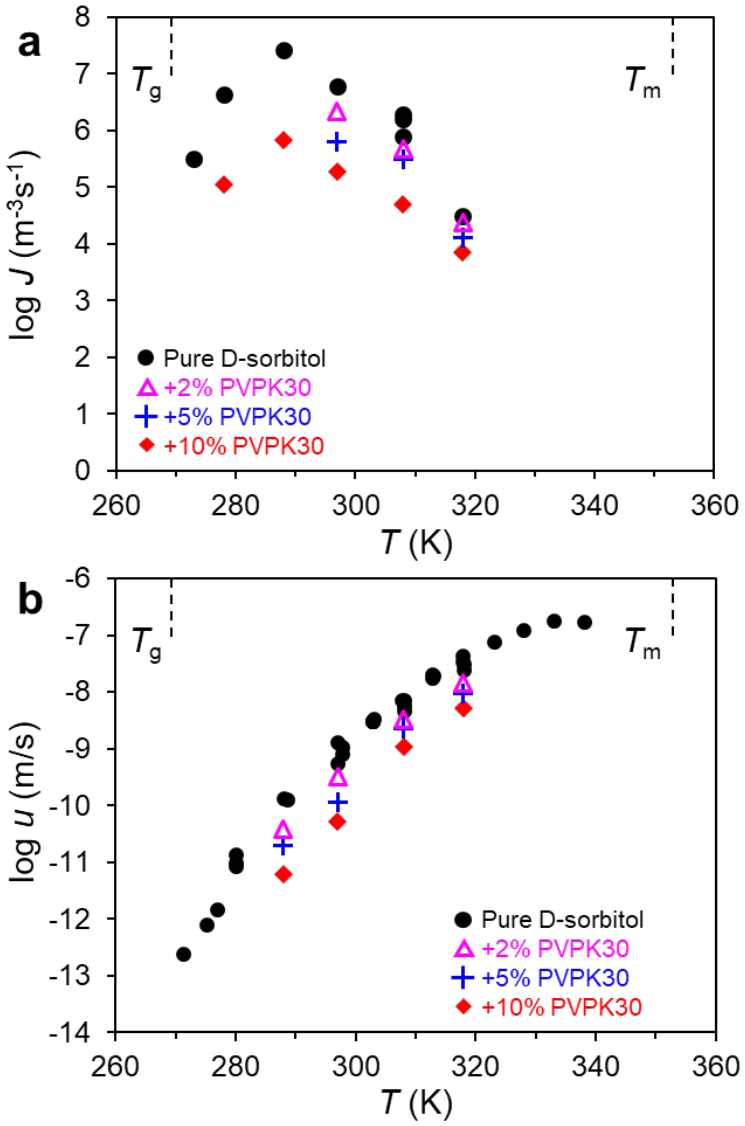

Figure 5. Effect of PVP K30 on the rate of crystal nucleation (a) and growth (b) in D-sorbitol. The polymer concentration ranges from 0 to 10 wt %.

In Figure 6, the rates of nucleation and growth are plotted against the PVP K30 concentration. Figure 6a shows that at a given temperature, log *J* decreases approximately linearly with polymer concentration. Furthermore, with cooling, the slope of each line becomes steeper. This signifies that PVP has a greater inhibitory effect on nucleation at lower temperatures.

Figure 6b reveals a similar effect of PVP on the rates of crystal growth. At a given temperature, log *u* decreases almost linearly with PVP concentration, and the slope of the line becomes steeper at lower temperatures. Thus, the presence of PVP slows down crystal growth in D-sorbitol in a similar manner as it does nucleation.

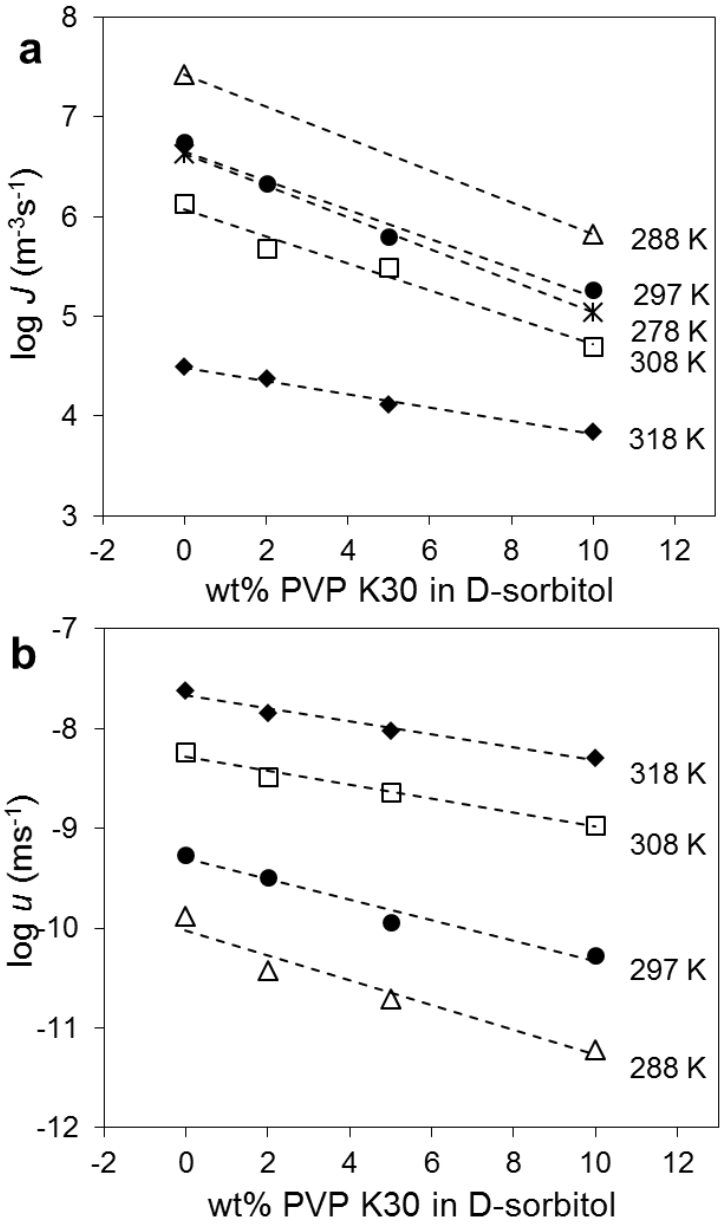

Figure 6. The rate of crystal nucleation *J* (a) and growth *u* (b) in D-sorbitol containing PVP K30 of different concentrations. Note that in most of the temperature range studied, *J* and *u* have opposite temperature dependence.

Effect of Polymer Molecular Weight on Crystal Nucleation and Growth. Figure 7 summarizes the data collected to test the effect of polymer molecular weight on crystal nucleation and growth in D-sorbitol. For these experiments, the PVP concentration was held at 10 wt %. For the molecular-weight fraction "K30", measurements were made at nearly all the temperatures investigated for the pure system, while for the other fractions, only three temperatures above T_{max} were investigated. Figure 7a shows that at 10 wt %, all PVP fractions suppress the rate of crystal nucleation, but the effect depends strongly on the molecular weight. The VP dimer has very little effect, while the highest molecular-weight fraction PVP K90 reduces the nucleation rate by nearly two orders of magnitude at 297 K. The data indicate that at a fixed temperature, the inhibitory effect of PVP increases with molecular weight, and that for a given PVP fraction, the inhibitory effect becomes stronger with falling temperature.

In Figure 8, the rates of crystal nucleation and growth are plotted against the molecular weight of PVP at the constant polymer concentration. Figure 8a shows that at a given temperature, J decreases systematically with polymer molecular weight. These log J vs log M_w plots are almost (but not perfectly) linear; the slope of the line becomes slightly steeper with falling temperature (from - 0.3 at 318 K to – 0.4 at 297 K). Figure 8b shows a similar effect of PVP's molecular weight on crystal growth. At each temperature, log u decreases almost linearly with log M_w and the slope of the line becomes steeper with falling temperature (from -0.2 at 318 K to -0.4 at 297 K).

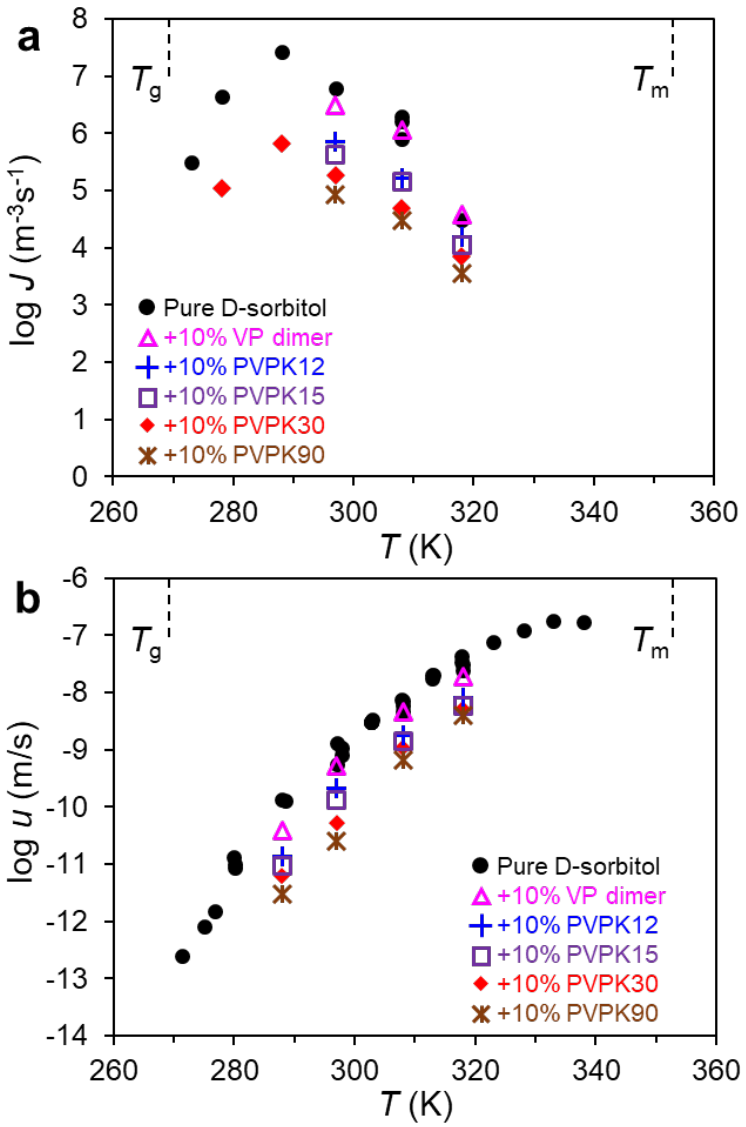

Figure 7. The rate of crystal nucleation (a) and growth (b) in D-sorbitol containing 10 wt % PVP of different molecular weights (VP dimer, PVP K12, PVP K15, PVP K30 and PVP K90).

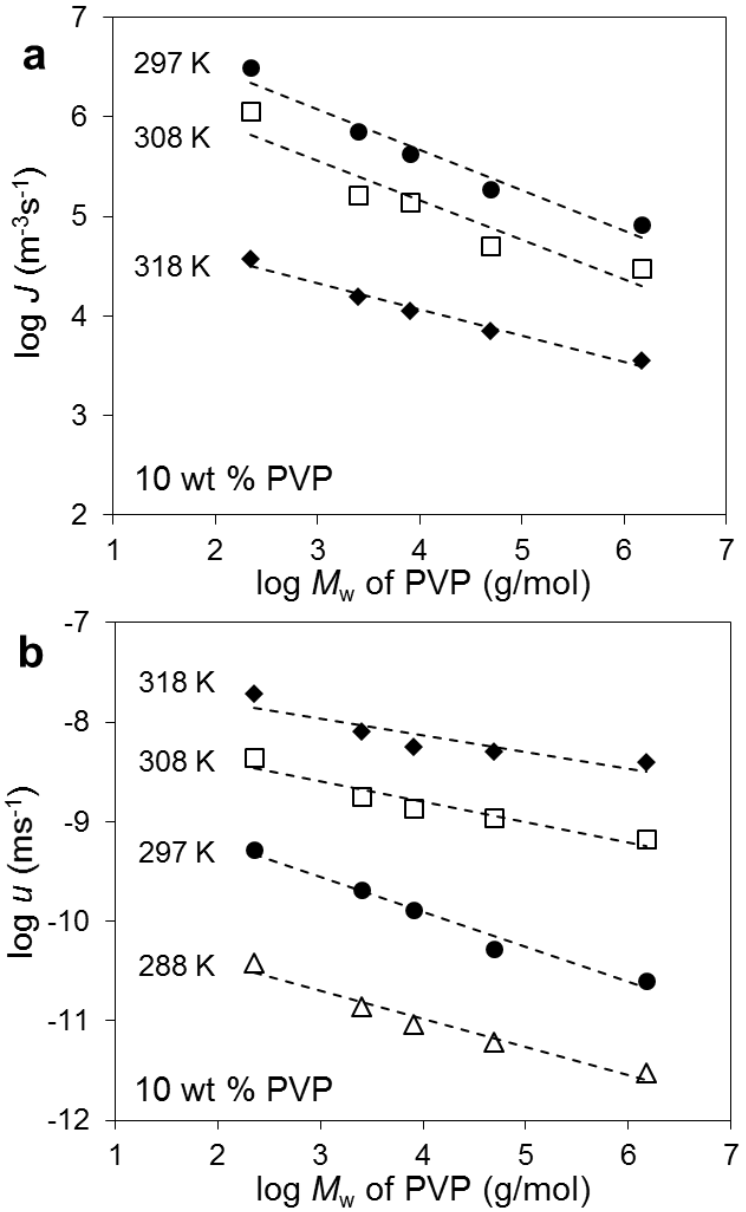

Figure 8. The rate of crystal nucleation (a) and growth (b) in D-sorbitol containing 10 wt % PVP as a function of PVP molecular weight.

5.5 Discussion

This study has examined the effect of PVP of different concentrations and molecular weights on the crystal nucleation and growth in D-sorbitol liquids. At the temperatures studied, PVP can significantly reduce the rates of both nucleation and growth, with its effect intensifying with increasing polymer concentration, increasing polymer molecular weight, and decreasing temperature. There seems to be strong similarity between the PVP effects on nucleation and growth. Here we further explore this similarity to understand the role of the polymer in the crystallization of the small-molecule host.

In Figure 9, the results in Figure 5 (same molecular weight, different concentrations) and Figure 7 (same concentration, different molecular weights) are plotted together in the format $u/u_{host} = J/J_{host}$, where u_{host} and J_{host} are the rates of crystal growth and nucleation in pure D-sorbitol, respectively. The diagonal line represents $u/u_{host} = J/J_{host}$, the condition where the polymer has the same effect on growth and nucleation. Figure 9 shows that all the data points approximately cluster together, and the overall trend roughly follows $u/u_{host} = J/J_{host}$. This indicates that at the temperatures of this study, the rates of nucleation and growth are similarly affected by the polymer. The deviation from the diagonal line reflects the fact that the polymer effect on nucleation is slightly stronger than on crystal growth (greater change in J than in u).

According to classical theories, the rates of nucleation and growth in a pure liquid can be written in a similar form:

$$J = k_J F_{thermo\ J}$$

$$u = k_u F_{thermo\ u}$$

In these equations, k is a kinetic factor specifying the frequency at which attempts are made to enlarge a nascent nucleus (k_J) or a macroscopic crystal (k_u), and F_{thermo} is a thermodynamic factor

relevant for nucleation ($F_{\text{thermo J}}$) or growth ($F_{\text{thermo u}}$). Given the relatively low polymer concentration (≤ 10 wt %), it is a reasonable first approximation to assume that the thermodynamic factors are not significantly altered relative to the pure system. Under this assumption, the simplest interpretation of our results is that the polymer reduces the kinetic factors k_J and k_u to a similar extent. For pure D-sorbitol, k_J and k_u have nearly the same temperature dependence,[9] suggesting a similar kinetic barrier for nucleation and growth. Thus, to a first approximation, the polymer effect observed can be attributed to an increase of the kinetic barrier common for nucleation and growth.

For a single-component system, the kinetic factors k_J and k_u are linked to motions of only one type of molecules. For a binary system, however, the motions of both components are potentially relevant. The magnitude of the polymer effect observed here, nearly two orders of magnitude suppression of J at the lowest temperatures, argues that the polymer's mobility may have an important role in inhibiting crystallization. This is because at a concentration 10 wt % or lower, PVP is not expected to reduce the mobility of host molecules by two orders of magnitude. Exactly how polymer mobility influences crystallization is still unclear. Previous studies of crystal growth in molecular glasses ($T < T_g$) have observed that a polymer's effect correlates with its segmental mobility.[15,17] That result is rationalized on the basis of a special mechanism of crystal growth in molecular glasses ("GC growth") involving crystallization-induced fracture and local transformation by surface diffusion, and the polymer's interference of the process. That conclusion has questionable validity here since crystal growth occurs in a viscous liquid where fracture cannot occur. Our results in Figure 8 show that the polymer's inhibitory effect on J and u increases steadily with molecular weight. This rules out segmental mobility as the controlling factor since segmental mobility becomes insensitive to molecular weight above approximately 100 monomers ($M_w \approx 10$ kg/mol for PVP).[21,22] Our results are weakly suggestive of a possible role for the polymer's center-

of-mass diffusion. The diffusion coefficient of a polymer chain in a dilute solution should scale with its molecular weight roughly as $M^{-0.5}$.[23,24,25] In comparison, our data in Figure 8 show that J and u vary with the PVP molecular weight as $M^{-\xi}$, where ξ = 0.2 to 0.4.

Further progress in this area will require a detailed evaluation of the effect of the polymer solute on the thermodynamic driving force of crystallization.[18] Given the very different temperature dependence of the thermodynamic factors for nucleation and growth, there could be a thermodynamic contribution to the different responses of nucleation and growth to a polymer impurity.

Effect of hydrogen bonding. It has been proposed that polymer-host hydrogen bonding has a controlling effect on the polymer's ability to inhibit crystal growth in a molecular glass.[26,27] Here, we evaluate this proposal against the results of this work, recognizing that the data were not collected in the glassy state, but in the liquid state. D-sorbitol is a donor and an accepter of hydrogen bonds; PVP is an acceptor of hydrogen bonds. At the same weight fraction of PVP, we expect the same number of hydrogen bonds per unit volume, regardless of the polymer's molecular weight. The hydrogen-bonding model would predict that all PVP molecular-weight fractions should have the same effect on nucleation and growth. However, our results show a strong molecular weight dependence of the polymer's effect on crystallization. Our results are consistent with the view that the polymer's mobility plays an important role in controlling the crystallization of host molecules.

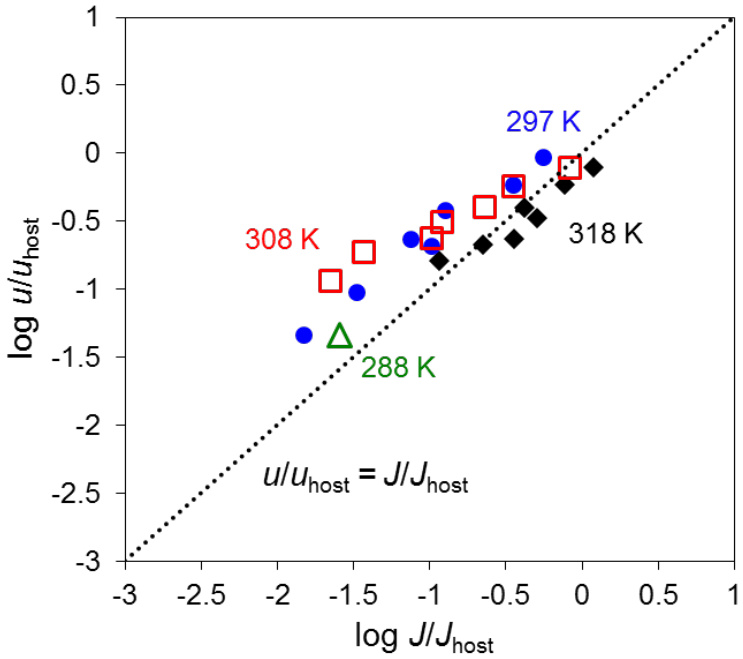

Figure 9. Correlation between the PVP effects on nucleation and growth. Normalized crystal growth rate u/u_{host} plotted against normalized crystal nucleation rate J/J_{host} in PVP doped D-sorbitol. This plot includes the data in both Figure 3 (same M_w, different concentrations) and Figure 5 (same concentration, different M_w). The line represents $u/u_{host} = J/J_{host}$ (the polymer has the same effect on growth and nucleation).

5.6 Conclusion

We have measured the rates of crystal nucleation and growth in D-sorbitol liquids in the presence of polyvinylpyrrolidone (PVP) of different concentrations and molecular weights. We find that PVP can significantly reduce the rate of nucleation and its effect increases with increasing polymer concentration, with increasing polymer molecular weight, and with falling temperature. The polymer's effect on crystal growth rate is quite similar to that on nucleation rate, suggesting a similar kinetic control of the two processes at the temperatures studied. These results suggest that the polymer's mobility (possibly center-of-mass diffusion) may be involved in its inhibitory effect on crystal nucleation and growth. Our results do not support the view that polymer-host hydrogen bonding is the controlling factor.

5.7 Acknowledgments

We thank AbbVie Inc. for supporting this work.

5.8 References

[1] Hasebe, M.; Musumeci, D.; Powell, C. T.; Cai, T.; Gunn, E.; Zhu, L.; Yu, L. Fast surface crystal growth on molecular glasses and its termination by the onset of fluidity. *J. Phys. Chem. B* **2014,** *118*, 7638-7646.

[2] Shi, Q.; Cai, T. Fast crystal growth of amorphous griseofulvin: relations between bulk and surface growth modes. *Crystal Growth & Design* **2016,** *16*, 3279-3286.

[3] Sun, Y.; Zhu, L.; Kearns, K. L.; Ediger, M. D.; Yu, L. A. Glasses crystallize rapidly at free surfaces by growing crystals upward. *Proc. Natl. Acad. Sci. U. S. A.* **2011,** *108*, 5990-5995.

[4] Wu, T.; Yu, L. Surface crystallization of indomethacin below Tg. *Pharmaceutical Research* **2006,** *23*, 2350-2355.

[5] Wu, T.; Yu, L., Origin of Enhanced Crystal Growth Kinetics near Tg Probed with Indomethacin Polymorphs. *The Journal of Physical Chemistry B* **2006,** *110* (32), 15694-15699.

[6] Hikima, T.; Adachi, Y.; Hanaya, M.; Oguni, M. Determination of potentially homogeneous-nucleation-based crystallization in o-terphernyl and an interpretation of the nucleation-enhancement mechanism. *Phys. Rev. B* **1995,** *52*, 3900-3908.

[7] Sun, Y.; Xi, H. M.; Chen, S.; Ediger, M. D.; Yu, L. Crystallization near glass transition: transition from diffusion-controlled to diffusionless crystal growth studied with seven polymorphs. *J. Phys. Chem. B* **2008,** *112*, 5594-5601.

[8] Zhu, L.; Wong, L.; Yu, L. Surface-enhanced crystallization of amorphous nifedipine. *Molecular pharmaceutics* **2008,** *5*, 921-926.

[9] Huang, C.; Chen, Z.; Gui, Y.; Shi, C.; Zhang, G.; Yu, L. Crystal nucleation rates in glass-forming molecular liquids: D-sorbitol, D-arabitol, D-xylitol, and glycerol. *The Journal of Chemical Physics* **2018** (In press)

[10] Powell, C. T.; Xi, H.; Sun, Y.; Gunn, E.; Chen, Y.; Ediger, M. D.; Yu, L. Fast crystal growth in *o*-terphenyl glasses: a possible role for fracture and surface mobility. *The Journal of Physical Chemistry B* **2015,** *119*, 10124-10130.

[11] Ishida, H.; Wu, T. A.; Yu, L. Sudden rise of crystal growth rate of nifedipine near Tg without and with polyvinylpyrrolidone. *Journal of Pharmaceutical Sciences* **2007,** *96*, 1131-1138.

[12] Kestur, U. S.; Lee, H.; Santiago, D.; Rinaldi, C.; Won, Y. Y.; Taylor, L. S. Effects of the molecular weight and concentration of polymer additives, and temperature on the melt crystallization kinetics of a small drug molecule. *Crystal Growth & Design* **2010,** *10*, 3585-3595.

[13] Kestur, U. S.; Taylor, L. S. Role of polymer chemistry in influencing crystal growth rates from amorphous felodipine. *CrystEngComm* **2010,** *12*, 2390-2397.

[14] Cai, T.; Zhu, L.; Yu, L. Crystallization of organic glasses: effects of polymer additives on bulk and surface crystal growth in amorphous nifedipine. *Pharmaceutical Research* **2011,** *28*, 2458-2466.

[15] Powell, C. T.; Cai, T.; Hasebe, M.; Gunn, E. M.; Gao, P.; Zhang, G.; Gong, Y. C.; Yu, L. Low-concentration polymers inhibit and accelerate crystal growth in organic glasses in correlation with segmental mobility. *J. Phys. Chem. B* **2013,** *117*, 10334-10341.

[16] Kothari, K.; Ragoonanan, V.; Suryanarayanan, R. The role of drug–polymer hydrogen bonding interactions on the molecular mobility and physical stability of nifedipine solid dispersions. *Molecular pharmaceutics* **2015,** *12*, 162-170.

[17] Huang, C.; Powell, C. T.; Sun, Y.; Cai, T.; Yu, L., Effect of Low-Concentration Polymers on Crystal Growth in Molecular Glasses: A Controlling Role for Polymer Segmental Mobility Relative to Host Dynamics. *The Journal of Physical Chemistry B* **2017,** *121* (8), 1963-1971.

[18] Sun, Y.; Tao, J.; Zhang, G. G. Z.; Yu, L. Solubilities of crystalline drugs in polymers: an improved analytical method and comparison of solubilities of indomethacin and nifedipine in PVP, PVP/VA, and PVAc. *Journal of Pharmaceutical Sciences* **2010,** *99*, 4023-4031.

[19] V. M. Fokin, E. D. Zanotto, N. S. Yuritsyn, and J. W. P. Schmelzer, Journal of Non-Crystalline Solids **352**, 2681 (2006).

[20] G. Tammann, and E. Jenckel, Zeitschrift für anorganische und allgemeine Chemie **193**, 76 (1930).

[21] Horinaka, J.; Aoki, H.; Ito, S.; Yamamoto, M. Molecular weight effect on local motion of polystyrene studied by the fluorescence depolarization method. *Polymer Journal* **1999,** *31*, 172-176.

[22] Rubinstein, M.; Colby, R. H. *Polymer Physics*; OUP Oxford: 2003.

[23] King, T. A.; Knox, A.; Lee, W. I.; McAdam, J. D. G. Polymer translational diffusion. 1. Dilute theta solutions, polystyrene in cyclohexane. *Polymer* **1973,** *14*, 151-155.

[24] Adam, M.; Delsanti, M. Dynamical properties of polymer-solutions in good solvent by Rayleigh-scattering experiments. *Macromolecules* **1977,** *10*, 1229-1237.

[25] Wheeler, L. M.; Lodge, T. P., Tracer diffusion of linear polystyrenes in dilute, semidilute, and concentrated poly(vinyl methyl ether) solutions. *Macromolecules* **1989,** *22* (8), 3399-3408.

[26] Kestur, U. S.; Taylor, L. S. Role of polymer chemistry in influencing crystal growth rates from amorphous felodipine. *CrystEngComm* **2010,** *12*, 2390-2397.

[27] Kothari, K.; Ragoonanan, V.; Suryanarayanan, R. The role of drug–polymer hydrogen bonding interactions on the molecular mobility and physical stability of nifedipine solid dispersions. *Molecular pharmaceutics* **2015,** *12*, 162-170.

Chapter 6. Hydrogen Bonding in Supercooled Polyalcohols Studied by Synchrotron X-Ray Scattering: D-Mannitol, Dulcitol and D-Arabitol

Chengbin Huang[1], Zhenxuan Chen[1], Men Zhu[2], Chris Benmore[3], Lian Yu[1,2,*]

[1] School of Pharmacy and University of Wisconsin-Madison, Madison, WI, 53705, United States

[2] Department of Chemistry, University of Wisconsin-Madison, Madison, WI, 53705, United States

[3] X-ray Science Division, Advanced Photon Source, Argonne National Laboratory, IL 60439, United States

6.1 Abstract

Synchrotron total X-ray scattering has been used to characterize the hydrogen bonds (HBs) in three polyalcohols in the crystalline state and the amorphous state (liquid or glass). For each system, the atomic pair distribution function (PDF) shows a well-resolved peak at 2.7 Å after removing intramolecular contributions. This peak corresponds to the O…O distance in an intermolecular HB. We find that the O…O bond length does not change significantly from the crystal to the liquid or glass, while the O…O coordination number (the number of HBs formed by each OH group) is ~10% lower in the amorphous phase. The distribution of the O…O distance is slightly narrower in the amorphous phase than in the crystal, perhaps a result of many distinct O…O distances in a crystal (static disorder) in order to achieve regular 3D packing. Furthermore, the O…O distance obtained from total is systematically shorter that that found in single-crystal structures (by ~0.03 Å). This might result from the fact that single-crystal diffraction yields mean atomic positions, whereas total scattering yields correlations between atomic pairs.

6.2 Introduction

X-ray scattering has been used to study the structure of liquids and glasses ever since the invention of the technique.[1,2] It is the standard method to measure a liquid's atomic pair distribution function (PDF). Experimental PDFs have provided critical tests for theories of atomic liquids[3,4] and water.[5] The availability of high-energy synchrotron X-ray sources has enabled measurements of "total scattering" up to high momentum transfer, which is necessary to obtain high-quality PDFs through Fourier transform.[6] In this work, the method of total scattering is applied to characterize hydrogen bonds (HBs) in three polyalcohols in the liquid and glassy state.

HBs are prevalent in molecular materials. Thanks to single-crystal X-ray diffraction, much is known about hydrogen bonds in crystals.[7] The same is not true in the liquid state. The best studied

system is undoubtedly water owing to its importance and its "simplicity" (only three atom-atom correlations need to be determined). HBs have been studied in mono-alcohols.[8,9] After removing intramolecular contributions, the intermolecular PDF contains a peak at $R_{OO} \approx 2.7$ Å corresponding to the O…O distance in an intermolecular HB. By this method, the number of HBs formed by each OH group N_{OO} can be obtained. For mono-alcohols, N_{OO} is close to and slightly smaller than 2 (~1.8 for methanol and ethanol at 293 K), consistent with a HB network of finite size in which each OH is donor once and acceptor once. Vahvaselka *et al.* wrote, "Even though the number of C atoms in the alcohol molecule increases, the ability to form hydrogen bonds remains the same."[9]

The nature of HBs is less well understood in polyalcohol liquids. At present, only the lower members ethylene glycol ($C_2O_2H_6$) [10] and glycerol[11,12] have been studied, and there is considerable disagreement in the literature. For example, there is no consensus on whether HBs in polyalcohols are exclusively intermolecular or partially intramolecular.[13] (This question does not arise for mono-alcohols.) Another complexity for polyalcohols is that these molecules can potentially adopt different conformations in the liquid state. In the case of glycerol, there are six distinct conformers, and many have been proposed to dominate in the liquid state.[12]

To improve the understanding in this area, we have investigated the liquids of 3 higher polyalcohols: D-arabitol ($C_5O_5H_{12}$), D-mannitol ($C_6O_6H_{14}$), and dulcitol ($C_6O_6H_{14}$, a stereoisomer of D-mannitol); see Scheme 1. One reason for choosing these molecules is that they are expected to have straight carbon chains in the liquid state, and this simplifies the analysis of total scattering (see below). These are also the systems that have been studied in this thesis (Chapter 3) with respect to crystal nucleation. There, a key finding is that the liquids of these seemingly similar molecules have very different nucleation rates (10 orders of magnitude). One way to understand

this difference is to compare the liquid structure with the crystal structure, under the assumption that structural similarity might lead to facile nucleation.

6.3 Experimental Section

D-mannitol (purity ≥ 99 %) was purchased from Alfa Aesar; dulcitol (purity ≥ 97 %) and D-arabitol (purity ≥ 99 %) were purchased from Sigma-Aldrich. They were used as received. For scattering experiments, each sample was placed in an X-ray transmitting silica capillary tube (1.5 mm diameter, 10 μm wall thickness). A liquid or glass sample was prepared by melting the crystal in a capillary tube and quenching the sample into an ice-water bath. A crystalline sample was prepared by crystalizing the liquid in the capillary tube at an elevated temperature (373 K for 10 min for D-mannitol and dulcitol; 363 K overnight for D-arabitol). This procedure yielded a good Debye powder, with uniform rings in its 2D diffraction pattern. From the diffraction patterns, the crystal polymorphs were determined, and they are summarized in Table 1. In the case of D-mannitol, an apparently polyamorphic transition occurs if the supercooled liquid is heated above its T_g (284 K), but this transition does not occur under the conditions of this study (275 K, 15 min).

Synchrotron X-ray diffraction was performed on the 6-ID-D beamline at the Advanced Photon Source (APS), Argonne National Laboratory (Illinois, USA). The X-ray wavelength is λ = 0.12355 Å. A Perkin-Elmer amorphous silicon two-dimensional detector was utilized to collect the scattered X-ray intensity with an active area of 409.6 × 409.6 mm^2 (2048 × 2048 pixels with a pixel size of 200×200 μm^2). The capillary sample tube was placed horizontally on a sample holder, and the sample temperature was controlled using a cryostream system (Oxford Instruments). The sample-to-detector distance was 32.46 cm (determined by measuring the diffraction of a cerium dioxide standard). Multiple scans were performed to achieve a total acquisition time of 15 minutes for each sample.

Two-dimensional diffraction patterns of polyalcohols were integrated azimuthally using the program FIT2D[14] to obtain a one-dimensional intensity vs. q curve, where $q = (4\pi/\lambda) \sin\theta$ is the momentum transfer (2θ is the scattering angle). The program PDFGETX2[15] was used to perform various corrections of the data to obtain the structure factor $S(q)$ for coherent scattering, including container background, beam polarization, Compton effect, oblique incidence, sample absorption, and detector efficiency, and to Fourier transform the corrected data to obtain the pair distribution function (PDF). The usable $S(q)$ covers the range from q_{min} = 0.3 Å^{-1} to q_{max} = 21 Å^{-1}. The $S(q)$ values at lower q were obtained by linearly extrapolating the function $F(q) = q\,[S(q) - 1]$ to zero at $q = 0$.

The program DebyePDFCalculator in DiffPy-CMI[16] was used to calculate the structure factor for a single molecule in random orientations and the corresponding PDF. The single molecule was obtained from the known crystal structures in the Cambridge Structural Database (CSD): DMANTL08 for D-mannitol,[17] GALACT for dulcitol,[18] and VOZMAY for D-arabitol.[19] For these calculations, Diffpy-CMI used a single displacement factor U_{iso} for all atomic pairs ($U_{iso} = \sigma^2/2$, where σ is the width of the distribution for the atom-atom distance due to static disorder or thermal fluctuation).

NXFit was used to perform fitting of a peak in the PDF to obtain the characteristics of the atom-atom correlation responsible for that peak, including its distance R, its coordination number N, and its displacement factor σ.[20] For this purpose, NXFit calculates the peak that would appear in the PDF for a hypothetical atom-atom correlation by computing its contribution to the structure factor $S(q)$ and performing a Fourier transform of this contribution under the same conditions used to transform the experimental data (the same q_{max} and window function).[20] This procedure is

necessary since the width of a PDF peak depends on the conditions of Fourier transform. NXFit requires as input the atomic form factors, which we obtained from standard tabulations.[21]

6.4 Results and discussion

Figure 1 shows the structure factors $S(q)$ for the polyalcohols studied. In this work, $S(q)$ is defined by:[6]

$$S(q) = 1 + \frac{I(q) - \langle f^2 \rangle}{\langle f \rangle^2} \qquad (1)$$

In eq. (1), $I(q)$ is the coherent scattering of the sample scaled to oscillate about $\langle f^2 \rangle$ (atom-averaged self-scattering power of each molecule) at high q, and $\langle f \rangle$ is the atom-averaged scattering power of each molecule. Defined in this way, $S(q)$ contains both intramolecular and intermolecular contributions. The validity of the data reduction procedure can be tested against the $S(0)$ value obtained. Because of the low compressibility of solids (or liquids near T_g), the scattering intensity at $q = 0$ is weak and the $S(0)$ value defined by eq. 1 should be approximately $1 - \frac{\langle f^2 \rangle}{\langle f \rangle^2}$. For D-mannitol and dulcitol, this value is -0.66; for D-arabitol, it is – 0.68. They agree with the experimental $S(q)$ extrapolated to $q = 0$. A noteworthy feature in Figure 1 is that the crystal and the liquid have similar $S(q)$ at high q (> 8 Å^{-1}). This is a well-understood result for molecular liquids. Since strong covalent bonds within a molecule have well-defined distances, their contribution to scattering persists to higher q than less well-defined intermolecular correlations. This result suggests that the molecular structure in the liquid is similar to that in the crystal.

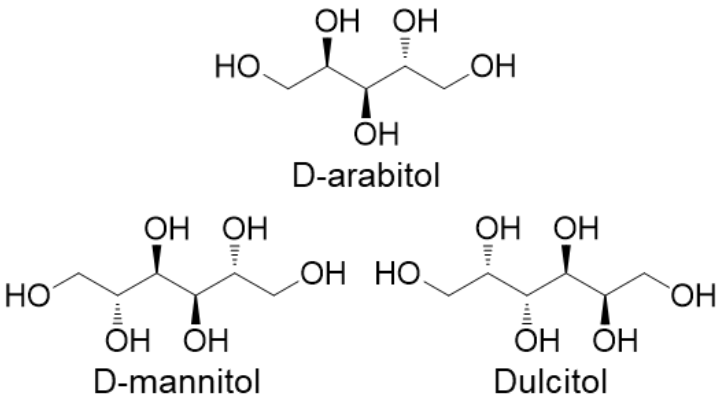

Scheme 1. Molecular structures of three polyalcohols studied here.

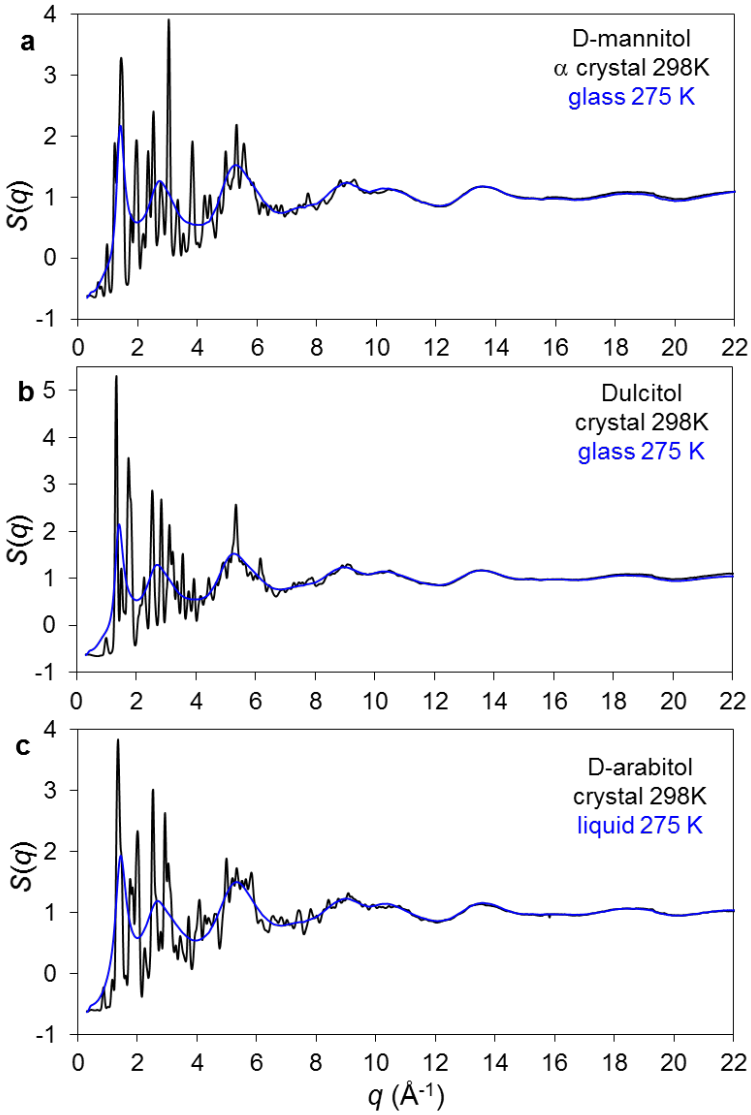

Figure 1. Total structure factors $S(q)$ for the crystals and the supercooled liquids of D-mannitol, dulcitol and D-arabitol. The crystal data were collected at 298 K and the liquid data at 275 K.

Figure 2 shows the differential PDF, $D(r)$, for the polyalcohols studied. $D(r)$ is obtained by a Fourier sine transform as follows,

$$D(r) = \frac{2}{\pi}\int_0^{q_{max}} q(S(q) - 1)\sin(qr)\, dq \qquad (2)$$

where q_{max} is the upper limit of the usable q range of experimental data. For our data, q_{max} = 21 Å^{-1} and no window function was used. $D(r)$ is related to two other types of PDF as follows: $T(r) = D(r) + 4\pi\rho r$, where ρ is the atomic number density (atoms/Å^3); $G(r) = T(r)/(4\pi\rho r)$, where $G(r)$ has the familiar physical meaning that the integral of $4\pi\rho\, r^2\, G\,(r)$ over some r range is the number of atoms within that range.

Figure 2 shows that for each polyalcohol, the PDFs of the crystal and the liquid are identical at short distances (< 2.5 Å), while significant differences are seen at longer distances. The agreement at short distances again, reflects the identical covalent bonds in the two phases. The peak at 1.5 Å corresponds to the covalent bonds in the molecule (C-C and C-O); the peak at 2.3 Å corresponds to the second-nearest-neighbor distance across two consecutive covalent bonds (its constancy is a result of nearly constant covalent bond angles). Given the length of each polyalcohol molecule (~ 7 Å for D-mannitol and dulcitol, ~ 6 Å for D-arabitol), the crystal and the liquid PDFs are expected to still resemble each other above 2.5 Å, but their difference should increase with distance owing to different molecular packing. This is indeed seen in Figure 2. For each system, there is significant corrleation between the crystal and the liquid for r = 2.5 – 6 Å, but at longer distances, no correlation is evident. For r > 6 Å, the crystal PDF is dominated by the regular spacings of crystal packing, whereas the liquid PDF by the damped oscillation characteristic of molecular packing in a dense liquid.

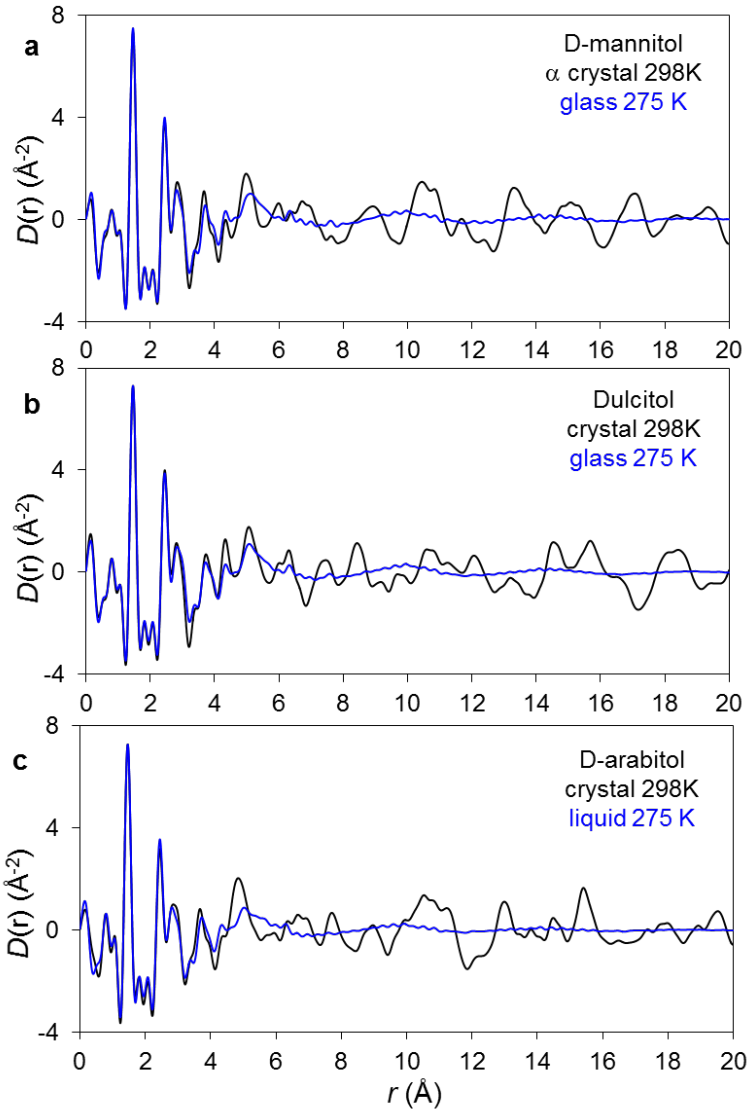

Figure 2. Differential PDFs *D*(*r*) for the crystals and supercooled liquids of D-mannitol, dulcitol and D-arabitol.

The next step in data reduction is to remove the intramolecular contribution to the total PDF to obtain the intermolecular PDF.[8] In terms of the $T(r)$ function, we have

$$T(r)_{inter} = T(r) - T(r)_{intra} \quad (3)$$

where $T(r)_{intra}$ is the X-ray weighted intramolecular PDF. In Figure 3, we illustrate the isolation of intermolecular PDF according to eq. (3) using crystalline D-mannitol (the α polymorph) as an example. The $T(r)$ trace (solid curve in Figure 3a) is obtained from the experimental $D(r)$ (Figure 2a) and the atomic number density ρ from single-crystal diffraction (Table 1). The $T(r)_{intra}$ trace (dotted curve) is calculated from the known molecular structure in this crystal[17] using the Debye model. The displacement factor σ in the model is varied to reproduce the widths of the peaks corresponding to covalent bonds (i.e., peaks at 1.5 Å and 2.3 Å). In this case, σ = 0.077 Å. The σ value describes the width of the unresolved distribution of the C-C and C-O covalent bond lengths and any thermal effect on them. Notice that the intramolecular $T(r)$ reproduces quite well the low r peaks corresponding to covalent bonds.

Figure 3b shows the intermolecular PDF $T(r)_{inter}$ obtained by subtracting $T(r)_{intra}$ from $T(r)$. The $T(r)_{inter}$ curve has no significant peaks below 2.5 Å as expected, and its first major peak is at 2.7 Å and almost fully resolved. It corresponds to the O…O correlation in an intermolecular HB. Fitting this peak using the program NXFit, we obtain R_{OO} = 2.72 Å for the bond length, N_{OO} = 1.9 for the coordination number of the oxygen atom (the number of HBs formed by each OH group acting both as donor and as acceptor), and σ = 0.099 Å. The parameter σ characterizes the width of the distribution of the O…O distance due to thermal fluctuation and static disorder.

The validity of these results from total scattering can be assessed by comparison with the values from single-crystal diffraction. In the single-crystal structure of D-mannitol at the same temperature (298 K), there are 6 distinct O…O distances with an average of 2.76 Å and a standard

deviation of 0.043 Å. The average O…O distance in the single-crystal structure is in reasonable agreement with the R_{OO} value from the PDF method. The PDF R_{OO} value seems slightly smaller than the single-crystal value, and the same decrease is also observed with other polyalcohols studied (Table 1). At present, we have no satisfactory explanation for this effect. Systematic differences have been reported between bond lengths obtained from single-crystal diffraction and from total scattering, and have been attributed to the fact that the former method determines the mean atomic positions while the latter, the atomic pair-correlation functions.[22] In the single-crystal structure of D-mannitol, N_{OO} is 2; that is, each OH group forms two HBs, serving as donor once and acceptor once. The slightly different N_{OO} value from total scattering (1.9) is attributed to the error of the method. A similar ~ 10 % discrepancy in N_{OO} is observed with the other polyalcohols (Table 1).

Having gained some confidence in the procedure to extract intermolecular correlations in crystals, for which the answer it known, we now apply it to liquids. Unlike the crystal case, there is no definitive knowledge of the molecular conformation in the liquid state. As a first approximation, it is not unreasonable to assume that the molecuclar conformation in the liquid is the same as that in the crystal. For the polyalcohols studied here, this assumption has additional justification. Based on an analysis of steric hindrance, Jeffrey and Kim[23] proposed that the carbon chain of a polyalcohol should be an extended zigzag if the configurations (D or L) on alternate carbons are different. This “rule” is based on the avoidance of short contact between two OH groups on alternate carbons. This model can predict polyalcohol conformations in crystals with considerable success. According to this model, D-mannitol, dulictol and D-arabitol should be extended zigzags, which is indeed the case in the actual crystal structures. Jefferey and Kim argue that this rule should be valid (perhaps more valid) in the liquid state, except that the terminal OH

group could be able to reorient relative to the carbon backbone. This prediction is consistent with the liquid-state NMR spectra of D-mannitol[24] and with the results of molecular simulations.[25]

Figure 4a shows the intramolecular PDFs of D-mannitol calculated using the four conformers consistent with the model of Jefferey and Kim. Starting from the conformation in the crystal, three additional conformations are generated by rotating the two terminal OH groups relative to the nearest C-C bond. The resulting $T(r)_{intra}$ curves are nearly indistinguishable below 2.9 Å, and differences are seen only at longer distances. Figure 4b shows the four intermolecular PDFs obtained by subtracting the four intramolecular PDFs from the total. All the results contain the peak of interest at 2.7 Å and there is no significant difference in this peak between the different models of removing the intramolecular contribution. The same conclusion is drawn upon analyzing the dulcitol and D-arabitol data the same way (Figures 5 and 6). For simplicity, we use the molecular conformation in the crystal to represent the conformation in the liquid.

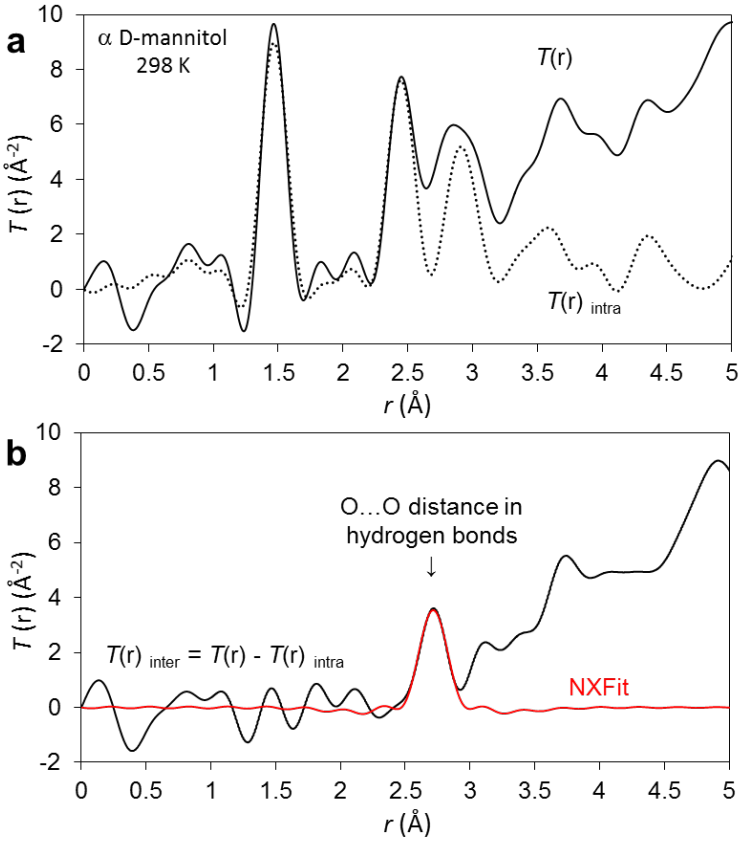

Figure 3. Illustration of the separation of intra- and intermolecular contributions of the total PDF. The system is D-mannitol in the α polymorph.

Table 1. Intermolecular hydrogen bonds in the polyalcohols studied.

	D-mannitol	Dulcitol	D-arabitol
Formula	$C_6O_6H_{14}$	$C_6O_6H_{14}$	$C_5O_5H_{12}$
Crystalline phase (298 K)			
Single-crystal diffraction:			
ρ, g/mL	1.471	1.496	1.493
ρ, atoms/Å^3	0.1264	0.1286	0.1300
R_{OO}, Å	2.764	2.717	2.763
σ (static), Å	0.043	0.059	0.066
N_{OO}	2	2	2
CSD ref. code	DMANTL01	GALACT	VOZMAY
Reference	26	18	19
Total powder scattering:			
R_{OO}, Å	2.72	2.69	2.72
σ (total), Å	0.099	0.097	0.102
N_{OO}	1.91	2.12	2.18
Glass or liquid (275 K)			
ρ, g/mL	1.442 (278 K)[27]	1.43	1.40
ρ, atoms/Å^3	0.1239 (278 K)[27]	0.123	0.122
R_{OO}, Å	2.72	2.69	2.72
σ, Å	0.094	0.088	0.082
N_{OO}	1.77	1.74	1.71
N_{OO} (amorph)/N_{OO} (cryst)	0.92	0.82	0.78

Notes: R_{OO} is the shortest O…O distance in an intermolecular HB. N_{OO} is the coordination number of the oxygen atom (the number of HBs formed by each OH group acting as donor or acceptor). σ is a parameter characterizing the width of the distribution of the O…O distance due to thermal fluctuation and static disorder.

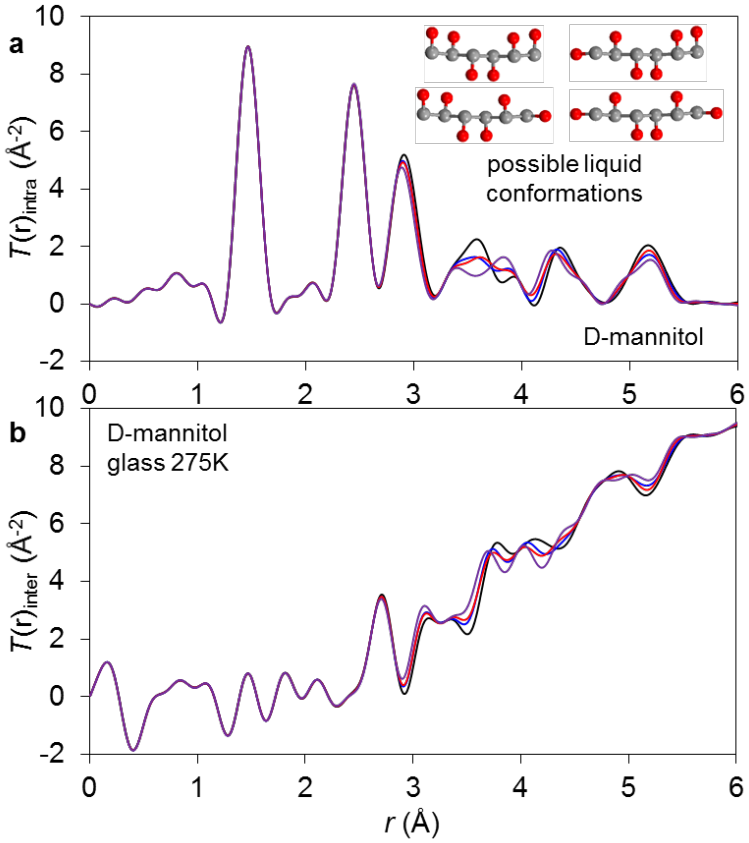

Figure 4. (a) Effect of terminal OH orientation on the intramolecular PDF of D-mannitol. (b) Calculated intermolecular PDF of the D-mannitol glass assuming different intramolecular PDFs in (a).

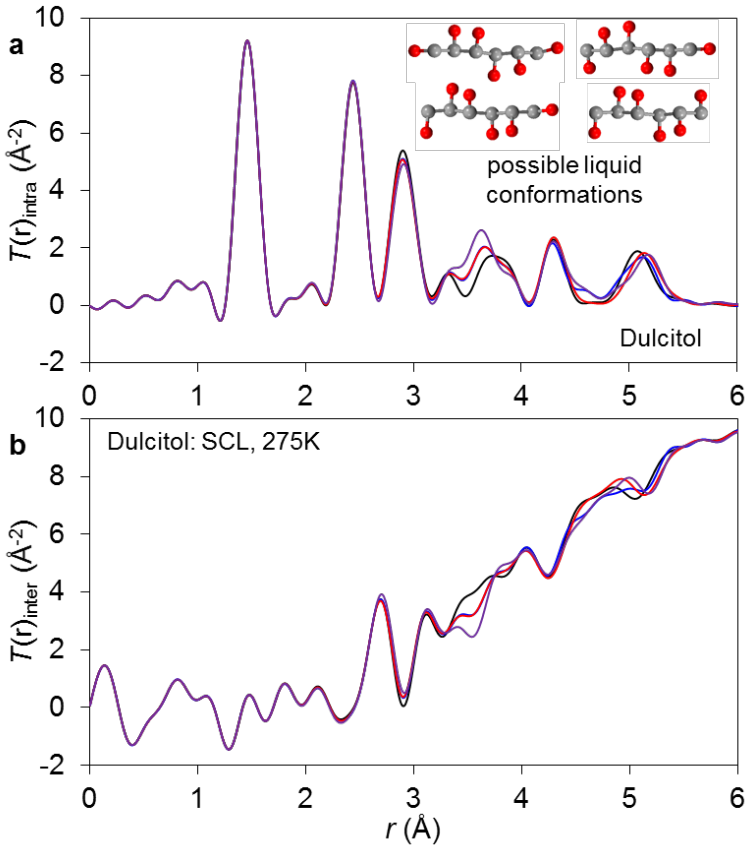

Figure 5. (a) Effect of terminal OH orientation on the intramolecular PDF of dulcitol. (b) Calculated intermolecular PDF of the dulcitol glass assuming different intramolecular PDFs in (a).

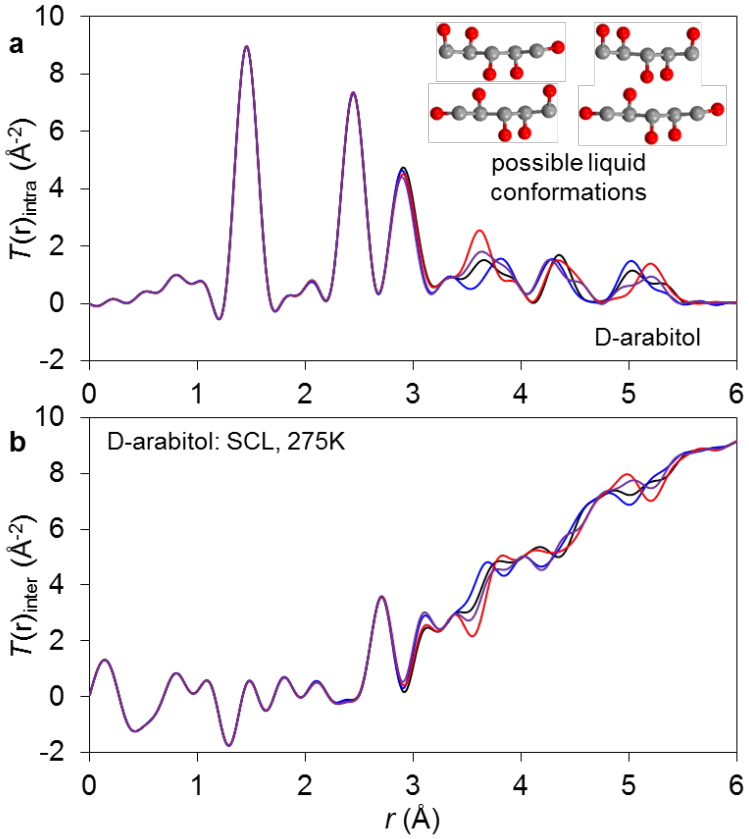

Figure 6. (a) Effect of terminal OH orientation on the intramolecular PDF of D-arabitol. (b) Calculated intermolecular PDF of the D-arabitol liquid assuming different intramolecular PDFs in (a).

Figure 7 shows the intermolecular PDFs $T(r)$ for the three polyalcohols studied. For each system, results are presented on both the crystalline phase and the amorphous phase. All the traces show a well-resolved peak at 2.7 Å corresponding to the O…O correlation in an intermolecular HB. There is no significant difference between the crystalline phase and the liquid phase in the position of this peak, indicating that the lengths of the intermolecular HBs are similar in the two phases. This is confirmed by numerical fitting using NXFit (Table 1).

Close inspection of Figure 7 shows that the 2.7 Å peak of the amorphous sample has a slightly smaller area and is slightly narrower than the peak in the crystalline sample. This is also supported by the analysis using NXFit. The coordination number for each oxygen is slightly smaller in the amorphous phase than in the crystal. For the three systems studied, the N_{OO} value in the amorphous phase is 10 – 20 % lower than that in the crystal. This means that on average, each molecule in the amorphous phase forms 10 % fewer hydrogen bonds than in the crystal. This conclusion is similar to that reached for mono-alcohol liquids,[8,9] though they were studied at higher temperatures relative to T_g than the polyalcohols studied here. Finally, we note that for all the three systems studied, the width of the O…O peak for the amorphous phase is slightly narrower (the σ value smaller) than that for the crystal. This argues that the HB bond length is better defined in the liquid than in the crystal. By this measure, the liquid is actually more “structured” than the crystal, despite its lack of long-range order. This could be a result of local optimization of HBs in the liquid state without the constraint of regular crystal packing. In the crystalline state, the need for regular and dense packing could mean that HBs cannot be optimized, leading to widely different O…O distances.

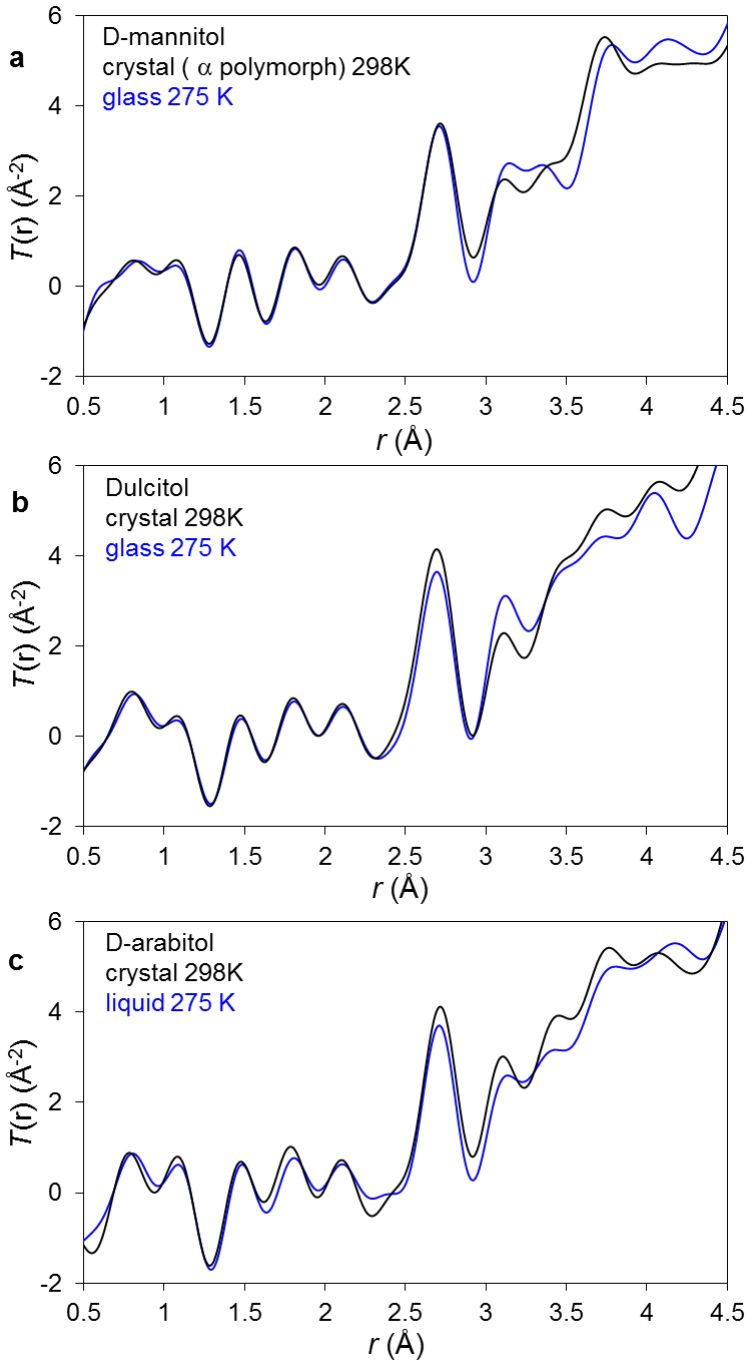

Figure 7. Intermolecular PDFs $T(r)_{inter}$ for the polyalcohols studied. For each system, results are shown for both the liquid phase and the crystalline phase.

6.5 Conclusion

We have used synchrotron total X-ray scattering to characterize the HBs in three polyalcohols in the crystalline state and the amorphous state. For each system, the atomic pair distribution function (PDF) shows a well-resolved peak at 2.7 Å after removing intramolecular contributions. This peak corresponds to the O…O distance in an intermolecular HB. We find that the O…O bond length does not change significantly from the crystal to the liquid or glass, while the O…O coordination number (the number of HBs formed by each OH group) is reduced by 10-20 %. The distribution of the O…O distance is slightly narrower in the amorphous phase than in the crystal, perhaps a result of the conflict between regular crystal packing and optimal hydrogen bonding.

6.6 Acknowledgments

We thank the NSF funded University of Wisconsin-Madison MRSEC (DMR 1720415) for supporting this work.

6.7 References

[1] G. W. Stewart, and R. M. Morrow, Phys. Rev. **30**, 232 (1927).

[2] B. E. Warren, Phys. Rev. **45**, 657 (1934).

[3] W. Ashcroft, J. Lekner, Phys. Rev. 145 (1965).

[4] J. L. Yarnell, M. J. Katz, R. G. Wenzel, and S. H. Koenig, Phys. Rev. A **7**, 2130 (1973).

[5] L. B. Skinner, C. Huang, D. Schlesinger, L. G. M. Pettersson, A. Nilsson, and C. J. Benmore, J. Chem. Phys. **138**, 074506 (2013)

[6] C. Benmore, *Modern Glass Characterization,* Ch. 6. (John Wiley & Sons, 2015).

[7] M. C. Etter, *Acc. Chem. Res*. **23**, 120 (1990).

[8] A. H. Narten, A. Habenschuss, J. Chem. Phys. **80,** 3387 (1984).

[9] K. S. Vahvaselka, R. Serimaa, and M. Torkkeli, J. Appl. Crvst. 28, 189 (1995).

[10] I. Bakó, T. Grósz, G. Pálinkás, M. C. Bellissent-Funel, J. Chem. Phys. **118,** 3215 (2003).

[11] S. Sarkar, R.N. Joarder, Phys. Lett. A **222,** 195 (1996).

[12] J.J. Towey, A.K. Soper, L. Dougan, Phys. Chem. Chem. Phys. **13**, 9397 (2011).

[13] S. P. Verevkin, D. H. Zaitsau, V. N. Emel'yanenko, A. A. Zhabina, Fluid Phase Equilibria 397, 87 (2015).

[14] A. P. Hammersley, S. O. Svensson, M. Hanfland, A. N. Fitch, D. Hausermann, High Press. Res. **14,** 235 (1996).

[15] X. Y. Qiu, J. W. Thompson, S. J. L. Billinge, J. Appl. Crystallogr. **37,** 678 (2004).

[16] P. Juhás, C. L. Farrow, X. Yang, K. R. Knox, S. J. L. Billinge, Acta Cryst. A **71,** 562 (2015).

[17] F. R. Fronczek, H. N. Kamel, and M. Slattery, Acta Crystallogr., Sect. C: Cryst. Struct. Commun. **59**, 567 (2003).

[18] H. M. Berman and R. D. Rosenstein, Acta Crystallogr. Sect. B **24**, 435 (1968).

[19] J. Kopf, M. Morf, B. Zimmer, and P. Köll, Carbohydrate Research **218**, 9 (1991).

[20] D. Pickup, R. Mossa and R. Newport, J. Appl. Cryst. **47**, 1790, (2014)

[21] P. J. Brown, A. G. Fox, E. N. Maslen, M. A. O'Keefe, and B. T. M. Willis, in International Tables for Crystallography Volume C, edited by E. Prince (Springer Netherlands, Dordrecht, 2004), pp. 554.

[22] M. T. Dove, M. G. Tucker, and D. A. Keen, Eur. J. Mineral. 14, 331-348 (2002).

[23] G. A. Jeffrey, and H. S. Kim, Carbohydrate Research **14**, 207 (1970).

[24] T. B. Grindley, M. S. Mckinnon, and R. E. Wasylishen, Carbohydrate Research **197**, 41 (1990)

[25] J. R. Grigera, Journal of the Chemical Society, Faraday Transactions 1**84** (1988) 2603.

[26] H. S. Kim, G. A. Jeffrey, R. D. Rosenstein, Acta Crystallogr., Sect. B: Struct. Crystallogr. Cryst. Chem. **24**, 1449 (1968).

[27] Zhu, M.; Yu, L. The Journal of Chemical Physics **2017,** *146* (24), 244503.

Chapter 7. Future Studies

This thesis work has contributed to the physical stability of molecular glasses and amorphous solid dispersions. To further improve our understanding on the relevant phenomena discussed in the previous chapters, some important questions should be further addressed. In this chapter, I would like to propose some future studies to provide some useful information on these questions.

7.1 Is there a correlation between molecular shape and surface diffusion coefficient in organic molecules?

In chapter 2 and Chen *et al.*[1], the two independent factors, molecular size and intermolecular hydrogen bonding, have been demonstrated to influence the surface diffusion coefficient in organic materials. It is interesting to study whether other molecular attributes can influence surface diffusion. In this proposal, the effect of molecular shape will be studied. I hypothesize that molecular shape will have a significant effect because for the same molecular size (molecular weight), the shape affects the depth of penetration into the similar mobility gradient, where the deeper penetration leads to the slower mobility.

Surface diffusion will be measured for molecules whose molecular weight and hydrogen bonding are similar, but their shapes are different. Here, one rod-like molecule (N,N'-Bis(naphthalen-1-yl)-N,N'-bis(phenyl)benzidine, CAS No.: 123847-85-8, known as NPB, M_w = 588.7 g/mol) and one spherical molecule (9,10-Bis[N,N -di(p-tolyl)-amino]anthracene, CAS No.: 177799-16-5, known as TTPA, M_w = 568.8 g/mol) are proposed (as shown in Figure 1). For these systems, no intermolecular hydrogen bonding can be formed, and the molecular weight are similar (588.7 vs. 568.8 g/mol). However, the two molecules have different shapes. NPB is rod-like, while

TTPA is sphere-like. My hypothesis is that the rod-like molecule has the slower surface diffusion than the sphere-like molecule because of the different penetration depths.

To quantify the surface diffusion of NPB and TTPA, the surface grating decay method, described in Chapter 2, using AFM and laser diffraction in flowing N_2 will be utilized. The decay of NPB and TTPA will be studied systematically over a wide temperature range. Considering the molecular weight of these molecules are fairly large relative to griseofulvin, the sinusoidal surface grating with a shorter wavelength ($\lambda < 1000$ nm) will be preferred to reduce the measurement time. Such information is expected to greatly improve our understanding of molecular factors, which influence surface mobility.

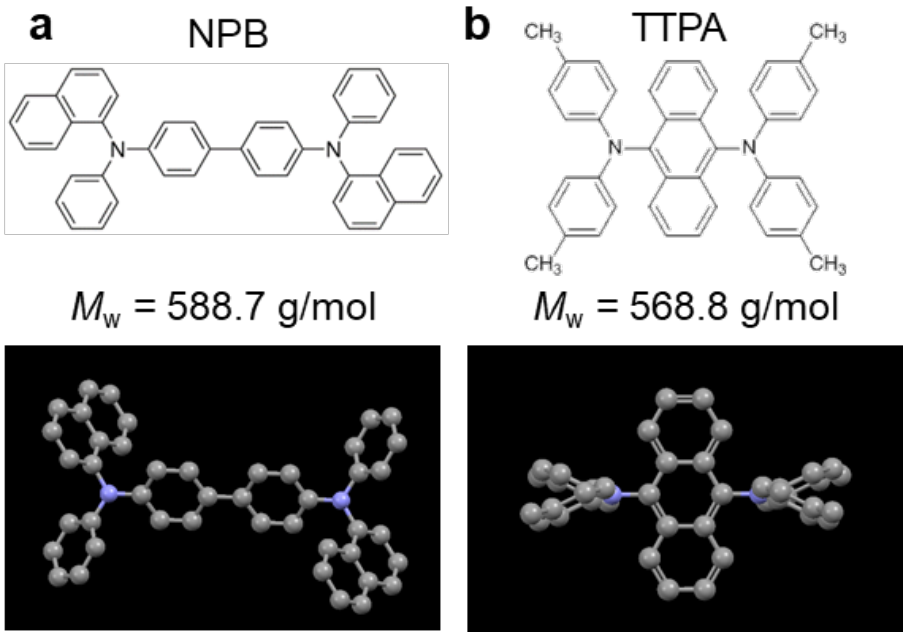

Figure 1. Molecular structure and conformation for (a) NPB and (b) TTPA proposed in this study. Note that the molecular conformation (without hydrogen atoms) for NPB is from Ref. [2], and for TTPA is computed from PubChem[3].

7.2 Can we directly observe the fracture at the front of GC crystals?

Some organic glasses are known to grow crystals rapidly in the bulk (so-called GC growth). Among its various explanations, the most recent by Powell *et al.*[4] argues that the GC growth process continuously creates voids and free surfaces through fracture (given the higher density of the crystal than the glass and the inability for the glass to flow during crystal growth, this must happen), which in turn enables fast local transformation. This mechanism is supported by the microstructure of GC crystals, which has been studied by AFM and SEM. However, where fracture occurs during GC growth (in the glass, at the crystal/glass interface, or somewhere else) is unknown. Therefore, it is interesting to directly investigate fracture during the process of GC crystal growth. Having this information is important for constructing a detailed model for GC growth.

In this proposal, we will study the griseofulvin (GSF) as a model system. Shi *et al.*[5] measured the GC crystal growth of GSF over the wide temperature range. From this information, we can select the appropriate crystal-growth temperature for the *in-situ* observation. The crystalline griseofulvin (GSF) is 8% denser than its glass, which might lead to the more obvious effect than other organics (*e.g. o*-terphenyl, nifedipine and indomethacin).

In sample preparation, the amorphous GSF should be annealed at an appropriate temperature ($T < T_g$, for example 353 K) to induce the GC growth, and prepare the observable crystals. The high resolution of the microscopy method is required to directly observe the fracture, for example atomic force microscope (AFM), scanning electron microscope (SEM) or even transmission electron microscope (TEM). Considering the TEM beam energy is high and might endanger the GSF film, the temperature controlled TEM might be applied to safely observe the samples (low temperature should be avoided for further fracture). My hypothesis is that the fracture might exist

in the glass, or on the crystal/glass interface. However, it will be helpful to scan the GSF sample from GC crystal region to glassy region through the crystal/glass interface.

7.3 Nucleation pre-factor of glass-forming molecular liquids

In the Chapter 3, the experimental nucleation rates in supercooled liquids of D-sorbitol and D-arabitol have been quantified at the temperature above the glass transition temperature, T_g. Under the classical nucleation theory (CNT), the exponential pre-factor, $A = f_u u_0$, can be estimated as 10^{20} $s^{-1}m^{-3}$, which is much smaller than the theoretical value ~ 10^{41} $s^{-1}m^{-3}$. In comparison, the discrepancy between experimental and theoretical pre-factor is observed in metallic liquid (Hg) and silicates (LS2). The experimental pre-factor can be *ca.* 15 orders of magnitude larger than the theoretical one for lithium disilicate,[6] and 7 orders of magnitude for mercury[7]. The discrepancies in LS2 and mercury are significantly different from molecular liquids, where the experimental pre-factor is smaller than theoretical one studied in polyalcohols. It is of interest to investigate whether this discrepancy between experimental and theoretical pre-factors is general for different types of organic molecules. In this proposal, several more organic molecules will be studied for homogeneous nucleation, and this information will provide a critical evaluation of the CNT.

To reach our goal, the organic molecules with homogeneous nucleation should be quantified and investigated by the CNT equation. Based on the preliminary data, the systems to be studied include nifedipine (NIF), griseofulvin (GSF), D-mannitol and ROY. For these systems, the crystal growth rate of nucleation polymorphs has been measured as a function of temperature, which can provide the growth temperature for two-stage method if necessary, and also represent the kinetics in the CNT equation. Besides, the thermodynamics will be evaluated based on Gibbs free energy difference between crystal and liquid, ΔG_v, and critical nucleus/liquid free energy, σ (estimated from the plot of ln (Ju) vs. $1/T/\Delta G_v^2$.

7.4 Do polyalcohols nucleate at temperature below the glass transition temperature? If so, does *J* still follow CNT?

The nucleation rates in lithium disilicate turns to deviate from CNT model at low temperatures (especially at $T < T_g$), and Gupta *et al.*[8] contributes this failure to the dynamic heterogeneity in deeply cooled liquid. In comparison, the experimental nucleation rates in supercooled liquids of D-sorbitol and D-arabitol (Chapter 3) follows the classical nucleation theory above the glass transition temperature T_g, and no deviation of CNT has been observed. We argue that the for D-sorbitol, there is no obvious indication that the CNT fails as a result of an increasing length scale of cooperative rearrangement. It would be interesting to measure the nucleation rate in D-sorbitol down to even lower temperatures ($T < T_g$) to see if the CNT continues to hold. This information is important to improve the understanding of the homogeneous nucleation rate at $T < T_g$ for molecular glasses, and also provide the critical evaluation of CNT at low temperatures.

Preliminary studies show that D-sorbitol nucleation rate is relatively slow in comparison to the studied temperature. Therefore, a large mass of D-sorbitol materials (*ca.* 1 gram) will be prepared, and nucleated at $T < T_g$ (269 K). In this proposal, D-sorbitol will be nucleated at 268, 263 and 253 K, which temperatures are easily accessed. Because the crystal growth rate of D-sorbitol glass is fairly slow (log u (m/s) < -12.6), the two-stage method will be utilized (the same growth temperature of 318 K).

7.5 Is there a fast “glass-to-crystal” nucleation model in molecular glasses?

Near and below T_g, molecular glasses are known to exhibit a fast mode of crystal growth (the so-called “glass-to-crystal” or GC growth mode). This growth mode is apparently unlimited by bulk dynamics in the liquid state, and has been given a number of explanations, including

homogeneous nucleation, shrinking critical-nucleus size to below the dynamic length scale, and micro-fracture and surface mobility. Such phenomenon has been observed in many molecular glass-formers (though not the ones studied here). It would be of interest to learn whether there is a fast "glass-to-crystal" nucleation mode in molecular glasses. In this proposal, the organic molecules, which have shown the fast GC growth in the bulk, will be studied at $T < T_g$. My hypothesis is that GC nucleation model might not exist because critical nucleus is nanometer scale which might not lead to fracture inside the bulk material. Knowing this information is still important to improve the understanding of the homogeneous nucleation rate at $T < T_g$ for molecular glasses, especially for pharmaceutical glasses whose storage temperature is usually below their glass transition temperatures.

The model systems include *o*-terphenyl, nifedipine, griseofulvin and ROY. The samples will be sandwiched between two coverslips and held at $T < T_g$. For T is close to T_g, the crystal growth rate is fast enough in the bulk to utilize the one-stage method, while the two-stage method can be adopted at lower temperatures. It is worth to note that the fracture resulting from low temperatures should be avoided, which might contribute to heterogeneous nucleation. In this proposal, the fracture temperature, $T_{fracture}$, will be assessed by Powell *et al.*[9] The steady state nucleation rate will be studied in the temperature range from $T_{fracture}$ to T_g.

7.6 Can free surface influence nucleation behavior?

Free surface of molecular materials is known to have the faster mobility than the bulk, and it is responsible for the fast surface crystal growth.[10] It is interesting to study the effect of free surface on crystal nucleation in molecular materials. I propose to study this effect by measuring the nucleation rate on the free surface for the open sandwich sample. Considering the fast surface

mobility of molecular materials and preferred sites on free surface, I hypothesize that free surface will result in the heterogeneous nucleation with a fast rate.

In this proposal, the studied systems will include different types of molecules: griseofulvin (no hydrogen bonding), nifedipine (limited hydrogen bonding) and D-arabitol (extensive hydrogen bonding). The open sandwich sample will be prepared by detaching sandwich samples by bending its edges away from the organic glass, creating a glass film with a free surface. It is worth to note that the fracture induced by cooling should be avoided for this study (the fracture-induced heterogeneous nucleation has been demonstrated for the crystal nucleation[11]). The open sandwich sample can be nucleated at appropriate temperatures, if necessary the two-stage method can be applied. With these data, it would be interesting to see whether the free surface will influence nucleation or not. If so, the further comparison among griseofulvin, nifedipine and D-arabitol data might provide us some information about molecular attributes on surface nucleation rate.

7.7 References

[1] Chen, Y.; Zhang, W.; Yu, L. Hydrogen bonding slows down surface diffusion of molecular glasses. *The Journal of Physical Chemistry B* **2016,** *120*, 8007-8015.

[2] Cheng, J.-A.; Cheng, P.-J., Crystal Study of N,N′-diphenyl-N,N′-bis(1-naphthyl)-1,1′-biphenyl-4,4′-diamine. *Journal of Chemical Crystallography* **2010,** *40* (6), 557-560.

[3] URL: https://pubchem.ncbi.nlm.nih.gov

[4] Powell, C. T.; Xi, H.; Sun, Y.; Gunn, E.; Chen, Y.; Ediger, M. D.; Yu, L. Fast crystal growth in *o*-terphenyl glasses: a possible role for fracture and surface mobility. *The Journal of Physical Chemistry B* **2015,** *119*, 10124-10130.

[5] Shi, Q.; Cai, T. Fast crystal growth of amorphous griseofulvin: relations between bulk and surface growth modes. *Crystal Growth & Design* **2016,** *16*, 3279-3286.

[6] Fokin, V. M.; Zanotto, E. D.; Yuritsyn, N. S.; Schmelzer, J. W. P., Homogeneous crystal nucleation in silicate glasses: A 40 years perspective. *Journal of Non-Crystalline Solids* **2006,** *352* (26–27), 2681-2714.

[7] Turnbull, D., Kinetics of Solidification of Supercooled Liquid Mercury Droplets. *The Journal of Chemical Physics* **1952,** *20* (3), 411-424.

[8] Gupta, P. K.; Cassar, D. R.; Zanotto, E. D., Role of dynamic heterogeneities in crystal nucleation kinetics in an oxide supercooled liquid. *The Journal of Chemical Physics* **2016,** *145* (21), 211920.

[9] Powell, C. T.; Chen, Y.; Yu, L., Fracture of molecular glasses under tension and increasing their fracture resistance with polymer additives. *Journal of Non-Crystalline Solids* **2015,** *429*, 122-128.

[10] Huang, C.; Ruan, S.; Cai, T.; Yu, L., Fast Surface Diffusion and Crystallization of Amorphous Griseofulvin. *The Journal of Physical Chemistry B* **2017,** *121* (40), 9463-9468.

[11] Su, Y., Yu, L., Cai, T., private communication.